Dissertation

submitted to the

Combined Faculties for the Natural Sciences and for Mathematics

of the Ruperto-Carola University of Heidelberg, Germany

for the degree of

Doctor of Natural Sciences

presented by

Rui Cao, M.Agr.

born in Nanjing, China

Oral-examination: 21.10.2020

Evaluation of a prophylactic L2-based vaccine in the pre-clinical model *Mastomys coucha* and establishment of an *in vitro* infection model for the cutaneous papillomavirus MnPV

Referees:

Prof. Dr. Martin Müller

Prof. Dr. Frank Rösl

Eidesstattliche Erklärung

Ich erkläre hiermit, dass ich die vorliegende Dissertation selbst verfasst und mich keiner anderen als der von mir ausdrücklich bezeichneten Quellen und Hilfsmittel bedient habe. Diese Dissertation wurde in dieser oder anderer Form weder bereits als Prüfungsarbeit verwendet, noch einer anderen Fakultät als Dissertation vorgelegt. An keiner anderen Stelle ist ein Prüfungsverfahren beantragt.

Heidelberg, den 15.08.2020

Rui Cao

Table of Contents

Summary

Non-melanoma skin cancer (NMSC) is the most frequent cancer in the Caucasian population. Infections with cutaneous human papillomaviruses (HPVs) in conjunction with UV and immunosuppression are risk factors in the development of this type of cancer. As known by *in silico* analyses, an epitope within the N-terminus of the HPV minor capsid protein L2 is highly conserved across numerous HPV types and theoretically should elicit a pan cross-neutralizing response. To study this subject in a preclinical system, a MnPV L2-based vaccine was developed and evaluated in *Mastomys coucha*, a rodent naturally and persistently infected with MnPV. Vaccination with MnPV L2 or VLPs can induce a strong humoral immune response against L2 or VLPs. Moreover, UV irradiation did not influence antibody reactivity to MnPV L2 or VLPs. However, L2-specific antibodies were not persisting as long as the antibody response induced after VLP vaccination. Furthermore, there was no significant difference in the appearance of skin tumors among unvaccinated and vaccinated animals suggesting that an L2-based vaccine only should be considered with caution. Additionally, in order to gain a deeper insight into cutaneous papillomaviruses and UV in the development of skin cancer, a short-term *in vitro* infection system was established. Transcripts from both the early (*E6*, *E7* and *E1^E4*) and the late (*E1^E4*, *L1*) promoter as well as the viral early protein E4 and E7 were detectable in infected keratinocytes, supporting the investigation of the MnPV/host cell interplay. Moreover, the infected keratinocytes were committed to differentiation via increased cell-to-cell contact, differentiation inducers and UV exposure, leading to an increase of *L1* mRNA. This indicates that UV-induced differentiation might influence the productive MnPV life cycle.

Taken together, the current study provides a basis for the development of L2-based vaccines against cutaneous papillomavirus infection especially together with frequent sun exposure and further research on the cutaneous papillomavirus- and UV-driven skin tumorigenesis.

Zusammenfassung

Weißer Hautkrebs („non-melanoma skin cancer“, NMSC) ist die häufigste Krebsart in der hellhäutigen Bevölkerung. Infektionen mit kutanen Humanen Papillomviren (HPVs) in Verbindung mit UV-Strahlung und Immunsuppression sind Risikofaktoren für die Entstehung dieser Krebsart. *In silico* Analysen haben gezeigt, dass ein Epitop im N-Terminus des HPV Capsidproteins L2 hoch konserviert zwischen zahlreichen HPV-Typen ist und theoretisch pan-kreuzneutralisierende Immunreaktionen auslösen könnte. Um diese Annahme in einem präklinischen Modell zu untersuchen, wurde ein MnPV L2-basierter Impfstoff entwickelt und in *Mastomys coucha* untersucht, einem Nagetier, das natürlicherweise mit MnPV infiziert ist. Die Vakzinierung mit MnPV L2 oder VLPs kann eine starke humorale Immunantwort gegen diese Antigene hervorrufen. Desweiteren hatte UV-Bestrahlung keinen Einfluss auf die Antikörper-Reaktivität gegen L2 oder VLPs. Jedoch blieben Antikörper gegen L2, im Gegensatz zu denen, die nach Impfung mit VLPs gebildet wurden, nicht lange nachweisbar. Auch beim Auftreten von Hauttumoren waren keine signifikanten Unterschiede zwischen vakzinierten und unvakzinierten Tieren zu erkennen, weswegen L2-basierte Impfstoffe mit Vorsicht betrachtet werden sollten.

Um ein besseres Verständnis für die Rolle von kutanen Papillomviren und UV bei der Entstehung von Hautkrebs zu erlangen, wurde außerdem ein *in vitro* System für eine transiente Infektion mit MnPV etabliert. Sowohl Transkripte des frühen (*E6*, *E7* und *E1^E4*) und späten Promotors (*E1^E4*, *L1*), als auch die viralen Proteine E4 und E7 konnten in infizierten Keratinozyten nachgewiesen werden, was die Untersuchung des Zusammenspiels von MnPV und Wirtszelle ermöglicht. Infizierte Keratinozyten konnten außerdem durch erhöhten Zell-Zell-Kontakt, verschiedene Behandlungen und UV-Bestrahlung zur Differenzierung angeregt werden, was zu einem Anstieg der *L1* mRNA Level führte. Dies deutet darauf hin, dass UV-vermittelte Differenzierung den produktiven Lebenszyklus von MnPV beeinflusst.

Zusammenfassend liefert die aktuelle Studie eine Grundlage für die Entwicklung eines L2-basierten Impfstoffes gegen kutane Papillomviren, vor allem unter häufiger Sonnenbestrahlung und für weitergehende Untersuchungen zu durch kutane Papillomviren und UV hervorgerufene Hauttumor.

1. Introduction

1.1 Infection and Cancer

Cancer, also known as malignant neoplasm or tumor, is caused by uncontrolled growth and division of abnormal cells with the possibility to invade and destroy other normal tissues or organs [1]. Genetic changes which can be inherited from one's parents, and several environmental "drivers" such as alcohol consumption, tobacco smoking, sun exposure and infectious agents, may account for the initiation of tumor development and progression [2]. A recently released database analysis estimated that infectious agents have caused around 2.2 million newly diagnosed cancer cases (13% of all cases) worldwide in 2018 [3]. In particular viruses, mainly Human papillomavirus (HPV), Epstein-Barr virus (EBV), Hepatitis B virus (HBV), Hepatitis C virus (HCV), Human herpes virus 8 (HHV-8) and Human T-lymphotropic virus (HTLV), contributed to 64.5% of infection-related cancers [3]. In addition to the abovementioned cancer-causing viruses, Merkel cell polyomavirus (MCPyV) is linked to the rare human skin cancer called Merkel cell carcinoma (MCC) that typically occurs in immunosuppressed individuals [4]. Although the infection with Human immunodeficiency virus (HIV) cannot directly cause cancer by itself, it can however weaken the immune system through infection, consequently favoring susceptibility to other human pathogens and malignancies [5].

Despite being classified into distinct viral groups and variation-specific oncogenic mechanisms, these cancer-causing viruses share some common strategies to promote tumorigenesis. These "oncoviruses" can hijack host cells by dysregulation of numerous genes involving cell cycle, proliferation or apoptosis after entry and then utilize the host cellular machinery for viral replication and propagation. Moreover, oncoviruses can subvert host immunity by causing chronic inflammation-even without obvious symptoms-for decades, which eventually cause tissue damage and cancer development [6, 7].

1.2 Papillomaviruses

Papillomaviruses (PV) are non-enveloped DNA viruses with a strong tropism for mucosal or cutaneous epithelia across a broad range of host species. Since the first papillomavirus (cottontail rabbit PV, CRPV) was isolated and characterized in 1933, currently, over 220 types of HPVs and around 200 types of animal papillomaviruses have been identified [8]. Based on the nucleotide sequence identities of the late gene *L1*, HPVs are classified into the five genera alpha, beta, gamma, mu and nu, where each newly designated type has to display at least 10% sequence difference to the closest known type [9-11]. Moreover, according to the International Committee on Taxonomy of Viruses (ICTV), animal papillomaviruses are organized into 48 genera so far and the genus classification of papillomaviruses keeps increasing due to next-generation sequencing [12].

Out of the group of mucosal HPV types, some are also known as high-risk (HR) types due to their high oncogenic potential in both women and men, mainly through sexual transmission. According to International Agency for Research on Cancer (IARC), 13 mucosal HPV types (HPV16, 18, 31, 33, 35, 39, 45, 51, 52, 56, 58, 59 and 66) from the alpha genus are referred to as HR HPV genotypes [13]. These account for 100% of cervical, 84% of anal, 70% of vaginal, 47% of penile, 40% of vulvar and 17% of oropharyngeal cancers [14, 15]. Of these types, at least 70% of cervical cancers are attributable to HPV 16 and 18. Low-risk (LR) HPV types (HPV6, 11, 40, 42, 43, 44, 54, 61, 70, 72 and 81) can cause genital warts and respiratory papillomatosis, which are rarely linked to cancer [16, 17]. Multiple HPV infections, including both HR and LR types, are commonly found and have a higher prevalence at the uterine cervix [18]. The cutaneous HPV types, comprising mainly of genus beta and gamma, are frequently associated with benign, premalignant and malignant skin lesions, such as keratoacanthomas (KAs), actinic keratosis (AKs), and squamous cell carcinomas (SCC) [19, 20], and also detected in healthy skin, even in children [21]. Additionally, serology and viral DNA analyses revealed type-specific beta HPVs, especially HPV5, 8 and 38, linked to increased risks of cutaneous SCCs in immunocompetent individuals [22, 23]. Few cutaneous types (HPV2, 3, 7, 10, 27 and 57) are classified in genus alpha, and can cause verruca vulgaris, verruca plantaris, and verruca plana as well as Butcher warts [24].

1.2.1 Papillomavirus Genome

The HPV genome, a double-stranded, circular DNA of approximately 8 kb, codes for non-structural early proteins (E1, E2, E4, E6, E7 and E5, which is absent in the genome of beta HPV types) and structural late proteins (L1 and L2). It also contains a non-coding long control region (LCR), which is located between the *L1* and *E6* genes (**Fig. 1.2.1**) [25].

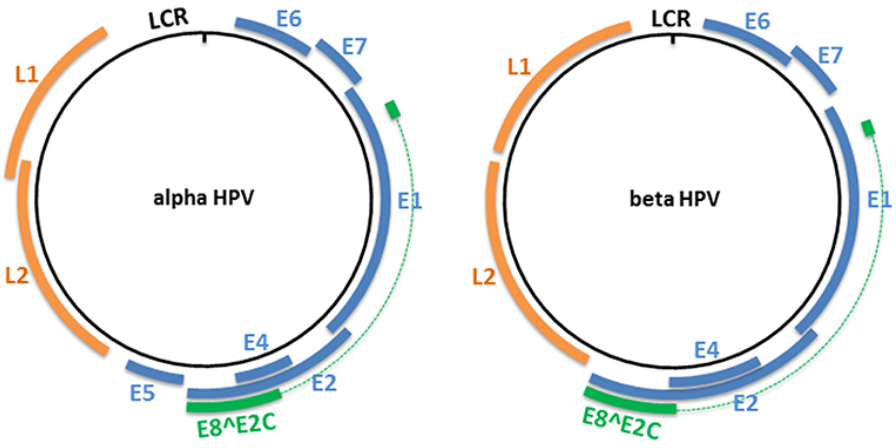

Fig. 1.2.1 Genomic organization of alpha and beta HPV types [25]. The genome of alpha (left panel) and beta (right panel) HPVs is composed of early genes (*E1, E2, E4, E6, E7* and *E5*, which is absent in the genome of beta HPV types) depicted in blue and late genes (*L1* and *L2*) shown in orange. LCR, long control region. This figure is adapted from [25].

E6 and E7, two well-known oncoproteins, are directly responsible for HPV-induced tumorigenesis by targeting cellular tumor suppressor proteins. In HR HPVs, E6 directly binds to the E6-associated protein (E6AP, harboring a LXXLL motif) and degrades p53 as well as other PDZ domain-containing proteins in a proteasome-mediated way. It thereby transcriptionally activates telomerase reverse transcriptase (hTERT) to increase telomerase activity [26]. E7 inactivates retinoblastoma protein pRb, thereby releasing transcription factor E2F from the pRb/E2F complex. It destabilizes pRb-associated proteins p130 and p107 through similar mechanisms [27]. The abovementioned E6/E7-driven progresses lead to inhibition of apoptosis, uncontrolled cell proliferation, immortalization of host cells and malignant transformation. Eventually the persistently infected epithelia progress to cervical intraepithelial neoplasia (CIN) or invasive carcinoma within decades. Notably, the HR HPV genome is capable of integrating into the host genome resulting in the disruption of *E2* and the continuous expression of *E6/E7*. Viral genome integration can be detected in more than 80% of HPV-positive cervical cancers [28, 29]. In contrast, it is not evident that cutaneous HPV genome integration occurs at infected areas, due to its episomal maintenance. However, in cutaneous HPV types, E6 and E7 show different affinities to p53 and pRb respectively, therefore, alternative strategies are employed by beta HPVs to facilitate viral propagation and ultimately induce skin lesions or carcinoma [25]. E6 of several beta HPVs can promote BAK degradation to inhibit apoptosis and target MAML1, a transcriptional coactivator of the NOTCH signaling pathway to prevent host cell differentiation. E7 of some cutaneous HPVs (HPV38 and 49) has the capacity to hyperphosphorylate pRb to uncouple the pRb/E2F complex in order to perturb cell cycle and differentiation [30].

The well-studied function of the E1 protein is the regulation of viral replication through the interaction with several cellular proteins, such as Histone H1, α-DNA polymerase, Replication protein A (RPA), and topoisomerases to favor the maintenance of the viral genome [31, 32].

The E2 protein, containing DNA binding and transactivation domains linked by an unstructured hinge, also plays an important role in viral replication and transcription. E2 recognizes and binds E2-binding sites (E2BSs) within the LCR to initiate viral DNA replication via loading the E1 helicase, which in turn recruits the host's DNA replication machinery onto the replication origin [33]. E2 also interacts with topoisomerase I, subsequently stimulating its DNA relaxation activity to favor the replication process [34]. E2 can act as either an activator or a repressor in viral transcription depending on the HPV type and the interaction between E2 and host cellular proteins.

The *E4* open reading frame (ORF) is located in the hinge region of the *E2* gene and primarily translated from spliced *E1^E4* transcripts. Despite varying sizes and structures formed, the abundant E4 protein has been found in cervical and skin lesions, and therefore together with p16 or minichromosome maintenance complex (MCM), is commonly used as a biomarker indicating productive infection [35, 36]. E4 causes a G2 cell cycle arrest by preventing the nuclear import of host Cyclin/Cdk complexes and

inhibits host cellular DNA replication by disrupting the loading of replication licensing proteins, consequently facilitating viral genome amplification [37]. Furthermore, E4 can interact with Serine-arginine protein kinase 1 (SRPK1) to prevent phosphorylation of not only host serine-arginine (SR) proteins but also serine residues in the hinge domain of E2 that alters the subcellular localization of the viral replication and transcription regulator E2 [38].

Cutaneous HPV types do not encode the E5 protein. It can contribute to cervical neoplasia *in vivo* and represents the smallest hydrophobic viral protein [39].

The LCR harbors binding sites for several viral and cellular transcription factors (E2, AP-1, NF-1, Sp-1, YY-1, etc.), the viral origin of replication, the early promoter and the late polyadenylation (pAL) site. The late promoter is usually positioned within the *E7* gene and tightly controlled by host cellular differentiation events [40].

1.2.2 Papillomavirus Capsid

The papillomavirus capsid is composed of two late proteins, the major capsid protein L1 and the minor capsid protein L2. L1, with a size of approximately 55 kDa, can spontaneously self-assemble into virus-like particles (VLPs) which comprise a highly immunogenic structure but are not contagious since no encapsidation of viral genomic DNA (vDNA) occurs [41]. Subsequently, five L1 monomers (a "jelly roll" β sandwich structure) form an L1 capsomer (**Fig. 1.2.2A**), and 72 capsomers are arranged into a T = 7 icosahedral capsid with a 55-60 nm diameter, which is linked by inter-disulfide bonds [42]. 12 pentavalent capsomers are located at the icosahedral five-fold axis and the remaining 60 hexavalent capsomers are present at the pseudo six-fold axis. The hexavalent capsomers of HPV16 L1 reveal more distinct C-terminal arms, different loop structures and L2 densities compared to pentavalent capsomers (**Fig. 1.2.2B**) [43]. For the structure and assembly of native capsids, a certain number of L2 proteins are incorporated into the capsomer via the L1-binding region of L2, which contains a conserved PxxP motif. Although up to 80 molecules of L2 are incorporated into the HPV16 capsid during baculovirus-based viral production [44], 24 to 36 molecules of L2 on average are distributed asymmetrically and randomly in one native capsid, where the L2 protein density starts from inside the base of the capsomer (**Fig. 1.2.2C**), and eventually present at the outside center of the capsomer [43, 45]. L2, with a molecular weight of 64-78 kDa, contains a DNA binding domain, a furin cleavage site, an RG-1 epitope (amino acid 17-36), a transmembrane domain (TMD), a chromatin binding region (CBR), a promyelocytic leukemia (PML) localization domain and an L1 binding domain to facilitate viral assembly, viral genome encapsidation and viral entry [46, 47]. The DNA binding capacity was proven for both L1 and L2 *in vitro* and *in vivo*, suggesting the binding of L2 to L1 is critical for vDNA packaging [48, 49]. L2 hydrophobically interacts with L1 even under high salt concentrations, weak detergents, urea (up to 2 M) and acidic pH conditions [50]. However, L1 alone as well as VLPs assembled with N-terminally

truncated or partially C-terminally deleted L2 protein exhibit less efficient packaging of plasmid DNA than capsids assembled from intact L1 and L2. Moreover, host cellular histones can be detected in native virions as well as mature HPV pseudoviruses (PsVs), suggesting a role in vDNA packaging [49, 51, 52]. Other double-stranded circular DNAs (pseudogenomes) as long as it is not larger than the natural PV genome size (~8 kb) can also be packaged into capsids, providing the basis for PsV- or quasivirions- (QVs) based-assays [53, 54]. Bovine papillomavirus 1 (BPV1) VLPs have been demonstrated to encapsidate plasmid DNA with a size of up to 10.2 kb, indicating the packaging capacity is PV type-specific [55].

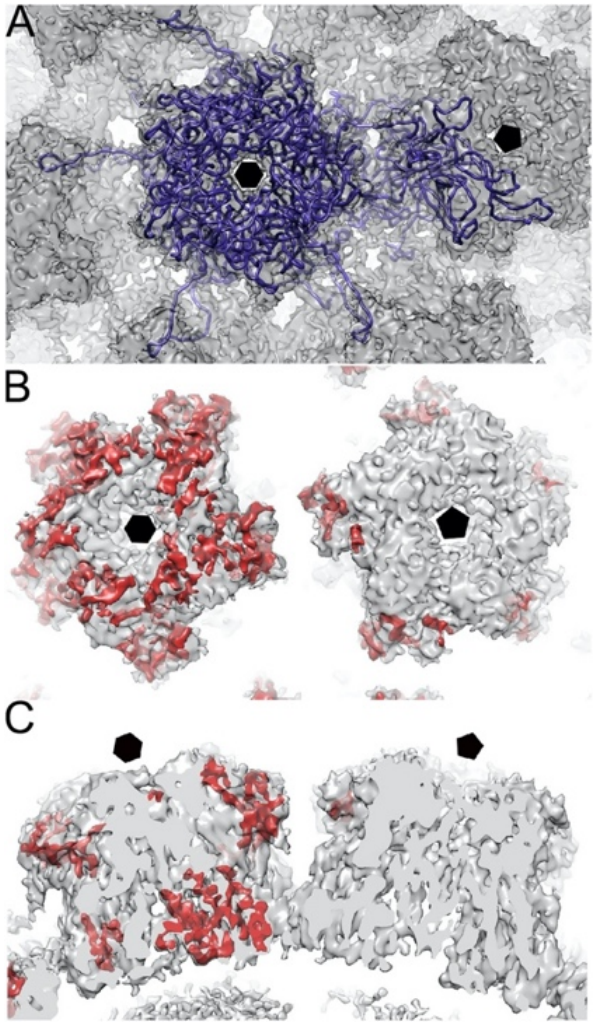

Fig. 1.2.2 Cryoelectron microscopy maps of HPV16 capsomer and putative L2 densities [43]. (**A**) Five L1 monomers (blue) form a capsomer and one extra L1 monomer is shown to indicate the interaction with neighboring capsomers. The pentavalent (right) and hexavalent (left) capsomers are presented as a black pentagon and hexagon respectively. (**B**) Different putative L2 densities (red) map on the surfaces of both pentavalent and hexavalent capsomers. (**C**) Cross-section view shows the difference of putative L2 densities inside the pentavalent and hexavalent capsomers. This figure is adapted from [43].

1.2.3 Entry and Life Cycle of Papillomaviruses

In the canonical model of PV entry, when micro abrasions occur at mucosal or cutaneous epithelium, the virions can bind to heparan sulfate proteoglycans (HSPGs) that are located on the host's basement membrane *in vivo*. *In vitro*, the binding to HSPGs or to laminin-332 (previously named laminin-5) occurs on the extracellular matrix (ECM). The virions then undergo a conformational change and are primed by Cyclophilin B (CYPB) and Kallikrein-8 (KLK8) to expose the N-terminus of the L2 proteins on the capsid surface [56]. In general, the L2 proteins are largely hidden within the base of the capsomer lumen depending on the estimation of L2 densities [57], and become exposed to be cleaved by the proprotein convertase furin at a highly conserved site (around amino acids 9-12 in HPV16 L2), leading to decreased binding of the capsid to HPSGs and higher affinity to non-HSPG cell receptors on the surface of basal cells [58, 59]. Subsequently, HPV virions enter host cells through endocytosis [60].

The HPV life cycle is tightly associated with the differentiation program of the infected epithelium (**Fig. 1.2.3**). Following nuclear entry and localization to ND10, vDNAs benefit from the integrity of ND10 which is commonly destroyed by viruses for infection and reorganize the components of ND10 (PML, Sp100, and Daxx) for the initiation of viral amplification and transcription [61]. Thereafter, the nuclear vDNA replication is synchronized with host DNA synthesis at a low copy number (50-100 copies/cell) with limited gene expression to avoid intrinsic cellular defenses, and vDNAs still maintain as an episomal status. In the maintenance stage, the early protein E2 interacts with Bromodomain-containing protein 4 (BRD4), which acts as a receptor for chromosomal binding, to tether episomal vDNAs to mitotic chromatins. However, HPV8 E2 exhibits a BRD4-independent tethering manner by locating to ribosomal DNA (rDNA) loci [62]. This tethering process efficiently partitions the episomal viral genomes to the daughter cells during cell division marking the late and persistent infection stage. In addition, the aforementioned proteins E2 and E1 are associated with early viral genome replication in the basal layer of the epithelium. At the same time, the oncoproteins E7 and E6 inactivate pRb and p53 respectively to drive potentially differentiation-initiated cells back into unscheduled S-phase re-entry and inhibit apoptosis. The vegetative amplification of viral genomes (up to thousands of copies/cell) is triggered by differentiation in the host cells [63]. To achieve a productive replication, HPVs hijack host DNA repair factors associated with the Ataxia telangiectasia mutated (ATM)- and Ataxia telangiectasia and Rad3 related (ATR)-dependent DNA damage response (DDR) [63]. Eventually, upon the terminal differentiation in the granular and cornified layers of the epithelium, the viral late promoter is activated, leading to increased expression of the capsid proteins L1 and L2. After virus assembly and viral genome encapsidation, the progeny virions are released upon the E4-induced collapse of keratin networks [64].

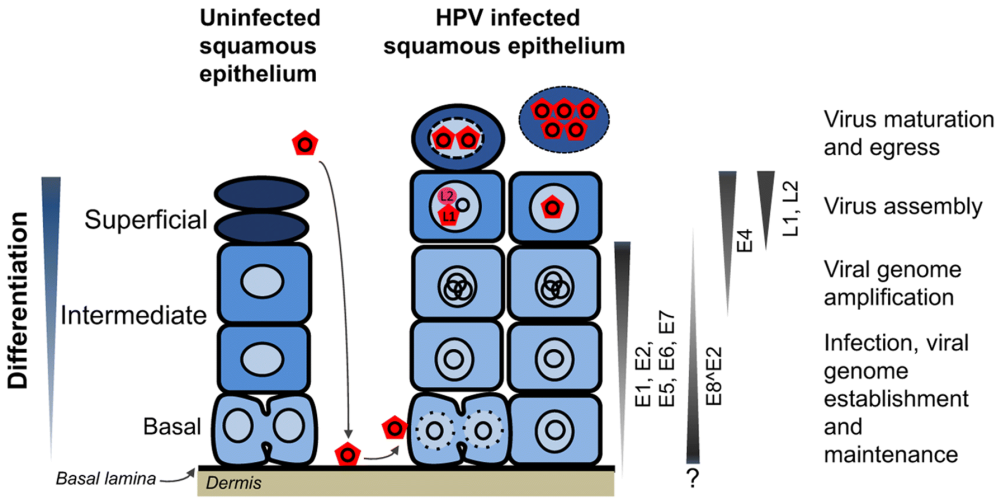

Fig. 1.2.3 Life cycle of alpha HPV [65]. The HPV life cycle is tightly associated with the differentiation program of the infected epithelium. The virions (red pentagon) gain access to the basal membrane through a micro-trauma. After entry, viral genomes (black circle) are initially replicated driven by E2 and E1 and maintained at a stable but low level in basal cells. Meanwhile, the early proteins E5, E6 and E7 promote cellular proliferation and evade apoptosis. Upon cell differentiation, the viral amplification enters the productive phase utilizing the host DNA repair machinery. Finally, the cells are committed to a terminal differentiation where the late viral proteins L1 and L2 are produced enabling capsid assembly and virus genome packaging. Afterwards the newly formed virions exit the cells with the aid of E4 in the superficial squamous epithelium. This figure is adapted from [65].

1.2.4 *In vitro* Model Systems for Papillomavirus Research

The abovementioned models of HPV entry and life cycle greatly profit from *in vitro* cell systems developed during the last few decades. Noteworthy are the immortalized cervical cancer cell lines such as HeLa (HPV18 positive, 20-50 integrated genomes/cell), SiHa (HPV16 positive, 1-2 integrated genomes/cell), CaSki (HPV16 positive, approximately 500 integrated genomes/cell) as well as W12 (HPV16 positive, at early passages contains about 100 episomes/cell), and CIN 612 (HPV31 positive, about 50 episomes/cell). These contributed tremendously to the investigation of chromosomal integration sites of HR HPVs, mechanisms of HPV transformation and carcinogenesis, and potential antineoplastic agents [66-68]. To clearly delineate the specific role of individual viral proteins in the life cycle, primary human keratinocytes were widely used, which are commonly isolated from foreskin or oral mucosa and immortalized either spontaneously or by ectopic telomerase expression [69, 70]. Thereafter, these keratinocytes are usually transduced with different viral genes and selected by antibiotics. These cell systems provide broad insights into individual and synergistic effects of viral gene products of different HPV types, especially when combined with genomic, transcriptomic and proteomic analyses [71]. This approach can overcome the natural limitations of studying LR and beta HPVs, since it has been reported that their viral genomes cannot be maintained in cultured keratinocytes and are gradually lost over time [72, 73]. In addition, human keratinocytes or other cell lines can also be infected with PsVs or QVs containing a reporter gene, to uncover pathogenic mechanisms arising from native promoters and maintenance of viral genomes during early infection [74]. Furthermore, these cell

systems are amenable to terminal differentiation by growth in culture medium containing high calcium concentrations or suspension culture using semi-solid methylcellulose medium, allowing the investigation of productive viral propagation in certain aspects [75]. Despite the multiple advantages, no monolayer-based *in vitro* systems can decipher how papillomaviruses truly complete their productive life cycle or promote tumorigenesis in tightly packed and continuous epithelial tissue.

Three-dimensional (3D) cell systems, so-called organotypic raft culture, are eminently suited to support the papillomavirus life cycle *in vitro* [76]. In these systems, transfected or infected keratinocytes continuously grow, stratify, differentiate and eventually form multilayered epithelium within 10-12 days [76]. These culture systems were successfully implemented for HPV16 and 18, but remain technically challenging for LR and beta HPV infection due to their unstable genome maintenance [77]. Nevertheless, a de-epidermalized dermis-based raft culture was generated by the overexpression of *E6* and/or *E7* from beta HPVs, which allowed identification of the proven invasive properties of HPV8 E7 to extend the understanding of HPV-directed skin cancer [78, 79].

1.3 Non-melanoma Skin Cancer

Non-melanoma skin cancer (NMSC) is one of the most common cancers affecting the fair-skinned population, with approximately one million new cases in 2018 according to the GLOBOCAN 2018 database [80]. NMSC includes basal cell carcinoma (BCC, approximately 80% of skin cancers) and squamous cell carcinoma (SCC, about 20% of skin cancers), and for both kinds, sunlight exposure and immunosuppression represent the main risk factors. Particularly, organ transplant recipients (OTRs) who are under immunosuppressive conditions, suffer from an increased risk and highly aggressive skin cancers [81]. A high prevalence of beta HPV DNA has been identified in NMSC patients with the rare hereditary disease *Epidermodysplasia verruciformis* (EV) [68]. Additionally, serology revealed that type-specific beta HPVs, especially HPV5, 8, 17, 20, 24 and 38, are linked to increased risks of cutaneous SCCs [82]. Despite the association between beta HPVs and NMSC, which is evident by the detection of HPV DNA and seroepidemiology, the underlying mechanism of pathogenesis is inadequately understood. Unlike HR HPVs, beta HPV viral load has been found remarkably higher in pre-malignant lesions AKs, rather than in SCC which may progress from AKs, particularly on sun-exposed sites, proposing a "hit-and-run" hypothesis that beta HPVs facilitate the initial and progressive stages of carcinogenesis, but are not required for tumor maintenance [83].

With the development of *in vitro* model systems, many investigations revealed new insights into beta HPV-induced malignancies, especially the role of E6 and/or E7. Although p53 inactivation is one of the core events in HR HPV-induced transformation, beta HPV E6 proteins have various impacts on host p53 as they: i) reduce p53 levels (HPV49 and 76); ii) induce *TP53* expression or stabilize p53 protein (HPV17, 38 and 92); or iii) have no effects (HPV5, 8 and 20) [84-86]. The binding affinity of E6 from

genus beta to p53 varies, no matter whether E6 affects p53 stability or not. For instance, both HPV49 and 76 can decrease p53 protein levels but HPV76 shows no binding ability to bind p53, suggesting alternative strategies of p53 inactivation [84, 86]. Some beta HPV E6 proteins (HPV5 and 8) are able to bind and degrade p300 by disrupting its association with AKT and consequently hamper the activation of p53 transcriptional activity [87]. Moreover, HPV8 and 38 E6 proteins activate hTERT for host cell immortalization, similar to HR HPV E6 proteins, in an E6AP- and NFX1-91 (a transcriptional repressor of hTERT)- dependent manner in primary human keratinocytes [88]. HPV49 E6 and E7 efficiently immortalize primary human foreskin keratinocytes (HFK), consistent with HPV16 E6 and E7 oncoproteins [86]. Interestingly, impaired NOTCH activity due to loss of function mutations could be frequently found in SCC, indicating that such mutations in *NOTCH* can counter its role as a tumor suppressor in epithelia [89, 90]. HPV8 and *Mus musculus* papillomavirus 1 (MmuPV1) E6 proteins bind to MAML1 in the NOTCH transcriptional activator complex (ICN/RBPJ/MAML), thus repressing target gene expression, ultimately inducing cell cycle arrest, delaying epithelial differentiation and sustaining proliferation [91]. Additionally, HPV8 and MmuPV1 E6 interact with SMAD2/3 to uncouple the SMAD2/3/4 transcription complexes and HPV5 E6 induces proteasome-mediated SMAD3 degradation to inactivate TGF-beta signaling, which causes the inhibition of differentiation [91]. Besides the interaction with pRb, HPV38 E7 can promote IKK-beta nuclear accumulation, which in turn stabilizes delta-p73, an antagonist of p53, by phosphorylation. Next, IKK-beta, delta-p73, DNMT1 and EZH2 form a repressive regulator that negatively regulates several pro-apoptotic p53 target genes [92]. HPV8 E7 also exhibits the ability to restrain differentiation by increasing the keratinocytes' "stemness" though upregulation of CD44 or EpCAM [93].

Given the fact that beta HPV-positive skin lesions are commonly found at sun-exposed sites, UV irradiation and beta HPV infection may act as co-activators for skin cancer development. Exposure to UVB radiation (280-315 nm) can cause DNA damage by forming cyclobutane pyrimidine dimers (CPDs) and 6-4 photoproducts (6-4 PP) [94]. If not properly repaired, DNA lesions can accumulate and induce mutations in tumor suppressor genes, such as *TP53* and oncogenes, which in turn lead to skin carcinogenesis. Beta HPVs actually favor UV-induced DNA lesions in infected cells. In response to UVB damage, beta HPV8 E6 protein has been shown to degrade p300, which subsequently loses the ability to activate ATM at the transcriptional level, resulting in the decrease of the ATM-regulated downstream gene *BRCA1* to disrupt DNA repair. In a similar way, p300 degradation-mediated ATR reduction leads to the attenuation of XPA (a repair factor that can bind to DNA damage sites) and POLη (a DNA polymerase that replicates across DNA lesions) [95-97]. HPV23 E6 co-localizes with HIPK2, a regulator involved in apoptosis, and inactivates p53 phosphorylation at Ser46, which is essential for the expression of pro-apoptotic genes after UV exposure [98]. In addition, beta HPV E6 degrades BAK, preventing the release of Cytochrome c (CYCS) from mitochondria and activation of the apoptotic caspase cascade [99].

Taking all this into account, beta HPVs target several pathways to favor persistence of thymine dimers and double strand breaks (DSBs) as well as to block apoptosis in UV-damaged cells.

1.4 HPV Vaccines

1.4.1 VLP-based Prophylactic HPV Vaccines

In the early 1990s, the production of VLPs with recombinant HPV major capsid protein L1 paved the way for the development of HPV vaccines. In 2006, the first HPV prophylactic vaccine with the trade name Gardasil was approved, followed by Cervarix in 2007, Gardasil-9 in 2014. Several other VLP-based vaccines are currently moving from pre-clinical studies forward into clinical trials (**Table 1.4.1**). Cervarix is a bivalent vaccine that protects against HPV16 and 18, which are attributable to most cervical and anal cancers. The recombinant quadrivalent vaccine, Gardasil, is directed against HPV16, 18, 6 and 11, preventing both cervical cancer and genital warts [100]. Moreover, the latest nonavalent vaccine, Gardasil-9, provides protection against HPV types responsible for 90% of cervical, vulvar, vaginal and anal cancers [101]. These approved vaccines were effective to reduce HPV-caused diseases in both women and men in the last decade. A recent meta-analysis covering more than 60 million people showed an 83% decline in HPV16 and 18 prevalence among girls aged 13 to 19 years and a 66% decline among women aged 20 to 24 years [102]. The recommendation for HPV vaccination by the World Health Organization (WHO) among females is from 9 to 14 years of age. However, women aged from 25 to 45 years vaccinated even with a single dose of Gardasil or Cervarix reached high HPV16 seropositivity, but less HPV18 seropositivity compared to that in younger females, indicating women older than 25 years still can partially benefit from HPV vaccination [103].

All three marketed bivalent, quadrivalent or nonavalent HPV vaccines raise high immunogenicity, long-term efficacy against HPV-associated diseases with acceptable safety profiles. However, their relatively high cost in turn affects the vaccination coverage rate (VCR) in low-income populations. HPV VLP-based vaccines provide type-specific protection. If cutaneous HPV-associated diseases were to be targeted, more L1 types would have to be included for the production of recombinant VLP vaccines. Therefore, developing a broadly prophylactic HPV vaccine with lower costs and higher thermal stability could contribute to further decrease of cancer cases and mortality attributable to HPV worldwide.

Table 1.4.1 VLP-based HPV vaccines that are licensed, in or advancing towards clinical trial. This table is adapted from [104]. 2vHPV vaccine, bivalent HPV vaccine; VLP, virus like particle; BEVS, balculovirus expression vector system; *E. coli*, *Escherichia coli*; MPL, monophosphoryl lipid A; AHSS, aluminum hydroxyphophate sulfate; cGMP, cyclic GMP.

Name	Antigen	System	Adjuvant	Status	Manufacturer
Cervarix (2vHPV vaccine)	L1 VLP of HPV16 and HPV18	BEVS	Aluminum hydroxide and MPL	Licensed	GSK
Gardasil (4vHPV vaccine)	L1 VLP of HPV6, HPV11, HPV16 and HPV18	Yeast	AHSS	Licensed	Merck
Gardasil (9vHPV vaccine)	L1 VLP of HPV6, HPV11, HPV16, HPV18, HPV31, HPV33, HPV45, HPV52 and HPV58	Yeast	AHSS	Licensed	Merck
Cecolin	L1 VLP of HPV16 and HPV18	*E. coli*	Aluminum hydroxide	Phase III clinical trial	Xiamen Innovax
Gecolin	L1 VLP of HPV6 and HPV11	*E. coli*	Aluminum hydroxide	Phase II clinical trial	Xiamen Innovax
L1 capsomers	L1 capsomers of HPV16	*E. coli*	Unknown	cGMP production	R. Garcea, University of Colorado-Boulder
L1-E7 VLP	HPV16L1-E7 VLP	BEVS	None	Phase I clinical trial	Medigene AG

1.4.2 L2-based Prophylactic HPV Vaccines

In the native condition, the major part of L2 is hidden under the capsid surface and only becomes partially exposed during viral entry. However, the N-terminus of L2 contains conserved and cross-neutralizing epitopes (especially aa 17-36, also known as RG1 epitope) and antibodies raised against these epitopes can provide efficient protection against papillomavirus-induced infection [105-108]. Thus, the minor capsid protein L2 came into the focus as a promising candidate for developing next generation vaccines. However, the titer of neutralizing antibodies raised against monomer L2 is relatively low when compared to those against type-specific VLP antigens [109]. Therefore, several strategies, such as various L2 peptide display platforms and the introduction of multiple L2 peptides from different HPVs, have been tested to enhance the immune response against the L2 protein.

VLPs, adeno-associated virus (AAV), and bacteriophages have been used as platforms to display L2 peptides. The HPV16 L2 RG1 peptide presented on the capsid's DE surface loop of HPV16 L1, for instance, did not affect the conformation and assembly of VLPs, but elicited cross-protection against different HPV types [110].

Table 1.4.2 L2-based HPV vaccines that are in or advancing towards clinical trial. This table is adapted from [104]. VLP, virus like particle; AAV, adeno-associated virus; TA, tissue antigen; CIN, cervical intraepithelial neoplasia; GW, genital warts; BEVS, balculovirus expression vector system; *E. coli*, *Escherichia coli*; MPL, monophosphoryl lipid A; AHSS, aluminium hydroxyphophate sulfate; cGMP, cyclic GMP.

Name	Antigen	System	Adjuvant	Status	Manufacturer
RG1-VLP	HPV16L1-L2(17-36)VLP	BEVS	Aluminum hydroxide	cGMP production	R.Kimbauer, NCI, Pathovax LLC
L2-AVV	L2 peptides of HPV16 and HPV31 displayed on AAV VLP	BEVS or 293T cells	unknown	cGMP production	2A Phama
L2 multimer	Fusion protein of L2~11-88 of HPV6, HPV16, HPV18, HPV31, and HPV39	*E. coli*	Alum	cGMP production	Sanofi, BracoVax
L2-thioredoxin	L2 peptides displayed on thioredoxin	*E. coli*	Unknown	cGMP production	M. Müller, DKFZ
AX03	L2 peptides displayed on bacteriophage	*E. coli*	Unknown	cGMP production	Agilvax, NIAID
TA-CIN	HPV16L2-E7E6 fusion protein	*E. coli*	None	Phase II clinical trial	Cantab Pharmaceuticals , Xenova
TA-GW	HPV6L2-E7 fusion protein	*E. coli*	Aluminum hydroxide or AS03	Phase II clinical trial	Cantab Pharmaceuticals , GSK

In addition, bacterial thioredoxin (Trx) is used as a scaffold to expose multiple L2 peptides. Bacterial thioredoxin is a small, non-toxic protein and capable of maintaining its structure even when multiple peptides are inserted into surface-exposed loops of thioredoxin [111]. Of tested Trx-L2 antigens containing 1-15 copies of different HPV16 L2 peptides, the variant with three or nine repeats of L2 aa 20-38 was the best in inducing neutralizing antibodies against HPV16, 31, 45 and 58 [111]. This indicates that immunogenicity and cross-reactivity of Trx-L2 can be influenced by the epitope region and tandem repeat number. Lately, *Pyrococcus furiosus* thioredoxin (PfTrx) replaced *Escherichia coli* thioredoxin (EcTrx) as a novel platform, since it is more resistant to thermal purification, protease degradation and is highly soluble. In addition, PfTrx elicits a similar immune response as EcTrx but unlike the latter does not show cross-reactions against thioredoxins of the vaccine recipient (human and murine), making PfTrx a safer vaccine scaffold [112]. PfTrx-L2 harboring tandems of three repeated copies of L2 aa 20-38 of HPV16, 31 and 51 induced broader protective immune responses when compared to PfTrx-L2 containing three copies of L2 aa 20-38 of HPV16 alone, suggesting that insertion of L2 from different HPV types can extend cross-reactivities [113]. Overall, as prominent candidates, several L2-based preventive or therapeutic HPV vaccines are currently moving from pre-clinical studies forward into clinical trials (**Table 1.4.2**).

1.5 Animal Models for Papillomavirus Research

With various *in vitro* tools, many host cellular events in response to papillomavirus infection have been explored. However, answers to questions regarding the progression of mucosal or cutaneous lesions, host immune responses against papillomaviruses, virus clearance, assessment of vaccine efficacy and so forth are ambiguous, where the *in vivo* animal models are required.

CRPV and BPV were the earliest virus-based model systems used to investigate papillomavirus-causing disease. However, considering the genetic diversity and housing condition, wild cottontail rabbits and bovines would not be the ideal model system. Lately, MmuPV1 was identified in athymic nude mice and found to infect both immunocompromised and immunocompetent (C57BL/6, hairless SKH-1 and FVB/NJ) laboratory strains of mice [114]. The formation of papillomas is regularly found on mucosal (oral cavity and anogenital tract) and cutaneous areas (muzzle and tail), which is significantly accelerated by exposure to a high dose of UVB [115, 116]. Intriguingly, the back sites of mice, even under immunosuppression, are more resistant to MmuPV1-caused papillomas compared to the muzzle or tail, probably due to less well-packaged virions at this area [117].

Considering host restriction and tissue tropism of papillomavirus infection, the natural animal models cannot elucidate some specific aspects of HPV-associated diseases. The generation of HPV transgenic mouse models can overcome these limitations to some extent. In this kind of model system, the expression of viral early genes, such as HPV16 *E6/E7*, HPV8 *E2/E6/E7*, HPV38 *E6/E7*, is under the control of the keratin 14 (K14) promoter, which is exogenous and keratinocyte-specific [118-120]. The formation of mucosal and cutaneous lesions and progressive changes were here rapidly driven by chronic estrogen administration or UVB. While these model systems focus on the function of one or two viral proteins, the viral late proteins are particularly missing, and ectopic gene expression is not regulated by the native viral promoter.

Mastomys coucha, another prominent existing experimental model, is a multimammate rodent from the family Muridae, commonly found in southern Africa and housed at the DKFZ since 1969 (**Fig. 1.5A**). *M. coucha* is naturally and persistently infected with *Mastomys natalensis* papillomavirus (MnPV, iota-type), and *Mastomys coucha* papillomavirus 2 (McPV2, pi-type) [121, 122]. Originally, *M. coucha* was misidentified as *Mastomys natalensis* due to similar appearance, but later distinguished by karyotyping (the chromosome number of *M. coucha* is 36 and that of *M. natalensis* is 32) and isoelectric focusing of serum proteins [123]. MnPV displays some features resembling cutaneous HPVs, such as episomal maintenance, the absent *E5* ORF in its genome and the induction of benign (corresponding to papillomas and KAs in human) and malignant (corresponding to SCCs) epithelial tumors in older animals (**Fig. 1.5B**) [121, 124]. McPV2, also lacking the *E5* ORF, infects mucosal sites and causes anogenital lesions (e.g. condylomas), thus, McPV2 is analogous to mucosal HPVs [122].

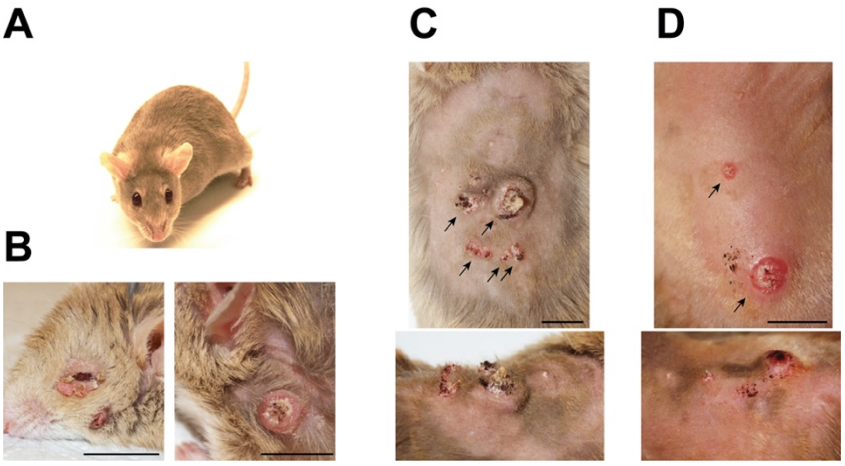

Fig. 1.5 *M. coucha* with spontaneous or UV-induced tumors [125]. (**A**) *Mastomys coucha* served as a model for investigating papillomavirus-associated diseases. (**B**) Spontaneously occurring skin lesions of naturally infected animals. (**C**) UV-induced keratinizing SCCs (KSCCs) occur on the shaved back of animals are indicated with black arrows. (**D**) Examples of UV-induced non-keratinizing SCCs (nKSCCs) occur on the shaved back of animals are indicated with black arrows. This figure is adapted from [125].

A virus-free *Mastomys* colony was generated by hysterectomy at the DKFZ. With these virus-free animals, the use of *Mastomys* as a promising model system for investigating the association of beta HPVs with NMSC is expanded to a broad range of research interests. It has been shown that the vaccination with VLP vaccine can elicit long-lasting and high levels of neutralizing antibodies and completely prevent the tumor formation in immunocompetent, immunosuppressed (corresponding to human OTRs) and experimentally infected virus-free animals [126]. Recently, the interplay of MnPV infection and UVB irradiation in NMSC development was described using the *Mastomys* model. Skin tumors appeared earlier and more frequently in chronically UVB-exposed virus-bearing animals in comparison to virus-free animals or unirradiated virus-infected animals [125]. Two types of UV-induced tumors were identified: i) keratinizing SCCs (KSCCs), which were well differentiated with a relatively high viral load (**Fig. 1.5C**); and ii) non-keratinizing SCCs (nKSCCs), which were a poorly differentiated with a low viral load even compared with unirradiated skin (**Fig. 1.5D**). KSCCs show a high degree of similarity in morphology and histology to human SCC precursor lesions, which commonly contain higher viral loads than SCCs. Moreover, transcriptional activation of MnPV early (*E6*, *E7*) and late (*L1*) genes can be detected in KSCCs rather than nKSCCs. The latter frequently harbored *Tp53* mutations, which is also observed in human SCCs, suggesting that the undifferentiated status of nKSCCs is due to a loss of function of p53. Intriguingly, a strong seroresponse against the MnPV major capsid protein L1 was detected in animals that only developed UV-induced nKSCCs, in which viral DNA was barely detectable. Therefore, for the first time, this model could support the proposed “hit-and-run” mechanism in the context of cutaneous PVs combined with UVB irradiation.

Furthermore, RNA sequencing analysis depicted the full transcription map of MnPV in productive skin tumors, revealing existing and potentially novel viral transcripts, the transcription start site (TSS) as well

as splicing junctions (SJs) for further understanding PV gene regulation [127]. The early mRNAs such as *E6* and *E7*, can be transcribed from the viral early promoter, which was identified within LCR region. The viral late promotor is located within the *E7* ORF, and largely regulates the expression of late *L1* and *L2* genes. The similar early and late promoters were also identified within the LCR and the *E7* ORF in other PVs, such as HPV5, 16 and 18 correspondingly, indicating the generally transcriptional regulations among various PVs [128-130]. Beside known viral genes, several novel *E2*, *E1^E4*, *E7* and *L2* isoforms are potentially expressed from alternatively spliced transcripts. In addition, 13 splicing junctions were validated and mapped to early and late transcripts, implying that alternative splicing is potentially involved in viral gene expression [131].

Moreover, *M. coucha*-derived keratinocyte (Kera5) and fibroblast (MaFi132) cell lines were established [132]. These two cell lines were spontaneously immortalized, allowing the exploration of the function of known and potentially novel viral proteins. Therefore, with the *in vivo* and *in vitro* models, further analysis can be conducted to complete the knowledge of molecular biology and pathogenesis of cutaneous papillomaviruses

1.6 Aims of the Thesis

Three licensed prophylactic vaccines can prevent the infection with certain mucosal HPV types. However, all of them are major capsid protein L1-based vaccines, which are type-restricted. Thus, there is still a need for broadly protective strategies to reduce or eliminate risks brought on by cutaneous HPV-associated NMSCs. The minor capsid protein L2 would be an ideal option, since the N-terminus of L2-derived polypeptides is highly conserved across numerous HPV types and can elicit pan-cross-neutralizing responses. In my thesis, an L2-based vaccine was developed and tested using *Mastomys coucha* as a unique pre-clinical model. *In vivo* the following issues were addressed:

i. Establishment of a vaccination protocol to determine the best formulation of the MnPV L2-based vaccine
ii. Examination of whether the MnPV L2-based vaccine will induce a strong and stable anti-L2 antibody response that can prevent tumor formation in naturally infected *Mastomys*, even under UV conditions
iii. Assessment of whether the MnPV VLP-based vaccine will protect irradiated virus-infected animals from the development of skin tumors
iv. Insight into the kinetics of antibody production and duration of protection

Since the mechanisms underlying the MnPV life cycle and pathogenesis still remain unclear, a novel *in vitro* infection model was developed to explore the MnPV/host cell interplay in response to extracellular stress (e.g. UV irradiation).

In this novel *in vitro* system the following issues were addressed:

i. Maintenance of viral genomes and viral transcriptional activity in the *in vitro* infection system
ii. Expression and localization of viral proteins
iii. Effects of differentiation induction and UVB exposure on infected cells

2. Material

2.1 Chemicals and Reagents

2-Propanol	Merck Calbiochem, Darmstadt
6 × DNA Loading Dye	Fermentas, St. Leon-Rot
Acetic acid	Merck Calbiochem, Darmstadt
Acrylamide-Bis (29:1), 30% w/v	Serva Feinbiochemica, Heidelberg
Actinomycin D	AppliChem, Darmstadt
AddaVax™	Invitrogen, Karlsruhe
Agarose	Sigma-Aldrich, Steinheim
Ammonium persulfate	Sigma-Aldrich, Steinheim
Ammonium sulfate	Carl Roth GmbH, Karlsruhe
Aqua ad iniectabilia	Braun, Melsungen
Bradford Reagent	Bio-Rad Laboratories, München
Briji 58, 10%	Sigma-Aldrich, Steinheim
Bromophenol blue	Serva Feinbiochemica, Heidelberg
BSA Molecular Biology Grade (20 mg/ml)	New England BioLabs, Frankfurt
Casein from bovine milk	Sigma-Aldrich, Steinheim
$CaCl_2$	Sigma-Aldrich, Steinheim
Chloroform	Merck Calbiochem, Darmstadt
Coomassie Brilliant Blue G-250	AppliChem, Darmstadt
CsCl	Roth, Karlsruhe
Dako Faramount Aqueous Mounting Medium	Dako Deutschland GmbH, Hamburg
DAPI	Sigma-Aldrich, Steinheim
Dithiothreitol (DTT)	Biomol, Hamburg
DMSO	Carl Roth GmbH, Karlsruhe
dNTPs Set PCR Grade	Invitrogen, Karlsruhe
EB buffer	Qiagen, Hilden
ECL SuperSignal West Femto	Thermo Fisher Scientific, USA
EDTA	Carl Roth GmbH, Karlsruhe
Enhanced Chemiluminescence Substrate (ECL)	PerkinElmer, USA
Ethanol, absolute	Merck Calbiochem, Darmstadt
Ethidium bromide, 1% solution	Sigma-Aldrich, Steinheim
Formaldehyde (4%) in PBS	Santa Cruz Biotechnology, Inc., Heidelberg
Gaussia-Juice BIG KIT	jpk GmbH, Kleinblittersdorf
Glucose	Carl Roth GmbH, Karlsruhe
Glycerol	AppliChem, Darmstadt

Glycine	Gerbu, Gaibach
Goat serum	Thermo Fisher Scientific, Darmstadt
H_2O_2	Merck Calbiochem, Darmstadt
H_3PO_4	Sigma-Aldrich, Steinheim
HEPES	Carl Roth GmbH, Karlsruhe
HCl	Carl Roth GmbH, Karlsruhe
IsoFlo 100% v/v inhalation gas, liquid	Toetis Österreich GmbH, Wien
KCl	Merck Calbiochem, Darmstadt
KH_2PO_4	Carl Roth GmbH, Karlsruhe
Lysozyme	Serva Feinbiochemica, Heidelberg
Methanol	Sigma-Aldrich, Steinheim
$MgCl_2$	Merck Calbiochem, Darmstadt
$MgSO_4$	Serva Feinbiochemica, Heidelberg
Milk powder, blotting grade	Carl Roth GmbH, Karlsruhe
Montanide ISA 720	Seppic, France
MTT	Sigma-Aldrich, Steinheim
Na_2CO_3	Carl Roth GmbH, Karlsruhe
Na_2HPO_4	Carl Roth GmbH, Karlsruhe
NaCl	Carl Roth GmbH, Karlsruhe
$NaHCO_3$	Sigma-Aldrich, Steinheim
NaOH	Carl Roth GmbH, Karlsruhe
OptiPrep™ Density Gradient Medium	Sigma-Aldrich, Steinheim
Phenol Red Solution	Sigma-Aldrich, Steinheim
Phenylmethylsulfonyl fluoride (PMSF)	Roche Diagnostics, Mannheim
Protease Inhibitor Cocktail Complete, EDTA-free	Roche, Mannheim
RiboLock RNase inhibitor	Thermo Scientific, St. Leon-Rot
RNase A/T1 Mix	Thermo Scientific, St. Leon-Rot
Roti-Phenol®	Carl Roth GmbH, Karlsruhe
Sigma Adjuvant System(SAS)	Sigma-Aldrich, Steinheim
Sodium dodecyl sulfate (SDS), ultra-pure	Carl Roth GmbH, Karlsruhe
Sodium deoxycholate	Merck Calbiochem, Darmstadt
Sucrose	Carl Roth GmbH, Karlsruhe
Tetramethylethylenediamine (TEMED)	Sigma-Aldrich, Steinheim
3,3',5,5'-Tetramethylbenzidine (TMB)	Sigma-Aldrich, Steinheim
Triton® X-100	Serva Feinbiochemica, Heidelberg
Triton® X-114	Sigma-Aldrich, Steinheim
Trizma® base (Tris)	Sigma-Aldrich, Steinheim
Tween® 20	Gerbu, Gaibach

β-Mercaptoethanol	Sigma-Aldrich, Steinheim

2.2 Reagents for Bacteria Cultivation

Ampicillin	Sigma-Aldrich, Steinheim
Bacto™ Agar	Becton Dickinson, Heidelberg
Bacto™ Trypton	Carl Roth GmbH, Karlsruhe
Bluogal	Invitrogen, Karlsruhe
Chloramphenicol	Sigma-Aldrich, Steinheim
Gentamycin	Sigma-Aldrich, Steinheim
Isopropyl-beta-D-thiogalactopyranoside (IPTG)	AppliChem, Darmstadt
Kanamycin	BIOTREND Chemikalien, Cologne
LB Medium	Carl Roth GmbH, Karlsruhe
Tetracycline	Sigma-Aldrich, Steinheim
X-gal	Sigma-Aldrich, Steinheim
Yeast extract	GERBU, Wieblingen

2.3 Reagents for Cell Culture

0.25% Trypsin/EDTA	Invitrogen, Karlsruhe
$CaCl_2$ solution (0.5 M)	PromoCell, Heidelberg
Dulbecco's Modified Eagle's Medium (DMEM)	Sigma-Aldrich, Steinheim
Dulbecco's Phosphate Buffered Saline (DPBS)	Invitrogen, Karlsruhe
Dulbecco's Phosphate Buffered Saline (DPBS) (+$CaCl_2$ +$MgCl_2$)	Thermo Fisher Scientific, Darmstadt
Dimethylsulfoxid (DMSO)	Carl Roth GmbH, Karlsruhe
EX-CELL™ 405 serum-free insect cell medium	Sigma-Aldrich, Steinheim
Fetal Bovine Serum (FBS)	Linaris GmbH, Wertheim
Grace's Insect Medium, supplemented	Sigma-Aldrich, Steinheim
Hank's Balanced Salt Solution (HBSS) (10 ×, -$CaCl_2$, -$MgCl_2$, -phenol red)	Thermo Fisher Scientific, Darmstadt
Hygromycin B	Sigma-Aldrich, Steinheim
L-glutamine (200 mM)	Thermo Fisher Scientific, Darmstadt
MEM Amino Acids 50 × (-L-glutamine)	Sigma-Aldrich, Steinheim
MEM Vitamin Solution 100 ×	Sigma-Aldrich, Steinheim
Methylcellulose, viscosity: 4,000 cP	Sigma-Aldrich, Steinheim
$NaHCO_3$, 7.5% (w/v)	Biochrom, Berlin
Non-essential amino acids (NEA) 100 ×	Biochrom, Berlin
Opti-MEM serum-free medium	Invitrogen, Karlsruhe
Penicillin/Streptomycin (10,000 U/ml)	Thermo Fisher Scientific, Darmstadt

Pluronic F-68	Sigma-Aldrich, Steinheim
TNM-FH Insect Medium	Sigma-Aldrich, Steinheim
Trypan blue	Biochrom, Berlin
Turbofect *in vitro* Transfection Reagent	Thermo Fisher Scientific, Darmstadt

2.4 Kits

Axygen™ AxyPrep™ Plasmid Miniprep Kit	Fisher Scientific GmbH, Schwerte
CloneJET PCR Cloning Kit	Thermo Fisher Scientific, Darmstadt
QIAGEN® Plasmid Maxi Kit	Qiagen, Hilden
QIAGEN® Plasmid Midi Kit	Qiagen, Hilden
QIAquick® Gel Extraction Kit	Qiagen, Hilden
RNeasy® Mini Kit	Qiagen, Hilden
TURBO DNA-free™ Kit	Thermo Fisher Scientific, Darmstadt

2.5 DNA and Protein Size Markers

GeneRuler™ 1 kb DNA Ladder	Thermo Fisher Scientific, Darmstadt
PageRuler™ Plus Prestained Protein Ladder	Thermo Fisher Scientific, Darmstadt

2.6 Universal Enzymes

Benzonase	Merck Calbiochem, Darmstadt
DreamTaq™ Green DNA Polymerase	Thermo Fisher Scientific, Darmstadt
DreamTaq™ Green PCR Master Mix (2 ×)	Thermo Fisher Scientific, Darmstadt
FastAP Thermosensitive Alkaline Phosphatase	Thermo Scientific, St. Leon-Rot
iTaq™ Universal SYBR® Green Supermix (2 ×)	Bio-Rad, München
Phusion® High-Fidelity DNA Polymerase	New England BioLabs, Frankfurt
Phusion® High-Fidelity PCR Master Mix (2 ×)	New England Biolabs
RevertAid Reverse Transcriptase	Thermo Fisher Scientific, Darmstadt
T4 DNA Ligase	New England BioLabs, Frankfurt

2.7 Restriction Enzymes

FastDigest BamHI	Thermo Fisher Scientific, Darmstadt
FastDigest EcoRI	Thermo Fisher Scientific, Darmstadt
FastDigest KpnI	Thermo Fisher Scientific, Darmstadt
FastDigest SacI	Thermo Fisher Scientific, Darmstadt
FastDigest XhoI	Thermo Fisher Scientific, Darmstadt

2.8 Consumables

Amersham™ Hybond™ P 0.45 PVDF	Th. Geyer, Renningen
Amicon® Ultra-15 10K Centrifugal Filter Devices	Sigma-Aldrich, Steinheim
Capillary tips (200 µl)	Biozym, Hessisch Oldendorf
Cell culture dishes (6, 10 cm)	TPP, Trasadingen, Switzerland
Cell culture flasks (25, 75 cm^2)	TPP, Trasadingen, Switzerland
Cell culture flasks 175 cm^2	Greiner, Frickenhausen
Cell culture plates (6, 12, 24, 96 well)	Greiner, Frickenhausen
Cell scraper	Corning Sigma, München
Centrifuge Tubes (14 × 89 mm)	Beckman Coulter.Inc, USA
Corning® Erlenmeyer culture flask with unvented cap, flat bottom, 500 ml	Corning Sigma, München
Cover slides Menzel-Gläser	Thermo Fisher Scientific, Darmstadt
Dialysis membrane Membra-Cel™, 34 mm, MWCO 14,000	Carl Roth GmbH, Karlsruhe
Fixogum Rubber Cement	Marabuwerke GmbH & Co KG, Tamm
Gloves (Microflex® XCEED)	MICRFLEX, USA
Incidin® Foam	Ecolab Deutschland, Monheim am Rhein
Locking clips Spectra/Por® Standard caps	Carl Roth GmbH, Karlsruhe
Luer-Lock Syringe (50 ml)	Terumo Detuschland, Eschborn
MF-Millipore Membrane Filter, 0.025 µm pore size, 47 mm diameter	Sigma-Aldrich, Steinheim
Minisart Syringe Filter	Sartorius, Göttingen
Multiplate™ PCR Plates 96-well, clear	Bio-Rad, München
Needles, sterile (20 G, 25 G, 27 G)	Braun, Melsungen
Nunc® Cryo Tubes	Sigma-Aldrich, Steinheim
Nunc™ F96 MicroWell™ White Polystyrene Plate	Thermo Fisher Scientific, Darmstadt
Objektträger Superfrost® Plus	Carl Roth GmbH, Karlsruhe
Optical Adhesive Covers MicroAmp	ABiosystems, Foster City, USA
PCR SingleCap 8er Soft Strips	Biozym, Hessisch Oldendorf
Phase Lock Gel Light	5PRIME GmbH, Hilden
Pipette Tips (10, 200, 1,000 µl)	Steinbrenner, Gießen
Pipette Tips RAININ LTS (20, 200, 1,000 µl)	Mettler-Toledo GmbH, Gießen
Polypropylene Tubes 12 ml	BD Falcon, Heidelberg
Polysorb Nunc-Immuno plates	Thermo Fisher Scientific, Darmstadt
Precellys Keramik-Kit, 1.4 mm ‘small’	VWR International, Darmstadt
Precision Wipes	Kimberly-Clark Professional, Reigate, UK

Protein LoBind Tube 1.5 ml	Eppendorf, Hamburg
Reaction Tubes (0.5, 1.5 and 2.0 ml)	Eppendorf, Hamurg
Reaction Tubes (15 and 50 ml)	Greiner, Frickenhausen
Scalpels, disposable	Feather Safety Razor, Osaka, Japan
Special autoclavable bags	Nerbe plus GmbH, Winsen/Luhe
Syringes, single use 1 ml	Th. Geyer GmbH, Renningen
TipOne sterile pipette filter tips	Starlab, Ahrensburg
Whatman 3 mm filter paper	GE Healthcare, Munich
X-ray films Super RX	Fuji, Japan

2.9 Laboratory Equipment

Analytical scale ABJ-120-4NM	Kern & Sohn GmbH, Balingen
Autoradiography Cassettes	Kodak, Stuttgart
Bacterial shaker G25	Infors, Bottmingen, CH
Cell Observer	Carl Zeiss, Oberkochen
Centrifuge Heraeus Fresco 17	Thermo Fisher Scientific, Darmstadt
Centrifuge Heraeus Pico 17	Thermo Fisher Scientific, Darmstadt
Centrifuge Megafuge 1.0R	Heraeus, Hanau
Centrifuge Rotina 380R	M&S Laborgeräte, Wiesloch
Centrifuge Sprout	Biozym, Hessisch Oldendorf
CoolCell® SV2	BioCision, San Rafael, USA
CFX96 Touch Real-Time PCR detection system	Bio-Rad, München
Confocal Olympus FluoView FV1000	Olympus, Hamburg
Developing machine CURIX 60	AGFA, Cologne
Duomax 2030 rocking platform	Heidolph Instruments, Schwabach
Easy-Cast™ Electrophoresis System	Thermo Fisher Scientific, Darmstadt
EVOS® XL Core Imaging System	Thermo Fisher Scientific, Darmstadt
French press (Emulsi Flex-C5)	Avestin, Ottawa, Canada
Freezer profi line	Liebherr, Ludwigshafen
Freezer VIP™ Series -86 °C	Sanyo, USA
Fridge Premium	Liebherr, Ludwigshafen
Gel documentation system GELSTICK	INTAS Science Imaging Instruments
Impulse Sealer	Tew Electric Heating Equipment, Taiwan
Incubator C200	LaBoTect, Göttingen
Kern EMB 1200-1 Tischwaage 1200 g	KERN & SOHN GmbH, Balingen
Liquid nitrogen tank CHRONOS Biosafe	Messer, Griesheim
Magnetic stirrer MR3000	Heidolph Instruments, Schwabach
Microscope Dialux 22	Ernst Leitz Wetzlar GmBH, Wetzlar

Microscope Olympus CK2	Olympus, Hamburg
Microwave	DéLonghi GmbH, Seligenstadt
Mini Trans-Blot® Cell	Bio-Rad, München
Mini-PROTEAN® 3 Cell	Bio-Rad, München
Moser ChroMini Pro Trimmer	Wahl GmbH, Unterkirnach
Moser Trimmer 1556	Wahl GmbH, Unterkirnach
Multichannel Pipette RAININ (50-200 µl)	Eppendorf, Hamburg
MyCycler thermal cycler	Bio-Rad, München
Neubauer hemocytometer	Bender&Hobein, Bruchsal
Overhead shaker REAX2	Heidolph Instruments, Schwabach
Peltier Thermal Cycler PTC-200	MJ Research, St. Bruno, Canada
pH-meter 761 Calimatic	Knick, Berlin
Pipette Boy	Integra Biosciences GmbH, Fernwald
Pipettes Research (2, 10, 20, 100, 200, 1,000 µl)	Eppendorf, Hamburg
Plate reader Synergy 2	BioTek® , Bad Friedrichshall
Plate Reader SPECTROstar Nano	BMG LABTECH Ortenberg
Power supply PowerPac™ HC/basic	Bio-Rad, München
Precellys 24 homogenizer	Peqlab, Erlangen
Roller Mixer SRT9D	Stuart, USA
Spectrophotometer NanoDrop® ND-1000	NanoDrop, USA
STERI-CULT 200 Incubator	Forma Scientifc, Marietta, USA
SterilGARD Hood	Baker Company, Sanford, USA
Thermal Cycler C1000™	Bio-Rad, München
Thermomixer compact/pico	Eppendorf, Hamburg
UV irradiation box & lid for animals	DKFZ fine mechanics workshop
UV irradiator Bio-Spectra	Vilber Lourmat Deutschland Eberhardzell
UV detector Variocontrol	Waldmann Medizintechnik, VillingenSchwenningen
UV table UV 181 BL	Waldmann Medizintechnik, Schwenningen
UV table N90	Benda Konrad, Wiesloch
Vortexer Reax top	Heidolph Instruments, Schwabach
Water bath	GFL-Gesellschaft für Labortechnik mbH, Burgwedel

2.10 Buffers and Solutions

Ammonium persulfate (APS)	10% (w/v) in water
Ampicillin	100 mg/ml
Blocking Buffer (Immunofluorescence)	1 × PBS 10% (v/v) Goat serum 0.3% (v/v) Tween 20
Cryo Medium	10% DMSO 30% FBS 60% Medium
Casein Blocking Buffer	0.2% (w/v) casein in PBST
Cesium Chloride Solution	58.8% CsCl (w/v) in VLP extraction buffer
Chloramphenicol	34 mg/ml
Coating Buffer (ELISA)	50 mM Carbonate buffer, pH 9.6 1 part 50 mM Na_2CO_3 4 parts 50 mM $NaHCO_3$
Colloidal Coomassie G-250 Staining Solution (1 L)	100 ml ddH_2O 100 ml H_3PO_4 100 g Ammonium sulfate 1.2 g Coomassie Blue G-250 Fill to 800 ml ddH_2O 200 ml Methanol (100%)
DPBS/0.8 M NaCl (50 ml)	42 ml DPBS (+$MgCl_2$ +$CaCl_2$) 8 ml 5 M NaCl
DTT	1 M
Kanamycin	50 mg/ml
LB Agar Plates	1.5% (w/v) Bacto Agar in LB medium supplemented with antibiotics
MTT	5 mg/ml
Lysis Buffer for DNA Extraction	50 mM NaCl 50 mM EDTA 0.5% SDS

Lysis Buffer for L2 Protein Extraction	300 mM NaCl 25 mM Tris 0.16% Tween 20 0.5 mM PMSF 0.1 mg/ml lysozyme pH 8.0
PBS (10 ×)	1.24 M NaCl 0.22 M Na_2HPO_4 0.1 M KH_2PO_4 Adjust the pH exactly to 7.2
PBST (1 ×)	1 × PBS, pH 7.2 0.1% (v/v) Tween 20
Permeabilization Buffer	1 × PBS 0.5% (v/v) TritonX-100
Pseudovirus Lysis Buffer	1 ml DPBS (+$MgCl_2$ +$CaCl_2$) 58.3 µl 10% Briji58 6.7 µl RNAse A/T cocktail
SDS Loading Dye (5 ×)	1% (w/v) SDS 0.03% (w/v) Bromophenol blue 12.5% (v/v) β-Mercaptoethanol 5 mM EDTA, pH 8.0 47.3% (v/v) Glycerol 0.3 M Tris, pH 6.8 2.5 mM NaF
SDS Running Buffer (10 ×)	1% SDS 0.25 M Tris 1.9 M Glycine

SOC Medium [133]	2% (w/v) Bacto-Trypton 0.5% (w/v) Yeast extract 10 mM NaCl 2.5 mM KCl 10 mM $MgCl_2$ 10 mM $MgSO_4$ 20 mM Glucose
Substrate Buffer (ELISA)	100 mM Sodium acetate pH 6.0 (with acetic acid)
Sucrose Solution	40% sucrose (w/v) in VLP extraction buffer
TAE Buffer (50 ×)	2 M Tris 0.25 M NaAc 0.05 M EDTA, pH 8.0 Adjust to pH 7.8 with acetic acid
TBS (10 ×)	Tris 0.5 M NaCl 1.5 M pH 7.5
TBST (1 ×)	1 × TBS, pH 7.5 0.1% (v/v) Tween 20
TMB Stock Solution	10 mg/ml TMB in DMSO
Transfection Buffer (for Sf9 cells)	25 mM HEPES 125 mM $CaCl_2$ 140 mM NaCl Adjust to pH 7.0, 7.1, 7.2
Trypan Blue Solution	0.25% Trypan blue in 1 × PBS
VLP Extraction Buffer	5 mM $MgCl_2$ 5 mM $CaCl_2$ 150 mM NaCl 0.01 % Triton X 100 20 mM HEPES, pH 7.4 2 mM PMSF (freshly added)

VLP Dialysis Buffer	0.3 M NaCl 50 mM HEPES pH 7.4
10 × Towbin Transfer Buffer [134]	0.25 M Tris 1.9 M Glycine
27% Iodiaxanol (4 ml)	1.8 ml Optiprep™ Density Gradient Medium 2.2 ml DPBS/0.8 M NaCl
33% Iodiaxanol (4 ml)	2.2 ml Optiprep™ Density Gradient Medium 1.8 ml DPBS/0.8 M NaCl
39% Iodiaxanol (4 ml)	2.6 ml Optiprep™ Density Gradient Medium 1.3 ml DPBS/0.8 M NaCl 80 µl Phenol red solution
4 × Minimal Essential Medium (524 ml)	40 ml HBSS 10 × 345 ml ddH_2O Autoclave 6 ml MEM Vitamin Solution 100 × 32 ml MEM Amino Acids 50 × 16 ml Non-essential amino acids (NEA) 100 × 4 ml L-glutamine (200 mM) 16 ml $NaHCO_3$, 7.5% (w/v) 5 ml Penicillin/Streptomycin 50 ml FBS pH 7.3
5 × Laemmli Buffer [135]	Tris-HCl (pH 6.8) 10% (w/v) SDS 25% (v/v) Glycerol 0.5% (w/v) Bromophenol blue Add 10% (v/v) β-Mercaptoethanol before use

2.11 Bacteria

DH10MultiBac^{Cre} Electrocompetent *E. coli*	Kindly provided by Prof. Dr. M. Müller, DKFZ
E. coli BL21	Kindly provided by Prof. Dr. M. Müller, DKFZ
E. coli Rosetta	Kindly provided by Prof. Dr. M. Müller, DKFZ
One Shot^{TM} TOP10 Chemically Competent *E. coli*	Invitrogen, Karlsruhe

2.12 Cell Lines

Table 2.12 Cell lines used in this study. All the cell lines used in this study are summarized below with their properties and respective references indicated.

Cell line	Properties	Reference
HEK293TT	Human embryonic kidney cells transformed with E1A/B of adenovirus 5, stably expressing two gene copies of SV40 large T-antigen.	[136]
HeLaT (HeLaT clone-4)	HPV18 human cervical carcinoma cell line stably expressing one copy of SV40 T-antigen under control of a CMV promotor	Kindly provided by Prof. Dr. M. Müller, DKFZ [137]
MaFi132	Spontaneously immortalized *Mastomys*-derived fibroblasts	[132]
MaFi191	*Mastomys*-derived fibroblasts harboring wildtype *Tp53*	Dr. D. Hasche, DKFZ
SF9	Insect cell line, clonal isolated from *Spodoptera frugiperda* Sf21 cells	Kindly provided by Prof. Dr. M. Müller, DKFZ
TN-High-Five	Insect cell line, ovarian cells of the cabbage looper *Trichoplusia ni*	Kindly provided by Prof. Dr. M. Müller, DKFZ
308 keratinocytes	Murine immortalized keratinocytes, contains activated *Hras* with mutation but wildtype *Tp53*	Kindly provided by Prof. Dr. P. Krieg, DKFZ [138]

2.13 Oligonucleotides

All oligonucleotides (primers) were synthesized by Sigma-Aldrich, Germany.

2.13.1 Primers Used for RT-PCR and qPCR

Table 2.13.1 Primers used for RT-PCR and qPCR in this study. The sequences of all the primers used for PCR experiments in this study are listed below. Size: Sizes of the amplicons.

Primer name	Sequence 5' to 3'	Application	Size
MnL1#1q-F	ACGGCAACTCATGCTTCTTC	qPCR	133 bp
MnL1#1q-R	CTCTGTGCCTGTCCATCCTT		
bGlobin-#1-qF	ACCATGGTGCACCTTACTGAC	qPCR	146 bp
bGlobin-#1-qR	TCCAGGCACCCAACTTCTAC		
MnPVL1-F	TCTACACCCGTCATTGTCCA	RT-PCR	380 bp
MnPVL1-R	GCCACGAGCTATCTCCACTC		
GAPDH-F	CTTCATTGACCTCAACTACATGGTC	RT-PCR	441 bp
GAPDH-R	GCAGTGATGGCATGGACTGTG		
F808//3144	TGAAGAAGCTCTACACCGCA	E1^E4 in RT-PCR	448 bp
R3559	GTCTCCTCCTTTCGGGTGC		
DH31	CGAGGTTTCTTACCCAGGAGG	E6 in RT-PCR qPCR	318 bp
DH32	TGCAAATTCTGCACCGTGC		
MnE7-cl-F2n	TATAGTTAACGCCATGATAGGACCTGACACC	RT-PCR	330 bp
MnE7-cl-R2	ATATGGATCCTCACTTGTCGTCATCGTCTTT GTAGTCAGATCTTCC		
Hprt F	GAAGGAGATGGGAGGCCATC	qPCR	185 bp
Hprt R	CTTTTATGTCCCCCGTTGACTG		
Rpl 32 F	AAGCGAAACTGGCGGAAAC	qPCR [139]	86 bp
Rpl 32 R	TAACCGATGTTGGGCATCAG		
MnPV E7 F1	GGTCAGCCTGTATTGTCACGAAG	qPCR	90 bp
MnPV E7 R1	AAGGTGTATTGTTCCGGTGGC		
Involucrin mc F	CAGCAGCAGCAACAGATAGAGC	qPCR	148 bp
Involucrin mc R	GATCCAGTGGCTGGTCTGAGAG		
Loricrin mc F	TGCAACGGAGACAACAGAGTT	qPCR	191 bp
Loricrin mc R	GGGAGGTAGTCATTCAGAAACCA		

2.13.2 Primers Used for Restriction Cloning

Table 2.13.2 Primers used for restriction cloning in this study. The Primers used for plasmid construction are listed below. All sequences and introduced restriction site are annotated in detail with texts of the same color.

Primer name	Sequence 5' to 3'	Restriction site
L1 wt F	AAAGAATTCGTCCCCATGTCATATATAGGGGCTATAATGGGA	EcoRI
L1 wt R	AAAGGATCCTTTTTTTCTCCGCTTGGTGGA	BamHI
L2 wt F	AAAGAATTCATTAGCATGTCTAGAAGGAGAAAGCGACATAC	EcoRI
L2 wt R	AAAGGTACCGGCAGCCAGTACGCCATCT	KpnI

2.14 Plasmids

Table 2.14 Plasmids used in this study. All the received and generated plasmids used in this study are summarized below with their features and references indicated.

Plasmid name	Features	Reference
847-MnL1short hum	Humanized MnPV $L1_{short}$ inserted into pGEM-IRES	Dr. Yingying. Fu, DKFZ
847-MnL2 hum	Humanized MnPV L2 inserted into pGEM-IRES	Dr. Yingying. Fu, DKFZ
pPK-CMV-E1E4	MnPV E1E4 wildtype, HA-tag at C-terminus	Dr. D. Hasche, DKFZ
pPK-CMV-E7	MnPV E7 wildtype, Flag-tag at C-terminus	M. Schäfer, DKFZ
pPK-CMV-$L1_{short}$	Humanized MnPV $L1_{short}$, HA-tag at C-terminus	Dr. Yingying. Fu, DKFZ [140]
pPK-CMV-$L1_{long}$	Humanized MnPV $L1_{long}$, 2 nd and 3 rd ATG mutation to GCG, HA-tag at C-terminus	Dr. Yingying. Fu, DKFZ [140]
pPK-CMV-$L1_{middle}$	Humanized MnPV $L1_{middle}$, 3 rd ATG mutation to GCG, HA-tag at C-terminus	Dr. Yingying. Fu, DKFZ [140]
pPK-CMV-L1 wt	MnPV L1 wildtype, HA-tag at C-terminus	Constructed in this study
pPK-CMV-L2 wt	MnPV L2 wildtype, HA-tag at C-terminus	Constructed in this study
pUC-MnPV	MnPV inserted in XbaI site	Dr. S. Vinzón, DKFZ

Plasmid name	Features	Reference
pET26 PfTrx-MnPV-L2(20-38)$_3$	3 copies of MnPV-L2 20-38 amino acids inserted in CpoI site	Dr. G. Spagnoli, University of Parma
pET26-PADRE$_{2\times}$ PfTrx-MnPV-L2(20-38)$_3$	3 copies of MnPV-L2 20-38 amino acids inserted in CpoI site, flanked with 2 copies of PADRE	Dr. G. Spagnoli, University of Parma

2.15 Antibodies

Table 2.15 Antibodies used in this study. All the antibodies used in this study are summarized below with their sources and usage indicated. WB, western blot; IF, immunofluorescence.

Antibody	Source	Application
Anti-actin, mouse polyclonal	Selfmade, provided by Dr. T. Hofmann, DKFZ	WB: 1:50,000
Anti-E4, mouse monoclonal	Selfmade, provided by Dr. D. Hasche, DKFZ	WB: 1:250 IF: 1:25
Anti-E7, mouse monoclonal	Selfmade, provided by Dr. D. Hasche, DKFZ	IF: 1:2
Anti-HA (3F10), rat monoclonal	Roche; Cat.#: 11867423001	WB: 1:1,000 IF: 1:1,000
Anti-Histone H3 (di methyl K4), rabbit monoclonal	Abcam; Cat.#: ab176878	WB: 1:5,000
Anti-Involucrin, rabbit polyclonal	Covance; Cat.#: PRB-140C	IF: 1:200
Anti-Involucrin, mouse polyclonal	USBiological; Cat.#: I8447-25	WB: 1:200
Anti-Loricrin, rabbit polyclonal	Covance; Cat.#: PRB-145P	WB: 1:1,000
Anti-p21, mouse monoclonal	BD Biosciences; Cat.#: 556431	WB: 1:2,000
Anti-p53, rabbit polyclonal	Santa Cruz; Cat.#: sc-9282s	WB: 1:1,000
Anti-Thioredoxin, mouse monoclonal	Selfmade, provided by Prof. Dr. M. Müller, DKFZ	WB: 1:5

Antibody	Source	Application
Anti-Vinculin (7F9), mouse monoclonal	Santa Cruz; Cat.#: sc-73614	WB: 1:4,000
Mouse monoclonal anti-SV40tag KT3	Selfmade, provided by Dr. Tim Waterboer, DKFZ	ELISA: 1:300
Mouse monoclonal anti-MnPV VLP (2D11, 3H8)	Selfmade, provided by Laura Katharina Schmitt, DKFZ	WB: 1:5 IF: 1:5
Serum Mix	Sera of five MnPV infected tumor bearing animals	ELISA: 1:1,000 WB: 1:1,000 IF: 1:1,000
AlexaFluor488 Goat-anti mouse IgG (H+L)	Invitrogen; Cat.#: A11029	IF: 1:1,000
AlexaFluor488 Goat-anti mouse IgG2a	Invitrogen; Cat.#: A21131	IF: 1:1,000
AlexaFluor594 Goat-anti mouse IgG2b	Invitrogen; Cat.#: A21145	IF: 1:1,000
AlexaFluor488 Goat-anti rabbit IgG (H+L)	Invitrogen; Cat.#: A11008	IF: 1:1,000
AlexaFluor488 Donkey-anti rat IgG	Invitrogen; Cat.#: A11006	IF: 1:1,000
Anti-Mouse IgG HRP Conjugate	Promega; Cat #: W402B	ELISA: 1:10,000 WB: 1:10,000
Anti-Rabbit IgG HRP Conjugate	Promega; Cat.#: W401B	ELISA: 1:10,000 WB: 1:10,000
Goat anti-Rat IgG (H+L) HRP	JacksonImmunoResearch; Cat.#: 112-035-143	WB: 1:10,000

3. Methods

3.1 MnPV L2 Protein Production

3.1.1 Transformation of Bacteria by Electroporation

The electroporation cuvettes were chilled on ice; meanwhile, bacteria were thawed on ice. 5-10 ng of plasmid DNA were gently mixed with 40 µl of *E. coli* BL21, Rosetta or DH10MultiBac^{Cre} Electrocompetent *E. coli* and transferred to the chilled electroporation cuvette. The mixture was pulsed once with 2.5 kV and then suspended in 250 µl SOC medium (room temperature). The transformed bacteria were shaken for 1 h at 250 rpm, 37 °C (for the MultiBac *E. coli*, the incubation time was extended to at least 6 h). Afterwards, 5-10 µl of bacterial culture were spread onto LB-agar plates containing the respective antibiotics and the plates were incubated overnight at 37 °C. Glycerol stocks were made for long-term storage at -80 °C the next day.

3.1.2 Expression and Induction of MnPV L2 Protein

A small amount of frozen pET26 PfTrx-MnPV-L2(20-38)$_3$ or pET26-PADRE$_{2\times}$ PfTrx-MnPV-L2(20-38)$_3$ bacteria glycerol stock were inoculated into 20 ml LB medium supplemented with 50 µg/ml chloramphenicol and 34 µg/ml kanamycin. The seed cultures were incubated overnight at 37 °C with shaking at 180 rpm and diluted 1:100 in 400 ml LB medium the next day. The growth of bacterial culture was measured at a wavelength of 600 nm (OD_{600}) until it reached 0.5-0.6. Subsequently, after taking a 1 ml sample of the bacterial culture, the expression of pET26 PfTrx-MnPV-L2(20-38)$_3$ or pET26-PADRE$_{2\times}$ PfTrx-MnPV-L2(20-38)$_3$ was induced by the addition of 1 mM Isopropyl β-D-1-thiogalactopyranoside (IPTG) overnight (16-18 h) at 16 °C with shaking at 150 rpm. Meanwhile, the French Press (Emulsi Flex-C5) was pre-cooled to 4 °C overnight.

3.1.3 Extraction of MnPV L2 Protein

After IPTG induction, the bacteria were pelleted by centrifugation for 10 min at 5,000 rpm and resuspended in 40 ml lysis buffer. The mixture was incubated at room temperature for 10 min, afterwards, chilled on ice for 20 min. Subsequently, the resuspended bacteria were transferred into the sample cylinder and lysed via French Press for 3-5 cycles with at least 15,000 psi. Regulator pressure was adjusted to approx. 40 psi, and the main pressure gauge would show 1,000-1,500 bar when stable lysing progress was achieved. The sample cylinder of the French Press was washed with 0.5 M NaOH, 10 mM HCl, autoclaved distilled water, and lysis buffer between different samples. The lysate was centrifuged for 1 h at 17,000 rpm at 4 °C. The supernatant was transferred to a new 50 ml Falcon tube and stored on ice until purification. 100 µl of supernatant and pellet were separately taken after the French Press process.

3.1.4 Thermal Purification of MnPV L2 Protein

The supernatant was supplemented with 5 M NaCl to a final concentration of 0.25 M. The solution was incubated at 70 °C, and the incubation time was dependent on the volume of solution (e.g. a 50 ml solution was incubated for 40 min, a 35 ml solution was incubated for 30 min). Subsequently, the solution was cooled on ice for 10 min and centrifuged at 17,000 rpm for 30 min. 100 µl of supernatant were taken after cooling down. After centrifugation, the supernatant was transferred into the dialysis membrane sealed by locking clips and dialyzed against 1 × PBS (with 300 mM NaCl) overnight at 4 °C.

3.1.5 Endotoxin Removal

15 ml of the dialyzed solution (12 ml if using a fixed-angle rotor) were transferred to Amicon Ultra centrifugal filters (unit 10K), then centrifuged at 4,000 × g maximum when using a swinging-bucket rotor (5,000 × g maximum for fixed-angle rotor) for approximately 15-40 min. Over-concentration can lead to precipitation and potential sample loss.

The concentrated MnPV L2 protein was aliquoted into fresh 1.5 ml Eppendorf tubes and mixed with 1% Triton X-114 and incubated on ice for 5 min followed by 5 min at 37 °C. In order to remove the Triton X-114, the samples were centrifuged at 12,000 g for 1 min at 37 °C. After 2 times of endotoxin removal, 500 µl of the supernatant was transferred into a Protein LoBind tube after passing through a 0.22 µm filter. Finally, samples were frozen at -80 °C for long-term storage (**Fig. 3.1.5**). Additionally, samples were taken before and after detoxification and after filtration (as final sample).

The quality and quantity of MnPV L2 proteins were monitored by Western blot and staining by Coomassie Blue. The methods are described in section 3.10.3 and 3.10.4, respectively.

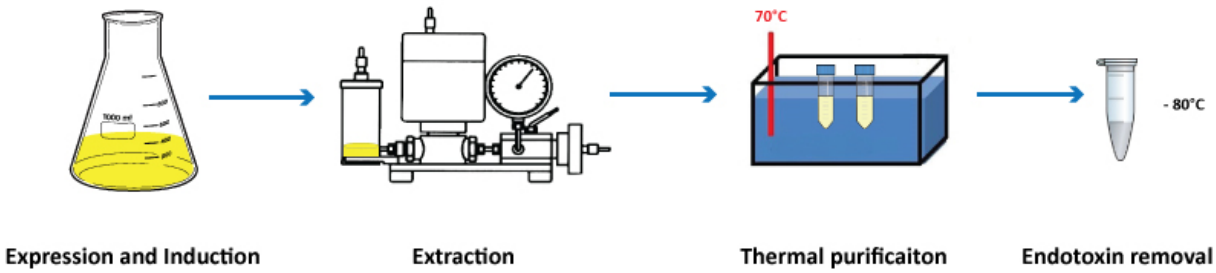

Fig. 3.1.5 Schematic overview of MnPV L2 protein production. Briefly, the production of MnPV L2 protein was induced by the addition of IPTG, and the bacterial cells were lysed via a French Press. Next, the extracted proteins were purified by heat incubation at 70 °C. After dialysis and endotoxin removal, the MnPV L2 protein was aliquoted and frozen at -80 °C for long-term storage.

3.2 VLP Production

3.2.1 Generation of Recombinant Baculoviruses

The generation of recombinant baculoviruses was performed as previously described with some modifications [126]. Briefly, Sf9 insect cells reaching 75% confluency in a T25 flask were transfected with recombinant MultiBac bacmids via the calcium phosphate precipitation method. After washing, cells were changed in 1 ml Grace's Insect Medium supplemented with 1% L-glutamine. 1 µg of MultiBac bacmid DNA was diluted in 1 ml transfection buffer and added dropwise to Sf9 cells. After incubation at 27 °C for 5 h, the cells were then washed twice and maintained in 10 ml TNM-FH supplemented medium for 6 days. The supernatant was used for the generation of a high-titer baculovirus stock. Sf9 cells with a density of 2×10^6 cells/ml were seeded in a T25 flask and infected with 1 ml supernatant for virus amplification for the next 6 days. This step was repeated by passaging increasing viruses in the supernatant for at least two weeks (3 ml supernatant for 1×10^7 Sf9 cells in a T75 flask and 5 ml supernatant for 2.5×10^7 Sf9 cells in a T175 flask). Each virus amplification for 6 days was referred as to one passage.

3.2.2 Expression Test of Recombinant Baculovirus

Sf9 cells in a T25 flask were infected with 1 ml supernatant from passage 2 and incubated at 27 °C for 3 days. Proteins were extracted and the expression of MnPV $L1_{short}$ was analyzed by Coomassie Blue staining and Western blot.

3.2.3 VLP Production and Purification

TN-High Five cells were grown to a density of 2.5×10^6 cells/ml in 250 ml suspension culture, subsequently centrifuged (2,000 rpm for 10 min in Sorvall GS-3 rotor) and resuspended in 42 ml EX-CELL™ 405 serum-free medium and 8 ml high-titer virus stock. The cells were shaken at low speeds at room temperature for 1 h and then incubated in 250 ml final volume of medium for 3 days at 27 °C. Cell pellets were harvested by centrifugation (3,000 rpm for 10 min at 4 °C in Sorvall GS-3 rotor) and washed twice in pre-chilled PBS (the washed cell pellets could be stored at -80 °C if necessary). Cell pellets were resuspended in 10 ml VLP extraction buffer containing 2 mM PMSF, followed by two rounds of sonication via a probe sonicator (2×1 min sonication, in between 5 min pause on ice, Output: 3). Clear cell lysate was collected by centrifugation at 10,000 rpm for 10 min at 4 °C in Sorvall F-28/50 rotor and carefully loaded onto the top of the CsCl layer. Meanwhile, a two-step gradient containing 7 ml of 40% sucrose on top of 7 ml CsCl solution (4.7 g CsCl in 8 ml VLP extraction buffer) was prepared. After centrifugation at 27,000 rpm for 2 h at 10 °C in SW-31Ti rotor, the interphase between sucrose and CsCl together with the complete CsCl layer was transferred into a Quickseal tube and balanced with VLP extraction buffer. After centrifugation at 48,000 rpm for 16 h at 20 °C in a Beckman 70Ti rotor, the fractions were collected in 1 ml aliquots and analyzed by Coomassie Blue staining and Western blot.

Small aliquots from the fraction with the highest and lowest protein yield were dialyzed against H_2O on a membrane filter and sent for electron microscopy.

3.2.4 Electron Microscopy

Micrographs were acquired with a Zeiss EM912 or EM910 electron microscope by Dr. Karsten Richter and Dr. Michelle Neßling (DKFZ, Heidelberg).

3.3 Animal Experiments

3.3.1 Animal Housing

Mastomys coucha from the naturally MnPV-infected breeding colony were maintained in the Zentrum für Präklinische Forschung (ZPF) S2 area at the DKFZ. They were housed in individually ventilated cages (IVC) at 22-24 °C with 55% relative humidity, mouse breeding diet and water *ad libitum*. Animals were closely monitored throughout their lifetime until they had to be sacrificed due to tumor development, bad health conditions or reaching the final timepoint in this study. *Mastomys coucha* from the MnPV-free colony were maintained in an isolator and were transferred to the ZPF Barriere D for experiments. *Mastomys coucha* at the DKFZ are housed and handled in compliance with German and European statutes. All animal experiments were undertaken with the approval of the responsible Animal Ethics Committee (Regional Council of Karlsruhe, Germany; G26/12 and G289/15).

3.3.2 Formulation of MnPV L2 Antigen-AddaVax™ Mixture

The AddaVax™ adjuvant was brought to room temperature and the capped bottle of AddaVax™ was shaken before opening. Meanwhile, the antigen, PfTrx-MnPV-L2(20-38)$_3$ or PfTrx-MnPV-L2(20-38)$_3$/PADRE$_{2\times}$, was diluted into the needed volume with sterile DPBS (filtered through a 0.22 µm sterile filter). Equal volumes of antigen and AddaVax™ (1:1, v/v) were mixed by pipetting with filtered tips. The antigen-AddaVax™ emulsion was taken in and out with a 27 G syringe needle until all air bubbles were eliminated prior to vaccination. 150 µl of antigen-AddaVax™ emulsion were injected subcutaneously into each animal.

3.3.3 Formulation of MnPV L2 Antigen-Montanide ISA 720 Mixture

The antigen was diluted into the needed volume with sterile DPBS and Montanide ISA 720 was taken out with a syringe through the rubber seal. Equal volumes of antigen and Montanide ISA 720 (1:1, v/v) were mixed thoroughly by passing through the syringe at least 25 times. The homogenization was repeated with a 25 G syringe needle at least 5 times prior to vaccination. 150 µl of antigen-Montanide ISA 720 emulsion were injected subcutaneously into each animal.

3.3.4 Formulation of MnPV VLP-Sigma Adjuvant System Mixture

The purified VLPs were dialyzed against VLP dialysis buffer using a Millipore membrane filter (0.025 μm pore size, 47 mm diameter) for 1 h at room temperature before vaccination. Prior to antigen addition, the contents of the Sigma Adjuvant System (SAS) were warmed to 40-45 °C. 1 ml of sterile DPBS (if the entire contents of the vial will not be used initially) was injected into the vial through the rubber stopper using a syringe fitted with a 20 or 21 G needle. The vial was vortexed vigorously for 2 to 3 min to mix well. This emulsion could be stored at 2-8 °C for up to 60 days (without freezing). To use the emulsion, it was warmed to 37 °C and vortexed briefly. Equal volumes of diluted antigen and SAS (1:1, v/v) were mixed well by vortexing for 1 min. 150 μl of VLP-SAS mixture were injected subcutaneously into each animal.

3.3.5 MnPV L2 Pilot Study

Eight-week old virus-free *Mastomys coucha* (five animals per group) were immunized with 80 μg of PfTrx-MnPV-L2(20-38)$_3$ or PfTrx-MnPV-L2(20-38)$_3$/PADRE$_{2\times}$ adjuvanted with either Montanide ISA 720 or AddaVax™ subcutaneously 5 times at biweekly intervals. Blood samples were collected before vaccination (pre-immune) and every two weeks after the immunization by puncture of the submandibular vein.

3.3.6 MnPV L2 Main Study

Eight-week old virus-bearing *Mastomys* were subcutaneously vaccinated with 80 μg of PfTrx-MnPV-L2(20-38)$_3$/PADRE$_{2\times}$ adjuvanted with AddaVax™ 5 times at biweekly intervals. Meanwhile, a subgroup of naturally infected animals was immunized with 10 μg VLPs (3 doses) in the presence of the SAS, which was used only in the first vaccination. At 18 weeks of age, some of the vaccinated or unvaccinated siblings from each cage were shaved on the back and irradiated with a dose of 150 mJ/cm^2 of UVB. The dose was increased by 50 mJ/cm^2 per week until the final dose (450 mJ/cm^2) was reached. Sera were collected every two weeks after the immunization (before 18 weeks of age) or every four weeks (after 18 weeks of age).

Blood was taken from the submandibular vein with a 25 G needle when the animals were under an isoflurane-anesthetized status. The blood droplets were collected in 1.5 ml Eppendorf tubes and incubated at room temperature for 1 h until they were completely clotted. The serum was carefully collected after centrifugation at 8,000 rpm for 20 min.

3.4 Enzyme-linked Immunosorbent Assay (ELISA)

3.4.1 Production of Glutathione-S-Transferase (GST)-tag Antigen

pGEX-4T-3 plasmids encoding MnPV L2 and McPV L2 were introduced into *E. coli* Rosetta bacteria by electroporation and cultivated in LB medium supplemented with 100 µl/ml ampicillin and 20 µg/ml chloramphenicol at 37 °C overnight (pre-culture). The vector containing the early gene E2 and empty vector (GST-SV40-tag) were introduced into *E. coli* BL21 and grown in LB medium containing 100 µl/ml ampicillin (pre-culture). 50 ml of pre-culture were transferred into 1 L LB medium containing the respective antibiotics and grown at 37 °C until the OD_{600} reached approximately 0.4. The culture was further grown at 25 °C until the OD_{600} value reached 0.5-0.6. Subsequently, the culture was induced with 250 mM IPTG. After the respective cultivation period at 25 °C (6 h for GST-SV40-tag; 18-20 h for McPV L2, MnPV L2 and E2), the cell pellets were collected by centrifugation for 20 min at 5,000 rpm at 4 °C in a Sorvall GS-3 rotor. The pellets were resuspended in 10 ml 1 × PBS containing 0.5 ml of protease inhibitor cocktail complete and 2 mM DTT. The lysates were sonicated with a probe sonicator 4 times for 15 s with 30 s interval on ice and then centrifuged at 14,000 rpm for 1 h in a Sorvall F-28/50 rotor. Finally, the supernatant was mixed with 1 volume of 100% glycerol and store at -20 °C.

GST-SV40-tagged viral antigens or GST-SV40-tag were quantified by titration in order to determine the total protein amount that completely saturated the GST-glutathione interaction. Titrations were performed in glutathione-casein coated plates. The antigens were diluted in a 1:3 serial dilution and detected using the monoclonal mouse antibody KT3 directed against the SV40-tag. The remaining steps followed the GST-capture ELISA standard protocol (see section 3.4.2). Proper dilution of the antigens used for GST-ELISA was determined by comparing the OD_{450} raw value with the one from the previously produced antigen.

3.4.2 GST-ELISA

The GST-capture ELISA was modified by Schäfer et al for detecting the seroreactivity of *Mastomys* sera [141, 142]. Briefly, glutathione is chemically crosslinked to casein and used to indirectly bind the fusion protein via its N-terminal GST-tag. The SV40-tag is fused to the C-terminus allowing the detection of the bound full-length fusion protein via KT3 (**Fig. 3.4.2**) [143]. The 96-well Polysorb Nunc-Immuno plates were coated with 200 ng/well of glutathione-casein, diluted in 100 µl 50 mM carbonate buffer, pH 9.6, overnight at 4 °C. Afterwards, the plates were blocked with casein blocking buffer (CBB, 180 µl/well) for 1 h at 37 °C. In the meantime, each *Mastomys* serum was incubated with a dilution of 1:50 in GST-blocking buffer (GST-SV40-tag was diluted in CBB based on the antigen titration described in section 3.4.1) for 1 h at room temperature with rocking agitation. This incubation step is essential to block unspecific reactivities of sera with bacterial proteins or GST/SV40 tags. After blocking, the ELISA plates were incubated with respective GST-SV40-tag fused viral protein and GST-SV40-tag lysates (100 µl/well)

for 1 h at room temperature. The ELISA plates were then washed with 1 × PBST for 4 times and incubated with diluted and preincubated sera for 1 h at room temperature. The washed ELISA plates were filled with 100 µl/well of HRP-conjugated goat anti-mouse IgG antibody diluted 1:10,000 in CBB for 1 h at room temperature. After washing, the bound antibodies were detected and quantified colorimetrically by incubation with 100 µl/well of substrate buffer (0.1 mg/ml tetramethylbenzidine and 0.006% H_2O_2 in 100 mM sodium acetate, pH 6.0) for 8 min. The enzyme reaction was stopped by adding 50 µl/well of 1 M sulfuric acid and the absorption was measured at a wavelength of 450 nm with the SPECTROstar Nano plate reader. The reactivity of serum against each antigen was calculated by subtracting the background GST-SV40-tag value from the respective viral antigen. Repetitive wells in each GST-tag fusion protein detection were incubated with serum mix, as a positive control, or KT3 antibody, checking antigen saturation during the sera incubation. All serological ELISAs were performed at least twice.

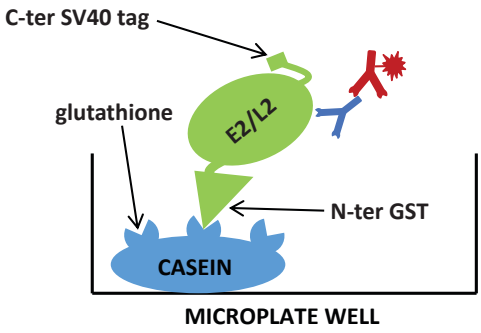

Fig. 3.4.2 Schematic view of the GST-capture ELISA. The viral protein (E2/L2) was fused to N-terminal GST and a SV40-tag was fused to the C-terminus of each viral protein. Glutathione-casein was used to capture the recombinant protein via an N-terminal GST-tag. Antibodies against respective viral proteins were detected by anti-mouse IgG conjugated to HRP.

3.4.3 VLP-ELISA

VLP-ELISA was used to detect antibodies, which specifically bind to the intact surface of MnPV VLPs (**Fig. 3.4.3**). Here, 96-well Polysorb Nunc-Immuno plates were coated with 100 ng/well of purified VLPs overnight at 4 °C. Afterwards, the ELISA plates were blocked with 180 µl/well of CBB for 1 h at 37 °C. 150 µl/well of diluted *Mastomys* sera (1:100 in CBB) were added to the first row of the ELISA plates and the remaining rows were filled with 100 µl/well of CBB. A 1:3 serial dilution was performed by transferring 50 µl from the previous row to the next row after mixing by using a multi-channel pipette. After incubation for 1 h at room temperature, the ELISA plates were washed with 1 × PBST for 4 times and incubated with 100 µl/well of HRP-conjugated goat anti-mouse IgG antibody diluted 1:10,000 in CBB. After washing, the bound antibodies were quantified colorimetrically by incubating with 100 µl/well of substrate buffer for 8 min. The enzyme reaction was stopped with 50 µl/well of 1 M sulfuric

acid and the absorption was measured at a wavelength of 450 nm with the SPECTROstar Nano plate reader. The antibody titer represents the last reciprocal serum dilution above blank.

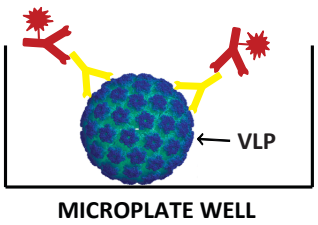

Fig. 3.4.3 Schematic view of the VLP-ELISA. The microplate well was coated with purified MnPV VLPs, allowing the detection of antibodies specifically binding to the intact surface of VLPs.

3.5 Pseudovirion-based Neutralization Assay (PBNA)

3.5.1 Generation of Pseudoviruses

293TT cells (3×10^6 cells in 10 ml medium) were seeded in a 10 cm dish and ten 10 cm dishes were prepared for a standard pseudovirus production. On the following day, 293TT cells were transfected with 5 µg of each plasmid (5 µg 847-MnL1short hum + 5 µg 847-MnL2 hum + 5 µg GAUSSIA luciferase/GFP) by using TurboFect transfection reagent (the transfection method is described in section 3.8.5). The cells were incubated for 48 h at 37 °C, 5% CO_2 and 95% humidity without changing medium.

3.5.2 Pseudovirus Extraction and Maturation

Transfected 293TT cells were resuspended and transferred into a 50 ml Falcon tube. After centrifugation at 1,900 rpm for 5 min at room temperature, cell pellets were resuspended in 1 ml DPBS containing $CaCl_2$ and $MgCl_2$ in a 1.5 ml Protein LoBind tube. After centrifugation at 5,000 rpm for 5 min at 4 °C, the supernatant was discarded and the pellets were resuspended in an equal volume of pseudovirus lysis buffer. Cells were lysed under rotation for 24 h at 37 °C.

3.5.3 Pseudoviruses Purification

An OptiPrep gradient solution with 27%, 33% and 39% iodixanol was prepared by diluting the original iodixanol solution (60%) in DPBS with 0.8 M NaCl and used for pseudovirion separation. In centrifuge tubes for SW41TI rotor, 3.3 ml of diluted iodixanol were added starting with 39% at the bottom and 27% on top. Phenol red was added to the 39% solution to make a distinction between 39% and 33%. The gradient was covered with parafilm and stored overnight at 4 °C to allow the formation of the gradient. For the following day, the 1.5 ml Protein LoBind tubes containing the pseudovirion lysate were placed on ice for 5 min. Afterwards, 0.17 volume of 5 M NaCl (17 µl per 100 µl of total volume in the tube, including pellet and lysis buffer) were added to the samples. The mixture was incubated on ice for 5 min. After centrifugation at 10,000 rpm for 10 min at 4 °C, the supernatant was transferred to a new Protein

LoBind and incubated with 2 µl Benzonase for 1 h at 37 °C. After incubation, the sample was centrifuged at 10,000 rpm for 10 min at 4 °C. Approximately 20 µl of pseudovirion containing crude extract was kept and stored at -80 °C before purification. The remaining supernatant was carefully loaded on the top of the Optiprep gradient and balanced with DPBS/0.8 M NaCl. The pseudoviruses were purified by ultracentrifugation through the gradient at 37,000 rpm for 5 h at 16 °C with TH641 rotor. 500 µl of fractions were collected in Protein LoBind tubes on ice by inserting a 20 G needle 1 cm below the 33%-39% interphase on the tube, allowing the solution to drip out. Fractions were labeled and stored at -80 °C. The crude extract as well as the purified fractions were analyzed in the *in vitro* infection assay to determine the dilution used in the *in vitro* neutralization assay.

3.5.4 Infection Assay

1.25×10^4 HeLaT cells (in 50 µl medium) were seeded in 96-well plates 2-5 h prior to the addition of pseudoviruses. Pseudoviruses from each fraction were diluted 1:200 and added to the HeLaT cells, and subsequently incubated for 48 h at 37 °C. Each fraction was tested in triplicates. After two days of incubation, the plates were placed at room temperature for 15 min before measurement. 10 µl of cell supernatant per well were transferred to white 96-well plates. 100 µl/well of substrate (10 µl of PKJ Coelenterazine per 1 ml of PJK GAUSSIA glow juice) were added to each well. The Gaussia luciferase signals were detected 15 min after substrate addition with a microplate luminometer Synergy2 reader.

3.5.5 Neutralization Assay

A pseudovirion-based neutralization assay was utilized to evaluate the neutralizing antibodies elicited by vaccine antigens (**Fig. 3.5.5**). Serum was diluted 1:60 with supplemented DMEM (without hygromycin B) in sterile tubes. Basically, 90 µl of pre-diluted sera were added to the wells of a 96-well plate in duplicates and 1:3 serial dilutions were performed by transferring 30 µl of sera from previous wells to next ones with a multichannel pipette (mix thoroughly). After that, 40 µl of pseudoviruses with the proper dilution were added to the wells containing serially diluted sera and incubated for 15 min at room temperature. The outside wells of the plate were left free of the serum-pseudovirus mixture but were filled with 150 µl of medium or 1 × DPBS. Next, 1.25×10^4 HeLaT cells (in 50 µl medium) were applied to the serum-pseudovirus mixture followed by two days of incubation at 37 °C. The amount of secreted Gaussia luciferase was determined as described in section 3.5.4.

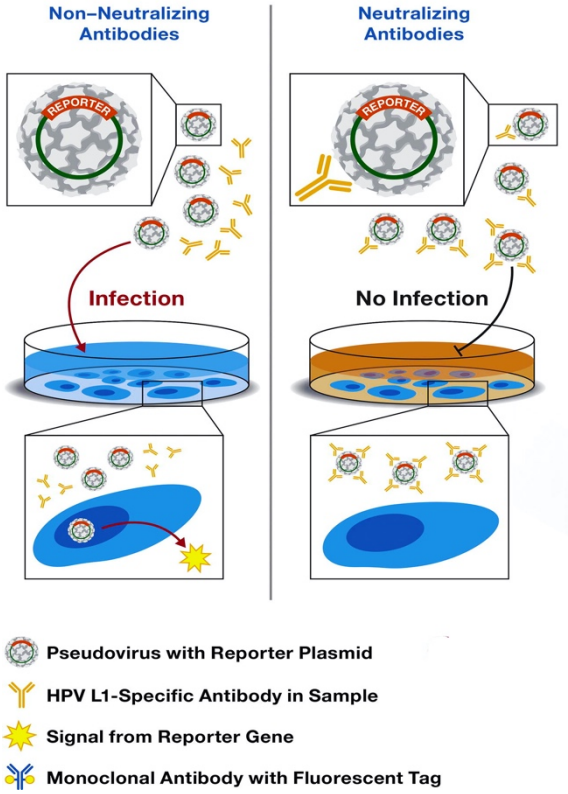

Fig. 3.5.5 Overview of the pseudovirion-based neutralization assay [144]. The neutralization assay is applied for the highly sensitive detection of neutralizing antibodies against papillomaviruses in sera. In principle, the major capsid protein L1, minor capsid protein L2 and encapsidated reporter gene, Gaussia luciferase, form pseudovirions, which are used to infect HeLaT cells. The pseudovirion infection can be determined by measuring the activity of secreted Gaussia luciferase in the culture medium upon substrate addition. However, the pseudovirion infection and the consequent expression of the Gaussia luciferase are prevented or reduced when the neutralizing antibodies are present during the pre-incubation with pseudovirions. This figure is adapted from [144].

3.6 Collection and Analysis of Animal Tissue Samples

3.6.1 Histological Samples

Animals were anesthetized with isoflurane and sacrificed by cervical dislocation, followed by shaving at the desired area with a razor. Skin biopsies and complete tumors were cut perpendicularly with scalpels and stretched out by pinning the specimen on a flat cork plate. The specimen for histological analysis were fixed with 4% paraformaldehyde (PFA) in a 12-well plate for at least 24 h at room temperature. Afterwards, the tissue was embedded in paraffin blocks and sliced in sections of 1-4 µm in the lab of Prof. Dr. Gröne, DKFZ.

3.6.2 Hematoxylin-eosin (HE) Staining

Prior to staining, tissue sections were immersed twice in xylol for 10 min to remove paraffin and then rehydrated with 2 × 100% ethanol, 1 × 96% ethanol, 1 × 70% ethanol and 1 × TBS or PBS for 5 min per step. Next, the slides were stained with hematoxylin for 2 min and rinsed with tab water for 5 min to allow the stain to develop. Afterwards, the slides were stained with eosin for 30 s and then dehydrated

with a graded ethanol series followed by incubation in xylene. The stained tissue sections were mounted in Mowiol and covered with coverslips. The images were obtained from stained sections by using a Keyence BZ-9000 microscope. HE stainings were kindly performed in the lab of Prof. Dr. Gröne, DKFZ.

3.6.3 Skin Samples for DNA Extraction

After taking samples for histology, the sliced tumor samples for molecular analysis were transferred to pre-cooled 1.5 ml Eppendorf tubes and snap-frozen in liquid nitrogen. Next, the sacrificed animals were immediately submerged into liquid nitrogen for snap freezing. The frozen animals were wrapped with paper towels for handling and the fine hairs left on the desired area were removed by carefully wiping with a paper towel. Next, the skin of the frozen animals was scratched with a scalpel onto aluminum foil placed on dry ice. The obtained skin powder was transferred to pre-cooled 1.5 ml Eppendorf tubes and stored at -80 °C. To avoid cross contamination among different tissues and animals, scalpels and aluminum foil were changed between handling each sample collection. Nitrogen bucket and surgical tools were cleaned with detergent, incubated for at least 1 min in sodium hypochlorite and rinsed with water after each extraction. The workplace was also cleaned with sodium hypochlorite. The surgical tools were thoroughly dried out and sent for autoclaving later.

3.6.4 DNA Extraction

DNA from animal samples was extracted using a phenol-chloroform method. Briefly, skin samples were incubated with lysis buffer (including Proteinase K and RNase A/T1 mix) at 37 °C for 30 min and at 56 °C for 1 h in a ThermoMixer at maximum speed. Afterwards, 1 volume of phenol was added to the lysate followed by shaking vigorously for 10 min. The mixture was centrifuged at 13,000 rpm for 10 min. Meanwhile, phase-lock tubes were centrifuged at 10,000 rpm for 2 min prior to use. The upper phase of the extraction was transferred to centrifuged phase-lock tubes to separate the phases of the lysate-phenol mix. 0.5 volume of phenol and 0.5 volume of chloroform-isoamylalcohol (CIA, 24:1) were added to the tubes. The mixture was shaken vigorously for 10 min and centrifuged at 13,000 rpm for 10 min. Next, additional 0.5 volume of CIA were added to the tubes to remove potentially remaining phenol. The shaking and centrifugation steps were repeated once. Afterwards, the upper phase was collected in a new tube with the addition of 0.1 volume of 3 M NaAc (pH 5.2) and 1 volume of isopropanol. To precipitate the DNA, the tubes containing the well-mixed solution were centrifuged at maximum speed for 20 min at 4 °C. The pellet was washed with 70% ethanol and air-dried. The DNA was dissolved in 50-100 µl EB buffer and incubated at 4 °C overnight.

3.6.5 Quantification of the Viral Load

The viral load of MnPV in each specimen was determined by quantitative PCRs (qPCR) to indicate the grade of skin lesions. A standard containing MnPV and β-globin plasmids in a molar ratio of 1:2 was

introduced to the assay. The *Mastomys Hbb* (β-globin) is a single copy gene accounting for two copies per cell [126]. Therefore, the viral load was defined as the number of MnPV DNA copies per cell/two copies of *Hbb* per cell. The specific primers were used to amplify MnPV and *Hbb*, respectively (see **Table 2.13.1**). All samples were tested in duplicates and normalized to the standard (in triplicates).

The qPCR reaction was set up as follows:

Reagent	Volume
iTaq™ Universal SYBR® Green Supermix (2 ×)	7.5 µl
Primer Mix (F + R, 20 µM)	0.375 µl
ddH_2O (PCR grade)	5.125 µl
DNA (20 ng)	2.0 µl

The respective qPCR program is shown in section 3.9.3.

3.7 Construction of Plasmids

3.7.1 Polymerase Chain Reaction (PCR) for Cloning

The respective PCRs were performed to amplify the DNA sequences of interest from the template DNA and introduce the desired restriction sites using Phusion DNA polymerase according to the manufacturer's instructions. In some cases, the forward primers contained a Kozak sequence upstream of the start codon. The reaction was set up as follows:

Reagent	Volume
Phusion DNA polymerase 2 × Master Mix	25 µl
Primer Mix (F + R, 20 µM)	2 µl
Template	50 ng
ddH_2O (PCR grade)	to 50 µl

The PCR was programmed in a thermo cycler with the following protocol:

Step	Temperature	Time	
Initial Denaturation	98 °C	30 s	
Denaturation	98 °C	10 s	30-35 cycles depending on the experiments
Annealing	58-60 °C	30 s	
Extension	72 °C	30-45 s 15-30 s/kb	
Final extension	72 °C	10 min	
	4 °C	Hold	

3.7.2 Agarose Gel Electrophoresis

The amplified PCR products were separated by electrophoresis on a 0.8 to 1.2% agarose gel (dissolved in 1 × TAE buffer) depending on the size of the amplicons. Next, the gel was stained with 0.5 µl/ml ethidium bromide for DNA visualization. GeneRuler 1 kb DNA ladder was loaded in parallel as a size marker. The DNA fragments were visualized at 260 nm wavelength in a gel documentation device or on a UV table.

3.7.3 Restriction Enzyme Digestion and Ligation

Prior to the restriction enzyme digestion, the target band was excised from the agarose gel and purified using the QIAquick Gel Extraction Kit according to the manufacturer's protocols. DNA concentrations were determined photometrically with a SPECTROstar Nano plate reader. The purified PCR products and vector backbones were digested at 37 °C for 1 h using FastDigest enzymes with the following protocol:

Reagent	Volume
10 × FastDigest Green Buffer	2 µl
DNA	1 µg
Restriction enzyme 1	0.5 µl
Restriction enzyme 2	0.5 µl
FastAP™ (for backbone)	1 µl
Nuclease-free H_2O	to 20 µl

The reaction was inactivated by heat incubation for 10 min at 65 °C or 5 min at 80 °C depending on the respective restriction enzymes. Digested PCR products and backbones were purified by agarose gel electrophoresis.

For ligation reactions, the vector to insert molar ratio was set between 1:3 and 1:5 (depending on the sizes of DNA fragments) and the required amount of insert was determined using the NEBioCalculator from NEW ENGLAND BioLabs (https://nebiocalculator.neb.com/#!/ligation) based on the following equation:

$$\frac{kb\ of\ insert}{kb\ of\ vector} \times\ ng\ of\ vector = ng\ of\ insert\ needed\ for\ a\ 1{:}\ 1\ molar\ ratio$$

100 ng of the vector DNA were used as default.

For each ligation the following reaction was set up:

Reagent	Volume
10 × T4 DNA Ligase Buffer	2 µl
Dephosphorylated vector	100 ng
Digested PCR product	X ng (determined by calculation)
T4 DNA Ligase	1 µl
Nuclease-free H_2O	to 20 µl

The gently mixed ligation reaction was incubated at 16 °C overnight.

3.7.4 Transformation of Chemically Competent Bacteria

1-5 µl (1-100 ng) of plasmid DNA were added to 50 µl of *E. coli* (TOP10) chemically competent cells. The mixture was mixed gently with a pipet tip and incubated on ice for 30 min followed by a heat shock at 42 °C for 1 min. The bacteria suspension was then immediately chilled on ice for 2 min. Afterwards, 250 µl of SOC medium was added and the suspension was incubated in a ThermoMixer at 550 rpm for 1 h at 37 °C. Subsequently, 50-100 µl of transformed cells were spread on pre-warmed agar plates with respective antibiotics and incubated at 37 °C overnight.

3.7.5 Identification, Propagation and Isolation of Expression Plasmids

Single colonies from the agar plate were isolated using a sterile pipette tip, transferred to 500 µl of LB medium containing the respective antibiotics and incubated for 2-3 h at 37 °C on a shaking platform. 2 µl of the bacterial cultures, which by then should show a cloudy haze in the medium, were used as templates for colony PCR using primers that amplify the target inserts. Positive clones were further cultivated in 4 ml LB medium for additional 5-6 h. Plasmids were extracted from 2 ml of bacteria suspensions using the Axygen™ Plasmid Miniprep Kit according to the manufacturer's protocol and sent for Sanger sequencing with universal primers provided by GATC or Eurofins Genomics. Larger amounts of plasmids with the correct sequences were isolated using the QIAGEN Plasmid Midi Kit for further experiments.

For bacteria cryopreservation, an absolute glycerol solution was added to bacterial cultures to a final 20-30% v/v glycerol concentration and mixed well. The glycerol stock tube was then frozen at -80 °C for long-term storage.

3.8 Cultivation and Treatment of Cells

3.8.1 Cultivation, Passaging and Seeding of Mammalian Cell Lines

HEK293TT, HeLaT, MaFi132 and MaFi191 were grown in Dulbecco's Modified Eagle's Medium (DMEM, high glucose, 4.5 g/L) supplemented with 10% fetal bovine serum (FBS), 1% penicillin/streptomycin and 1% L-glutamine. Hygromycin B (125 µg/ml, 1:400 dilution) was added to

the culture medium of HeLaT and HEK293TT cells to maintain the selection of the hygromycin phenotype of resistant cells.

Murine 308 keratinocyte cells were cultured in 4 × Minimal Essential Medium (MEM) supplemented with 1% penicillin/streptomycin.

All mammalian cell lines were maintained in a cell culture incubator at 37 °C, 5% CO_2 and 95% humidity and tested for possible *Mycoplasma spp.* contamination by PCR routinely.

For mammalian cells, after removal of medium, cells were washed once with 1 × DPBS prior to the addition of 1-2 ml of 0.25% trypsin-EDTA for detachment. After incubating at 37 °C for 1-5 min depending on the specific cell line, trypsin-EDTA activity was neutralized by adding 10% FBS-containing medium. Cells were suspended with fresh culture medium and collected in a 15 ml or a 50 ml Falcon tube and the cell pellets were collected by centrifugation at 350 g for 3 min and resuspended in fresh culture medium. For maintenance culture, cells were passaged at a ratio of 1:5 to 1:20.

For cell counting, 100 µl of the cell suspension was mixed with 100 µl of 0.25% trypan blue in PBS and the cell number per ml was determined by a Countess II FL automated cell counter.

3.8.2 Cultivation, Passaging and Seeding of Insect Cell Lines

Insect cell lines for VLP production were grown at 27 °C without CO_2 and humidity restriction. Sf9 cells for recombinant baculovirus production were cultured in TNM-FH insect medium supplemented with 10% FBS, 1% penicillin/streptomycin, 1% L-glutamine and 0.1% Pluronic F-68. TN-High-Five cells for baculovirus expression were cultured in EX-CELL™ 405 serum-free medium supplemented with 1% penicillin/streptomycin and 1% L-glutamine.

For adherent culture, cells were detached with a cell scraper and passaged at a ratio of 1:3. For suspension culture, 50 ml of 1 × 10^6 viable cells/ml TN-High-Five cells were seeded with 200 ml supplemented medium in an erlenmeyer culture flask and cultivated at a constant shaking speed of 125-150 rpm at 27 °C. After two or three days, when cell densities reached 1 × 10^6 viable cells/ml, cells were seeded to culture flasks according to the different uses.

3.8.3 Cryopreservation and Reactivation of Cells

For long-term storage, cell pellets were resuspended in 1 ml of pre-chilled Cryo Medium and transferred into a 2 ml cryotube. Cryotubes containing cells were then wrapped in several layers of tissue papers (ca. 1 cm in thickness) or put in a CoolCell® SV2 device and subsequently frozen at -80 °C. After one week, cells were transferred into a cryo-conservation tank filled with liquid nitrogen. Notably, the Cryo Medium for insect cells is different from that of mammalian cells, and contains 1 ml of 10% FBS, 10% DMSO and 80% TNM-FH supplemented insect medium for Sf9 cells; 10% DMSO and 90% EX-CELL™ 405 supplemented serum-free medium for TN-High-Five cells.

For reactivation of cells, frozen cells were thawed at 37 °C under gentle shanking. The thawed cells were transferred to 5 ml of pre-warmed culture medium in a 15 ml Falcon tube and centrifuged at 350 g for 4 min to remove DMSO. Next, cells were carefully resuspended in fresh culture medium and transferred to culture flasks or dishes.

3.8.4 *In vitro* Infection of Murine Keratinocytes

MnPV particles were extracted from MnPV-induced skin lesions of *Mastomys coucha*. Briefly, frozen tumors were cut into small pieces with a scalpel and transferred to 2 ml Precellys tubes filled with 6 glass beads. 400 µl of pre-chilled DPBS supplemented with 136.9 mM NaCl was added into tubes, subsequently, the mixture was homogenized 2 times using a Precellys 24 tissue homogenizer with the "5000-2x-2000-005" program (if additional tumor tissue was left, this step was repeated again). The tubes were centrifuged at 5,000 g for 10 min and the supernatant was removed prior to the addition of pre-chilled DPBS. The mixture was once again homogenized 2 times using the Precellys 24 tissue homogenizer with the "5000-2x-2000-005" program. The homogenized mixture was transferred to a 50 ml Falcon tube filled with 5 ml DPBS. Afterwards, the mixture was sonicated for 50 s with an output level of 3.0 (20-25%) and then centrifuged at 5,000 g for 10 min. The supernatant was harvested, aliquoted into 1.5 ml Eppendorf tubes and stored at -20 °C for further experiments.

1×10^5 308 cells were seeded in a 6-well plate one day before infection. Afterwards, 100-150 µl of tumor extract were added into culture medium and the plate was swirled gently. After 24 h of incubation, the cells were washed 2 times with DPBS and replaced with fresh culture medium for an additional 24 h incubation. Subsequently, the cells were harvested for DNA, RNA and protein isolation or re-seeded for routine cell culture. The infected cells were passaged every two or three days, and samples were collected in parallel.

3.8.5 Transfection of Expression Plasmids

Mammalian cells with a proper cell density according to the required experiments were seeded in petri dishes or plates and incubated overnight. On the following day, the culture medium was refreshed prior to transfection. Briefly, plasmids were diluted in 1 ml Opti-MEM, subsequently, 2 volumes of TurboFect (1:2 µg total DNA:µl Turbofect) were added. The DNA and Turbofect were mixed by vortexing and incubated at room temperature for 20 min. Afterwards, the DNA/Turbofect mixture was distributed evenly to the dish. The cells were harvested 24 or 48 h after transfection depending on the purposes of experiments. For instance, 4×10^5 MaFi132 cells were seeded in a 10 cm dish 24 h before transfection. Next, MaFi132 cells were transfected with pPK-CMV-L1$_{short}$ (5 µg), pPK-CMV-L1$_{middle}$ (10 µg), pPK-CMV-L1$_{long}$ (10 µg), or pPK-CMV-L1 wt (10 µg), respectively, using TurboFect. The transfected cells were harvested after additional 48 h of incubation.

3.8.6 UV Irradiation of Cells

6×10^5 infected 308 cells in a 6 cm dish were seeded one day prior to UVB irradiation. The lamps of the UV table (UV 181 BL) were turn on for a warm-up period of several minutes. At the same time, the cells attached to the dishes were washed once with DPBS. Thereafter, the dishes were inverted on the UV table without lids when irradiated with a dose of 50 mJ/cm^2. In addition, the irradiance was determined with a UV detector (Variocontrol, Spectrum: TL06). When reached the desired UV dose as shown in the detector, the UV lamps were turn off and fresh culture medium was added into the dishes. The cells were harvested 0.5, 1, 2, 4, 8, 24 and 48 h after irradiation.

3.8.7 Actinomycin D Treatment

In order to determine the mRNA half-life of MnPV viral transcripts, the addition of Actinomycin D (ActD) was employed. In brief, 6×10^5 infected 308 cells were seeded with 4 ml culture medium in a 6 cm dish. On the following day, the cells were treated with 5 µg/ml of ActD (dissolved in ethanol, stock solution: 1 mg/ml) and harvested 1, 2, 4 and 8 h after ActD treatment, respectively.

3.8.8 Calcium Chloride Treatment

To address whether uninfected or infected 308 cells can be differentiated by calcium, 3×10^5 or 9×10^5 uninfected or infected 308 cells were seeded with 4 ml culture medium in a 6 cm dish. On the following day, 308 cells were treated with 0.7, 1.4, 2.8 and 5 mM calcium chloride ($CaCl_2$, stock solution: 5 M) and infected 308 cells were treated with 2.8 mM $CaCl_2$. The cells were collected 48 h after treatment.

3.8.9 Methylcellulose Treatment

For preparation of 2% (w/v) methylcellulose stock medium, 4 g of sterile methylcellulose powder (4000 cPs) was weighed and transferred to 100 ml pre-heated 4 × MEM (60 °C, without penicillin/streptomycin and L-glutamine). The mixture was stirred using a magnetic stirrer for 20 min at room temperature. In particular, the mixture would not form an aqueous solution but an emulsion at this moment. The mixture was stirred at 4 °C overnight after the addition of 100 ml 4 × MEM containing the respective amount of penicillin/streptomycin and L-glutamine. On the next day, the clear and highly viscous medium was aliquoted into 50 ml Falcon tubes and centrifuged at 5,000 g for 90 min at room temperature. 90% of the supernatant was transferred into a new 50 ml Falcon tube. The 2% methylcellulose culture medium was stored at -20 °C and thawed at 4 °C overnight prior to use.

3×10^5 or 9×10^5 308 cells or 9×10^5 infected 308 cells (in 100 µl) were seeded in 6 cm dishes filled with 5 ml of 2% methylcellulose culture medium using a 10 ml syringe. To distribute cells evenly, a sterile pipette tip was used to stir the methylcellulose culture medium thoroughly. The suspended cells were incubated at 37 °C for 48 h. To harvest cells from this highly viscous medium, methylcellulose was diluted 1:10 with DPBS in a 50 ml Falcon tube and mixed well prior to the centrifugation at 1,000 rpm

for 4 min. 90% of the supernatant was discarded and the cell (invisible) pellets were resuspended with the liquid left in the 50 ml Falcon tube and subsequently transferred to a 15 ml Falcon tube. The cells were washed with 10 ml DPBS and collected by centrifugation at 2,000 rpm for 4 min.

3.9 Isolation and Analysis of Nucleic Acids

3.9.1 Isolation and Reverse Transcription of RNA

RNA was extracted from cells using the RNeasy Mini Kit according to the manufacturers' protocol. Briefly, attached cells were resuspended using trypsin and washed once with DPBS. The cell pellets were harvested by centrifugation at 350 g for 4 min and resuspended with 600 µl of RLT lysis buffer supplemented with 40 mM DTT. Cells were homogenized by passing through QIAshredder spin columns. 600 µl of 70% ethanol prepared with RNase-free water were mixed with the homogenized lysate. The lysate was transferred to a spin column and processed according to the manufacturer's protocol. The concentration of RNA eluted in 35 µl of RNase-free water was measured photometrically using a SPECTROstar Nano plate reader.

To remove contaminating DNA from RNA preparations, especially in infected 308 cells, the RNA was treated using the Turbo-free DNase free Kit. Briefly, 2 µl of 10 × DNase buffer and 0.6 µl DNase were added to the RNA (max. 20 µg) and the reaction volume was adjusted to 20 µl with nuclease-free water. The mixture was incubated for 30 min at 37 °C in a ThermoMixer at 550 rpm. 2 µl of DNase Inactivation Reagent was added to stop the reaction. The tube was incubated for 5 min and flicked every 1 minute to keep the inactivation beads in suspension. Afterwards, the mixture was centrifuged at 13,000 g for 2 min to remove the beads and DNase-free RNA was transferred to a new tube. The concentration was measured photometrically before reverse transcription or storage at -80 °C.

The RevertAid Reverse transcriptase and Oligo dT_{22} Primer were applied for the synthesis of first strand cDNA from RNA templates using the following two step protocol:

RT+ Reaction	RT- Reaction
200 ng-1 µg RNA	200 ng-1 µg RNA
1 µl Oligo dT_{22} Primer (20 µM)	1 µl Oligo dT_{22} Primer (20 µM)
Nuclease-free H_2O to 12.5 µl	Nuclease-free H_2O to 12.5 µl

All reactions were incubated at 65 °C for 5 min and placed on ice for 1 min prior to the addition of the following reagents to the reactions:

4 µl 5 × RT buffer	4 µl 5 × RT buffer
2 µl dNTPs (10 mM)	2 µl dNTPs (10 mM)
1 µl RevertAid RT (200 U/µl)	1.5 µl nuclease-free H_2O
0.5 µl Ribolock (20 U/µl)	

All reactions were incubated at 42 °C for 1 h, and then at 72 °C for 10 min

The reactions were carried out in 0.5 ml reaction tubes. The RT- reaction was performed in each reaction as a negative control to detect possible DNA contamination after DNase treatment. All cDNA samples were analyzed by RT-PCR using *Mastomys* Gapdh-specific primers, which is also suitable for murine samples. The DNase treatment was reprocessed when the RT- reaction of samples showed positive signals after PCR. Otherwise, the cDNAs were stored at -20 °C and freshly diluted depending on the purpose of further experiments.

3.9.2 Semi-quantitative PCR

The semi-quantitative polymerase chain reaction (RT-PCR) was performed using DreamTaq DNA Polymerase according to the following setup:

Reagent	Volume
DreamTaq Green 2 × Master Mix	10 µl
Primer Mix (F + R, 20 µM)	0.5 µl
cDNA	20 ng
ddH_2O (PCR grade)	to 20 µl

The PCR was programmed in a thermo cycler with the following protocol:

Step	Temperature	Time	
Initial Denaturation	95 °C	3 min	
Denaturation	95 °C	30 s	26-35 cycles depending on the experiments
Annealing	58-60 °C	30 s	
Extension	72 °C	20-30 s 60 s/kb	
Final extension	72 °C	10 min	
	4 °C	Hold	

The amplified products were analyzed by agarose gel electrophoresis.

3.9.3 Quantitative PCR

The quantitative real-time PCR (qPCR) was performed using iTaq™ Universal SYBR Supermix. The reaction was set up as follows:

Reagent	Volume
iTaq™ Universal SYBR® Green Supermix (2 ×)	7.5 µl
Primer Mix (F + R, 20 µM)	0.5 µl
cDNA	5 ng
ddH_2O (PCR grade)	to 15 µl

Each reaction was performed in duplicates. The sequences of interests were amplified in a Thermal Cycler C1000™ and the florescent signals during amplification were detected with a CFX96 Touch Real-Time PCR detection system using the following program:

Temperature	Time	
95 °C	10 min	
95 °C	15 s	40 cycles
60 °C	1 min	
Plate read		
95 °C	1 min	
60 °C	1 min	
65 °C	31 s	
65 °C + 0.5 °C/cycle Ramp 0.5 °C/s Plate read	5 s	60 cycles

3.10 Isolation and Analyses of Proteins

3.10.1 Extraction and Quantification of Proteins

Cells were washed once with DPBS and lysed in 1.25 × Laemmli buffer. Lysates were transferred into 1.5 ml Eppendorf tubes, then heated at 95 °C for 5 min, subsequently, chilled on ice and treated with 100 U/ml Benzonase for 5 min at room temperature. Thereafter, proteins were stored at -20 °C until quantification. Protein concentrations were measured at a wavelength of 280 nm using a NanoDrop spectrophotometer.

For harsh denaturation in transfected MaFi132 cells, additional DTT and β-mercaptoethanol were added to a final concentration of 100 mM and 4%, respectively, prior to incubation for 1 h at room temperature and heating at 95 °C for 10 min. The samples were chilled shortly before loading.

3.10.2 SDS-polyacrylamide Gel Electrophoresis (SDS-PAGE)

Proteins were negatively charged via the binding of sodium dodecyl sulfate in the buffer and subsequently separated based on their molecular weight via discontinuous sodium dodecyl sulfate polyacrylamide gel electrophoresis (SDS-PAGE). Typically, this system was set up with a stacking gel and a separating gel. The SDS gels were made according to the following protocol:

Separating gel (8%-12%)	Stacking gel (6%)
0.3 M Tris, pH 8.8	0.25 M Tris, pH 6.8
8-12% Acrylamide-Bis (29:1)	6% Acrylamide-Bis (29:1)
0.1% SDS	0.1% SDS
0.1% APS	0.1% APS
0.08% TEMED	0.16% TEMED

40-100 µg of total proteins were loaded to the SDS gel along with PageRuler Prestained Protein Ladder as a molecular weight marker. The electrophoresis was carried out in electrode buffer (1 × SDS running buffer) at 80 V for the stacking gel and 120 V for the separating gel and stopped when the desired size separation according to the marker was reached.

3.10.3 Western Blot

Well-separated proteins were electrophoretically transferred to a PVDF membrane (0.45 µm) in a Mini Trans-Blot® Cell. Prior to electrophoretic transfer, the PVDF membrane was activated by incubating with methanol for few minutes and the SDS gel was pre-equilibrated in transfer buffer to remove SDS and salts from the running buffer which could decrease the conductivity of the transfer. The transfer sandwich was assembled as shown in the left panel of **Fig. 3.10.3**. Afterwards, the electrophoretic transfer of proteins was performed at 400 mA for 1 h at 4 °C. After blotting, the PVDF membrane was blocked with 5% milk powder in 1 × TBST at room temperature for 1 h, subsequently incubated with

primary antibodies diluted in 5% milk/TBST at 4 °C overnight with agitation. The next day, the membrane was washed 4 times (15 min per washing) with 1 × TBST and incubated with a 1:10,000 dilution of HRP-conjugated secondary antibody in 5% milk/TBST at room temperature for 1 h. Additional 4 times washing was performed before signal development. The detected protein of interest was visualized by addition of enhanced chemiluminescent reaction (ECL) substrates for HRP on the membrane exposed to X-ray film.

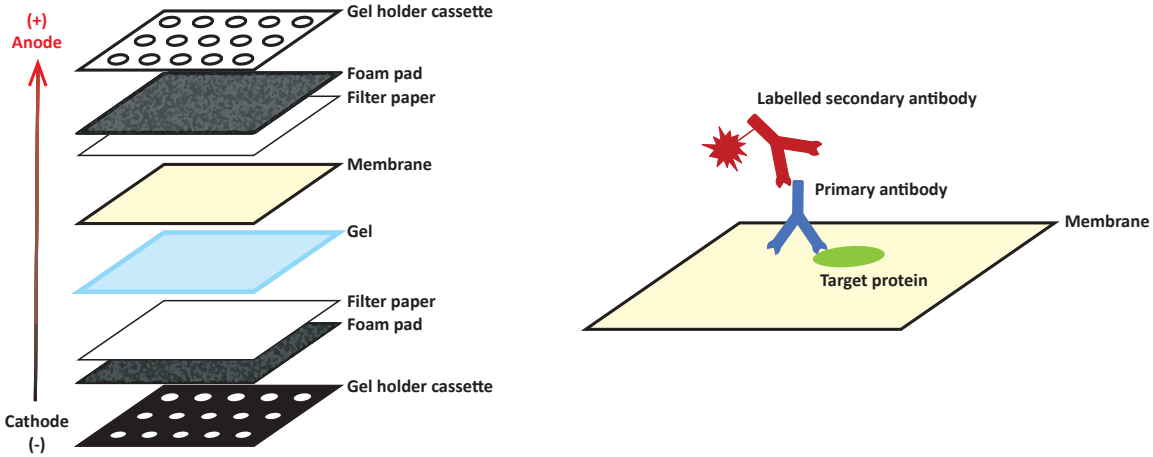

Fig. 3.10.3 The principle of Western blotting. The sandwich method was applied for the electrotransfer and assembled with a foam pad and a filter paper at each end, the membrane (anode) and the gel (cathode) in between. Next, the target protein was bound by specific primary antibody as well as enzyme-conjugated secondary antibody and detected via an enzyme reaction.

3.10.4 Coomassie Blue Staining

Colloidal Coomassie G-250 staining was performed to visualize proteins resolved by SDS-PAGE. After electrophoresis, the gel was washed in water for 5 min and transferred to the Coomassie G-250 solution at room temperature overnight with agitation. On the following day, the stained gels were rinsed in water several times until the background of the gel became clear. Afterwards, the image of the gel was acquired using a scanner.

For quantification of MnPV L2 protein and VLPs, bovine serum albumin (BSA) with a serial dilution was used as a standard for protein concentration. The concentration of antigens was determined by the comparison of band intensities between BSA standards and antigens using ImageJ.

3.10.5 Immunofluorescence Staining

Cells were seeded in either 6 or 10 cm dishes, into which several glass coverslips were placed prior to the treatment. After 24 or 48 h incubation depending on the specific experiment, the coverslips were transferred to a 24-well plate. The cells were washed once with 1 × PBS and fixed in 4% paraformaldehyde (PFA) in PBS at room temperature or ice-cold acetone at -20 °C for 10 min (especially

for Involucrin and Loricrin) and subsequently washed twice with 1 × PBS. Cells were then permeabilized with 0.05% Triton-X in PBS for 5 min and blocked with 10% goat serum in 0.05% Triton-X/PBS for 1 h at room temperature with agitation. After washing with PBS twice, the cells were incubated with the respective primary antibodies with an appropriate dilution in 10% goat serum/0.03% Triton-X/PBS at 4 °C overnight. The next day, the cells were washed with 1 × PBS 5 times and then incubated with the respective AlexaFluor-conjugated secondary antibody (1:1,000) at room temperature for 1 h with agitation. Plates containing the coverslips were covered with aluminum foil to avoid the fluorophore from photobleaching. The cells were then washed twice with 1 × PBS prior to nuclear staining with DAPI (0.3 μg/ml in PBS) at room temperature for 5 min. Thereafter, the stained cells were washed twice with PBS and rinsed once with absolute ethanol to remove salts and subsequently mounted on glass slides with a drop of Dako Faramount Aqueous Mounting Medium. The images were acquired by exciting fluorochromes at the respective wavelength with a Zeiss Cell Observer fluorescence microscope. The glass slides were placed in the dark at 4 °C for long-term storage.

3.11 Statistical Analysis

GraphPad Prism 8.0 was used for data analysis. The incidence of tumor development was calculated using Kaplan-Meier analysis with log-rank test. Statistics for qPCR results were assessed using non-parametric Kruskal-Wallis test followed by Dunn's multiple comparison test.

4. Results

4.1 MnPV L2 Pilot Study

To evaluate the best antigen and adjuvant formulation for MnPV L2 vaccination, virus-free *Mastomys coucha* (five animals per group) were immunized with 80 µg purified pET26 PfTrx-MnPV-L2(20-38)$_3$ (MnPV L2; **Suppl. Fig. 1**) or pET26-PADRE$_{2\times}$ PfTrx-MnPV-L2(20-38)$_3$ (MnPV L2/PADRE; **Suppl. Fig. 2**) adjuvanted with either Montanide ISA 720 or AddaVax™ (**Suppl. Table 1**). MnPV L2/PADRE consists of three copies of a conserved MnPV L2 epitope (amino acid 20-38) displayed on *Pyrococcus furiosus* thioredoxin (PfTrx), flanked by two copies of a pan HLA DR-binding epitope (PADRE; **Fig. 4.1.1A**). PADRE is a synthetically universal helper T cell peptide with a high-affinity to DR on the surface of antigen presenting cells (APCs), which consequently increases antibody responses [145].

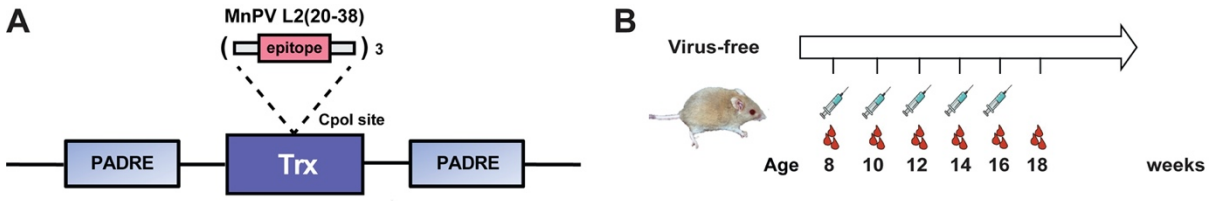

Fig. 4.1.1 Scheme of pET26-PADRE$_{2\times}$ PfTrx-MnPV-L2(20-38)$_3$ and MnPV L2 vaccination pilot study schedule. (**A**) Three copies of the MnPV L2 epitope (amino acid 20-38) were displayed on *Pyrococcus furiosus* thioredoxin (PfTrx), flanked by two copies of the pan HLA DR-binding epitope (PADRE). (**B**) Eight-week old virus-free *Mastomys coucha* were vaccinated biweekly and their age indicates the time of vaccination or sera collection, respectively.

Eight-week old virus-free *Mastomys* subcutaneously received five doses of MnPV L2 vaccines at biweekly intervals. Sera were collected before vaccination (pre-immune) and every two weeks after the immunization (**Fig. 4.1.1B**). Anti-L2 and neutralizing antibodies were assessed by GST-MnPV L2 ELISA and PNBA respectively. MnPV L2/PADRE formulated in Montanide ISA 720 or AddaVax™ elicited higher anti-L2 titers compared with other formulations (**Fig. 4.1.2A**). Consistent with these GST-MnPV L2 ELISA data, also neutralizing titers from animals vaccinated with MnPV L2/PADRE formulated in Montanide ISA 720 or AddaVax™ were evidently higher (**Fig. 4.1.2B**). Irrespective of the adjuvants, the mean titer of neutralizing antibodies raised against MnPV L2/PADRE reached 2.4×10^2. Surprisingly, MnPV L2 antigen elicited relatively high anti-L2 titers, but did not show neutralizing response to MnPV. Therefore, MnPV L2/PADRE was chosen for further experiments.

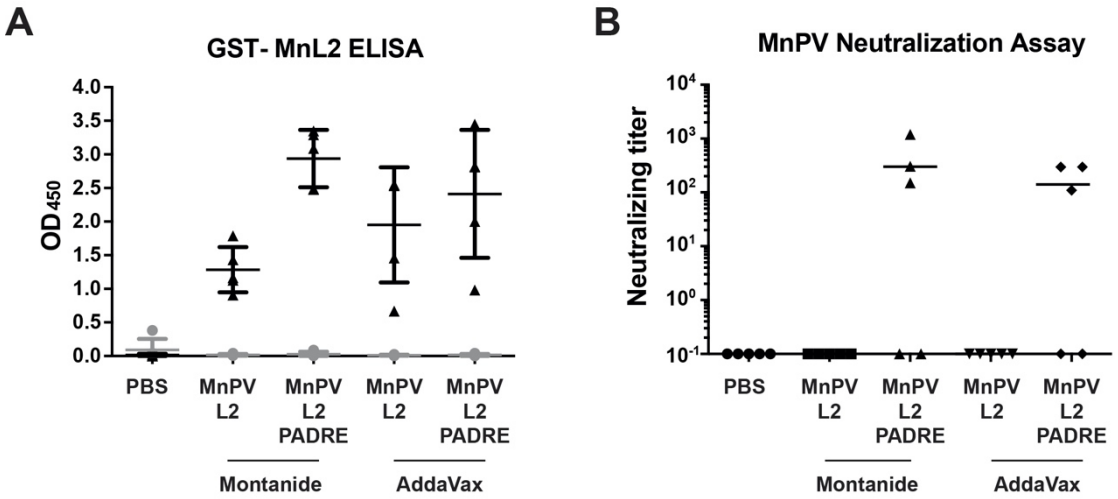

Fig. 4.1.2 Anti-MnPV L2 antibody response in the vaccination pilot study. Virus-free animals were vaccinated with different formulations of antigen. PBS: mock-vaccination with PBS; MnPV L2 + Montanide: vaccination with pET26 PfTrx-MnPV-L2(20-38)$_3$ containing Montanide ISA 720; MnPV L2/PADRE + Montanide: vaccination with pET26-PADRE$_{2\times}$ PfTrx-MnPV-L2(20-38)$_3$ using Montanide ISA 720; MnPVL2 + AddaVax: vaccination with pET26 PfTrx-MnPV-L2(20-38)$_3$ formulated in AddaVax™; MnPV L2/PADRE + AddaVax: vaccination with pET26-PADRE$_{2\times}$ PfTrx-MnPV-L2(20-38)$_3$ adjuvanted with AddaVax™. Sera were collected before immunization (gray dots) and two weeks after the 5th immunization (black dots). (**A**) Comparison between anti-L2 titers in pre-immune sera and in sera collected after the 5th injection of different formulations, which was measured by GST-MnPVL2 ELISA and displayed as mean ± SD. (**B**) Neutralization titers of sera after final immunization were tested against MnPV pseudovirus. Mean neutralization titers are indicated by horizontal bars.

Considering the conservation of the L2 N-terminus among different papillomaviruses, sera obtained from animals vaccinated with MnPV L2/PADRE formulated in Montanide ISA 720 or AddaVax™ were further used to assess the serological response against *Mastomys coucha papillomavirus* 2 (McPV2) L2 by GST-McPV L2 ELISA. Antibodies raised by MnPV L2/PADRE + Montanide (**Suppl. Fig. 3A**) or MnPV L2/PADRE + AddaVax (**Suppl. Fig. 3B**) indeed showed a weak cross-reactivity with McPV L2.

4.2 Antigen Production

To produce large amount of MnPV L2/PADRE protein for further experiments, an *E. coli* expression system and thermal purification were used. Expression of MnPV L2/PADRE was analyzed and quantified by Coomassie Blue staining (**Fig. 4.2A**) and Western blot (**Fig. 4.2B**), where the predominant band migrated at the predicted size of 23 kDa. The concentration of purified MnPV L2/PADRE was determined by comparing the band density of MnPV L2/PADRE to bands from different concentrations of BSA using ImageJ.

For VLPs production, the MultiBac baculovirus/insect cell expression system and a two-step sucrose/CsCl density gradient for purification were employed. The MultiBac expression system is widely used to express recombinant multiprotein complexes at high abundance for vaccine development and gene therapy [146]. After sucrose/CsCl density gradient centrifugation, pooled fractions (Fraction 2 to 6) containing VLPs were analyzed by Coomassie Blue staining (**Fig. 4.2C**). The concentration of VLPs was also determined by comparing the band densities using ImageJ. Additionally, the morphology of VLPs was visualized by negative stain electron microscopy (EM), where well assembled and uniformly sized particles with a diameter of approximately 55 nm were observed, demonstrating the high quality of VLPs (**Fig. 4.2D**).

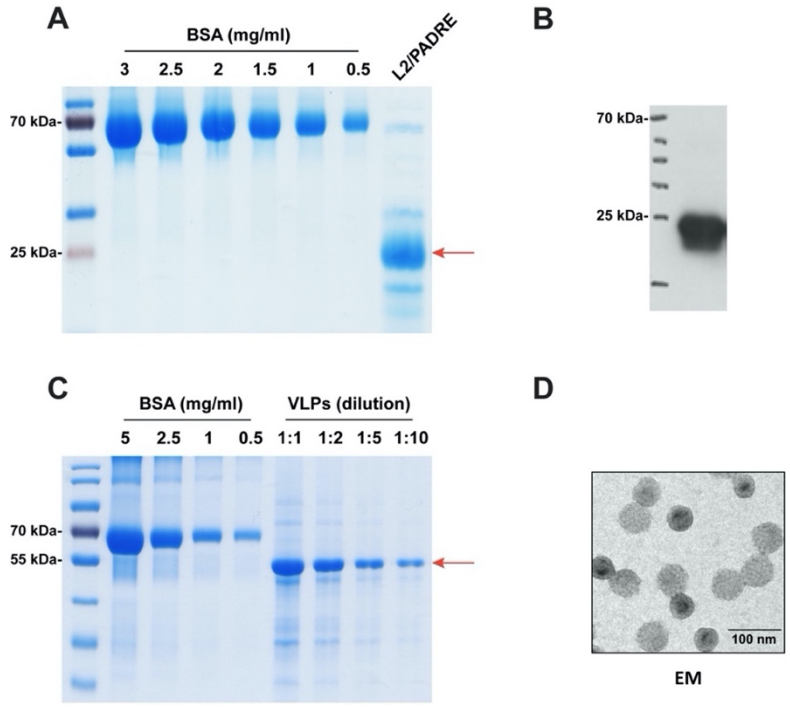

Fig. 4.2 Quantification and identification of pET26-PADRE$_{2\times}$ PfTrx-MnPV-L2(20-38)$_3$ and MnPV VLPs. The purified pET26-PADRE$_{2\times}$ PfTrx-MnPV-L2(20-38)$_3$ (L2/PADRE) were visualized by staining with Coomassie Blue (**A**) and analyzed by Western blot (**B**) using anti-Thioredoxin antibody. The purified VLPs were visualized by staining with Coomassie Blue (**C**) and examined by electron microscopy (**D**). The concentration of L2/PADRE or VLPs was determined by band densities using ImageJ when compared to different concentrations of BSA. The red arrow indicates L2/PADRE or VLPs respectively.

4.3 Study Design and Vaccination Schedule

To investigate the efficacy of MnPV vaccinations under UV conditions, animals from the naturally infected colony were divided into three groups (Control, MnPV L2/PADRE, VLP). A five-dose vaccination schedule at 8, 10, 12, 14 and 16 weeks was applied for animals in the MnPV L2/PADRE group and a three-dose vaccine was administered to animals in the VLP group according to the previous study [126]. A subset of each group was irradiated with UVB starting at the animal age of 18 weeks. The animal numbers in each subgroup are shown in **Table 4.3**.

Table 4.3 Overview of the MnPV L2 vaccine main study.

Group	n	Treatment (age)	
		Vaccine (8/10/12/14/16 w)	Start of UVB irradiation (18 w)
Control	16		
	19		+
MnPV L2/PADRE	16	+	
	18	+	+
VLP	11	+ *	
	14	+ *	+

n = number of animals, w = weeks
* Animals were immunized with VLPs at an age of 8, 10 and 12 weeks

Eight-week old virus-bearing *Mastomys* were subcutaneously vaccinated with MnPV L2/PADRE formulated in AddaVax™ at biweekly intervals. In parallel, a subgroup of naturally infected animals was immunized with 10 µg VLPs in the presence of the Sigma Adjuvant System (SAS), which was used only in the first vaccination. The irradiation schedule was followed as described previously with a slight modification in the present study [125]. Briefly, at 18 weeks of age, some siblings from each cage were irradiated with a dose of 150 mJ/cm^2 of UVB (three times per week). The dose was increased by 50 mJ/cm^2 per week until the final dose (450 mJ/cm^2) was reached and maintained for further treatments. Sera were collected every two weeks after the immunization (before 18 weeks of age) or every four weeks (after 18 weeks of age) (**Fig. 4.3**).

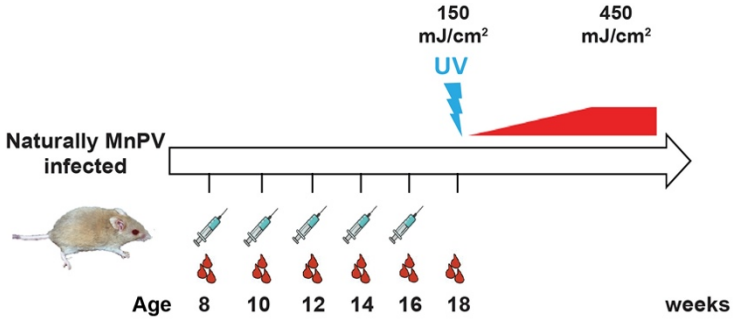

Fig. 4.3 Time schedule of the MnPV L2 vaccine main study. Eight-week old virus-bearing *Mastomys coucha* were biweekly vaccinated. The age indicates the time of vaccination or sera collection. Subsequently, animals from each cage were shaved on the back and irradiated with UVB starting at 18 weeks of age until the final dose of 450 mJ/cm^2 was reached.

4.4 Serological Responses to MnPV Vaccinations

4.4.1 Serological Responses in the Control Group

Serological responses against MnPV were measured in this long-term follow-up study to monitor the success of immunization and the infection status of the animals during their lifetime until the age of 82 weeks. In order to gain deeper insights into the effect of UV irradiation in all groups, serological data in this study were further separated based on whether animals were UV-irradiated or not. Consequently, 253 sera from 16 unirradiated animals and 295 sera from 19 irradiated animals in the control group were examined by GST-ELISA and VLP-ELISA.

The seroconversion of the virus-bearing animals was assessed by the appearance of antibodies against the viral early protein E2, as a marker of early infection [147]. The antibody response against MnPV E2 was detectable at eight-weeks of age and some animals showed strong anti-E2 responses even at late time points, indicating a persistent MnPV infection in the virus-bearing colony (**Fig. 4.4.1A**, cut-off = 0.2). Moreover, the seroreactivity against the viral minor capsid protein L2 was also measured in the unvaccinated control animals. Anti-L2 titers were overall much lower in the control group, and the mean anti-L2 titers were generally close to the baseline (**Fig. 4.4.1B**, cut-off = 0.2). Only one of 19 irradiated animals showed higher antibody responses against MnPV L2 at 54, 58 and 64 weeks of age, but antibody titers against MnPV E2 or L1 were below the cut-off, suggesting that the detectable positive anti-L2 titers probably resulted from unspecific reactions in the GST-ELISA.

In general, the seroreactivity against VLPs appeared at late infection stages, reflecting productive MnPV infections, consequently serving as an indicator of the occurrence of MnPV-induced skin tumors [147]. Therefore, 188 sera obtained from irradiated animals after 18 weeks of age were analyzed. The initial appearance of serological responses against VLPs was observed at week 46 in the irradiated animals and titers increased over time (**Fig. 4.4.1C**, cut-off = 300). At 26 weeks, one unirradiated animals showed high antibody titers against VLPs. However, this animal died prior to the end of the study at the age of 50 weeks. Although two unirradiated animals were tested positive for anti-VLPs antibodies, none of them developed tumors. Within the irradiated subgroup, tumors occurred in two out of six positive animals. This demonstrates that UV irradiation could possibly induce the seroreactivity against VLPs and accelerate the development of tumors, which is consistent with previous studies [125].

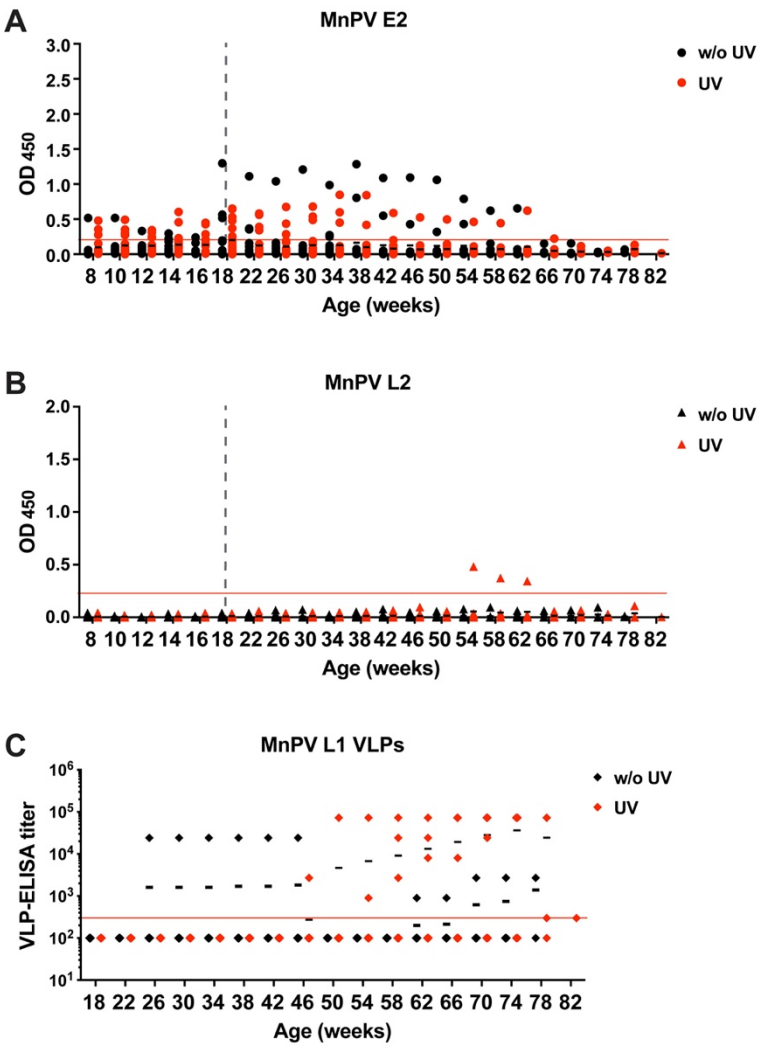

Fig. 4.4.1 Time course of anti-MnPV E2, -L2 and -L1 antibody response in naturally infected animals. Sera were collected every two weeks before the age of 18 weeks and every four weeks at older age. The seroreactivity against MnPV E2 (**A**) and L2 (**B**) was measured by GST-ELISA, and antibodies against the major capsid protein L1 (**C**) were determined by VLP-ELISA. Data are visualized by scattered dots and the mean values are shown as black horizontal lines. Black dots (n = 253 sera), triangles (n = 253 sera), and diamonds (n = 188 sera) indicate values of antibody titers from naturally infected unirradiated animals, and red dots (n = 295 sera), triangles (n = 295 sera), and diamonds (n = 213 sera) represent values of antibodies from naturally infected irradiated animals. Grey dashed lines in A and B indicate the start of the UVB irradiation and red lines represent the cut-off of the method (GST-ELISA = 0.2, VLP-ELISA = 300).

4.4.2 Serological Responses in the MnPV L2/PADRE-vaccinated Group

To evaluate the effect of the MnPV L2/PADRE vaccine in *Mastomys* during constant virus contact and additional irradiation with UVB, the serological responses against MnPV E2, L2 and VLPs were monitored. In this group of MnPV L2/PADRE-vaccinated animals, 261 sera from 16 unirradiated animals and 287 sera from 18 irradiated animals were examined by GST-ELISA and VLP-ELISA.

After vaccination, 56% (19/34) of animals after three and 68% (23/34) after four and five doses of vaccine, respectively, developed anti-L2 antibody responses above the cut-off, demonstrating the majority of MnPV-infected animals responded to the MnPV L2/PADRE vaccine in a dose-dependent manner (**Fig.**

4.4.2B). Moreover, the anti-L2 antibody levels reached the mean titer of 0.437 in all MnPV L2/PADRE-vaccinated animals (n = 33) after the final immunization, which is significantly higher ($p < 0.0001$) than that of 0.01 in naturally infected animals (n = 35) at 18 weeks of age but much lower ($p = 0.214$) than that of 2.413 in vaccinated virus-free animals (n = 5; **Fig. 4.1.2A**). Hence, vaccination of naturally infected *Mastomys* with MnPV L2/PADRE induced a strong anti-L2 response when compared to the control group (**Fig. 4.4.1B**). However, in general, the anti-L2 titers decreased below the cut-off after 46 weeks, which was not influenced by UV irradiation. At 54 weeks, one of 16 unirradiated animals that tested positive for anti-L2, was also positive for anti-VLP antibodies but negative for anti-E2, and did not develop a tumor. At the same time, one seropositive irradiated animal showed an antibody response against VLPs with a cut-off titer of 300 but was negative for E2 and also did not show any sign of tumor development.

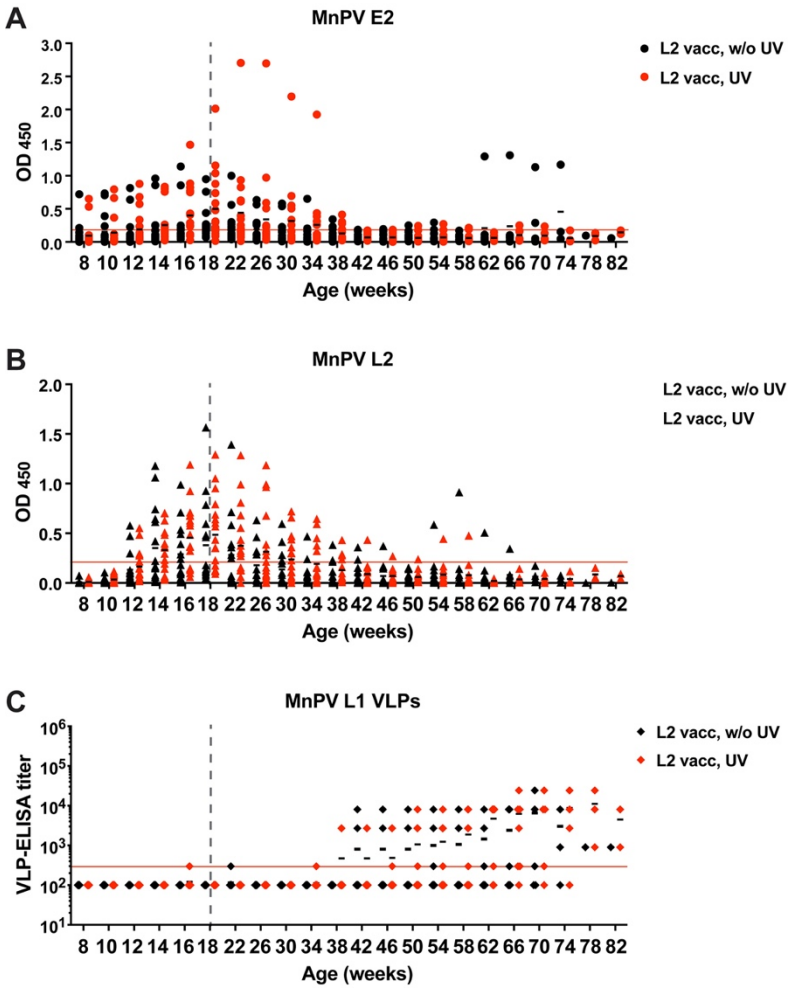

Fig. 4.4.2 Time course of anti-MnPV E2, -L2 and -L1 antibody response in the MnPV L2/PADRE group. Sera were collected every two weeks before 18 weeks of age and every four weeks after 18 weeks of age. The seroreactivity against MnPV E2 (**A**) and L2 (**B**) was measured by GST-ELISA, and antibodies against VLPs (**C**) were determined by VLP-ELISA. Data are visualized by scattered dots and the mean value is shown as a black horizontal line. Black dots, triangles and diamonds indicate values of antibodies from MnPV L2/PADRE-vaccinated animals without irradiation (n = 261), and red dots, triangles and diamonds represent values of antibodies from MnPV L2/PADRE-vaccinated animals with irradiation (n = 287). Grey dashed lines indicate the start of UVB irradiation and red lines represent the cut-off of the method (GST-ELISA = 0.2, VLP-ELISA = 300).

As serological read-outs for the MnPV L2/PADRE vaccination efficacy, the seroreactivities against E2 or VLPs were additionally analyzed. Compared to persistently infected unvaccinated *Mastomys*, anti-E2 titers in both unirradiated and irradiated vaccinated animals declined below the cut-off at week 42, indicating that MnPV L2/PADRE vaccination reduced the MnPV infection rate (**Fig. 4.4.1A** and **Fig. 4.4.2A**). The initial appearance of seroconversion against VLPs was observed at week 42 in unirradiated animals and at week 38 in irradiated animals (**Fig. 4.4.2C**). Three of the 16 unirradiated and six of the 18 irradiated vaccinated animals were tested seropositive for anti-VLPs. Of these anti-VLP antibody-positive animals, one unirradiated and two irradiated animals developed skin tumors, suggesting that protective antibodies against MnPV were probably lost in those animals.

4.4.3 Serological Responses in the VLP-vaccinated Group

In a previous study, the VLP-based vaccine could successfully prevent skin tumor formation in virus-bearing *Mastomys* even under immunosuppression [126]. However, it was also important to address whether vaccination with VLPs is also protective under UV irradiation. Therefore, 176 sera from 11 unirradiated animals and 242 sera from 14 irradiated animals in the VLP vaccination group were also examined by GST-ELISA and VLP-ELISA. Of note, since the anti-L2 titers were measured for monitoring the success of L2 immunization and they remained at undetectable or very low levels in the control group, the seroreactivity against L2 was not analyzed in the VLP-vaccinated group.

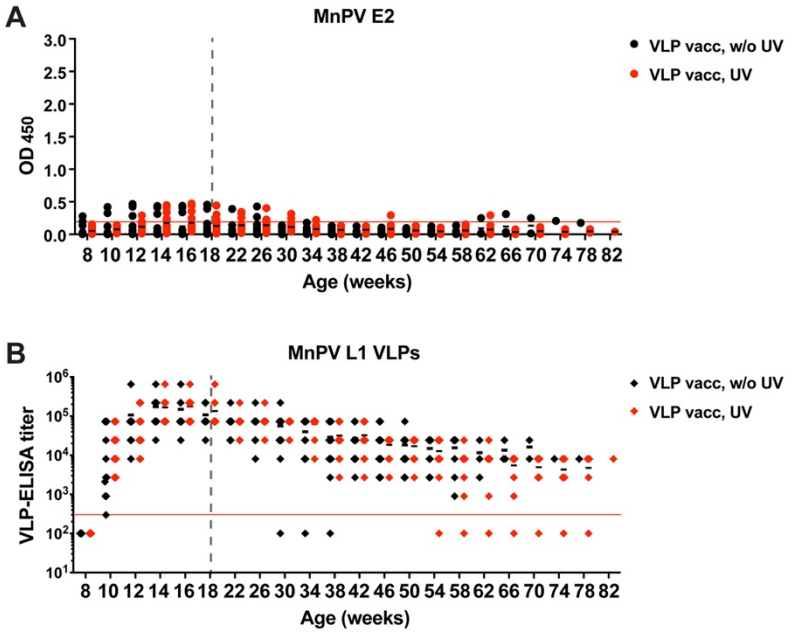

Fig. 4.4.3 Time course of anti-MnPV E2 and -L1 antibody responses in the VLP-vaccinated group. The seroreactivity against MnPV E2 (**A**) was measured by GST-ELISA, and antibodies against VLPs (**B**) were determined by VLP-ELISA. Data are visualized by scattered dots and the mean value is shown as a horizontal line. Black dots and diamonds indicate values of antibodies from VLP-vaccinated animals without irradiation (n = 176), and red dots and diamonds represent values of antibodies from VLP-vaccinated animals with irradiation (n = 242). Grey dashed lines indicate the start of UVB irradiation and red lines represent the cut-off of the method (GST-ELISA = 0.2, VLP-ELISA = 300).

Here, an immediate decrease in the serological response against MnPV E2 after VLP vaccination was also observed (**Fig. 4.4.3A**) when compared to the control group (**Fig. 4.4.1A**). In accordance with previous studies, anti-VLP antibody titers were remarkably induced in all animals and the geometric mean titer reached 1.7×10^5 after the third immunization (**Fig. 4.4.3B**, cut-off = 300). The induction of anti-VLP antibodies correlates with the production of neutralizing antibodies [126]. The seroreactivity against VLPs declined slowly in a time-dependent manner, demonstrating that the antibodies elicited by VLP vaccination are long lasting. Additionally, the UV irradiation did not affect the antibody response.

4.4.4 Correlation Analyses of Antibody Responses

The seroreactivity against E2 did not rapidly diminish in L2-vaccinated animals, additionally, few animals showed slightly higher anti-E2 titers after vaccination (**Fig. 4.4.2A**). Therefore, to further confirm the efficacy of MnPV vaccines, especially that the L2 vaccine can reduce the risk of MnPV infection, correlation analyses were performed between anti-E2 antibody titers and anti-L2/VLP antibody titers in the vaccinated group (**Fig. 4.4.4**). Since the majority of the L2-vaccinated animals was negative for anti-VLP responses and the tumor occurrence in few seropositive animals was already mentioned in section 4.4.2, the correlation of anti-L2 and anti-VLP antibody titers was not evaluated here. Furthermore, considering a possible effect of UV irradiation, correlation analyses were also separated according to whether animals were UV-irradiated or not.

In the L2 vaccination group, as expected, no significant correlation of antibody responses against E2 with L2 in unirradiated (left panel, n = 261 sera, $R^2 = 0.0672$) and irradiated (right panel, n = 287 sera, $R^2 = 0.1535$) animals was found (**Fig. 4.4.4A**). In other words, the increase of anti-L2 titers negatively correlated with the increase of anti-E2 titers. Moreover, the association between anti-E2 antibody titers and anti-VLP antibody titers (**Fig. 4.4.4B**) was also very weak in unirradiated (left panel, n = 176 sera, $R^2 = 0.1332$) and irradiated (right panel, n = 242 sera, $R^2 = 0.1821$) animals of the VLP vaccination group. Hence, these correlation analyses demonstrated that MnPV L2/PADRE or VLP vaccine was able to reduce MnPV infection in naturally infected animals.

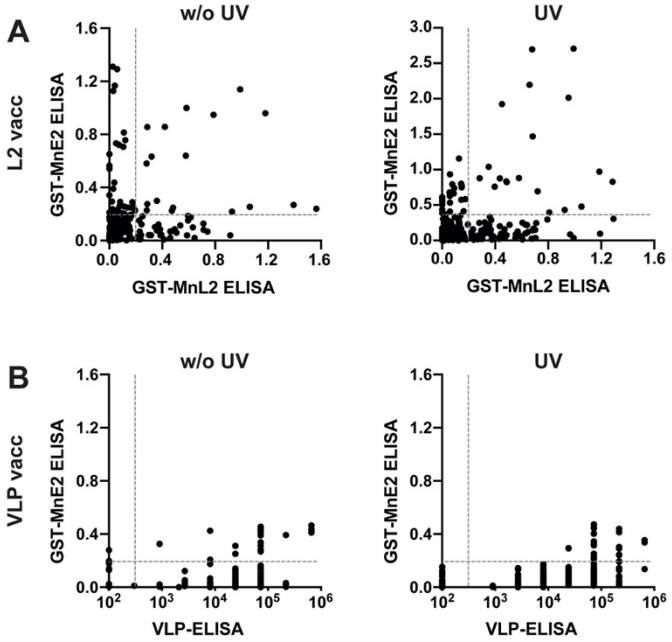

Fig. 4.4.4 Correlation analyses of antibody responses against MnPV E2, L2 and VLPs. (**A**) Correlation between anti E2 antibody titers and anti L2 antibody titers in unirradiated (left panel, n = 261, $R^2 = 0.0672$) and irradiated (right panel, n = 287, $R^2 = 0.1535$) animals of the L2 vaccination (L2 vacc) group. (**B**) Correlation between anti E2 antibody titers and titers of antibodies against VLPs in unirradiated (left panel, n = 176, $R^2 = 0.1332$) and irradiated (right panel, n = 242, $R^2 = 0.1821$) animals of the VLP vaccination (VLP vacc) group. Grey dashed lines indicate the method's cut-off (GST-ELISA = 0.2, VLP-ELISA = 300).

In conclusion, vaccination of naturally infected *Mastomys* with MnPV-L2/PADRE or VLPs elicited a strong anti-L2 or anti-VLP response, respectively, when compared to the control group. Additionally, decreasing anti-E2 responses after vaccination indicate that the MnPV-L2/PADRE and VLP vaccinations suppressed MnPV infection in the virus-bearing colony. Moreover, the rapid decrease of anti-L2 responses revealed that the persistence of anti-L2 antibodies after immunization was not as stable over time in comparison with the anti-VLP antibodies. However, UV irradiation did not affect stability of antibodies raised after immunization with either antigen.

4.5 Incidence of Tumor Development

MnPV VLP-based vaccination was shown to completely prevent papillomavirus-induced skin tumors even under immunosuppressive conditions [126]. Hence, to illustrate the protective efficiency of MnPV L2/VLP vaccines against UV-associated skin cancer, the tumor incidence in unvaccinated and vaccinated animals was assessed. Here, tumors that spontaneously developed on unirradiated areas of animals or in the case of UV-irradiated animals occurred on the shaved area of the back were defined as events in the Kaplan-Meier plot. The statistical analysis was performed using log-rank test.

At the end of the observation period in this study, regarding unirradiated animals, there were 25% tumor-bearing animals in both the control and the L2 vaccination groups, yet 0% in the VLP vaccination group (**Fig. 4.5**). Of the irradiated animals, 37.5% of control, 44.4% of L2- and 23.8% of VLP-vaccinated animals developed skin tumors (**Fig. 4.5**). Since the incidence was less than 50% in all groups, the median age of tumor formation could not be defined by statistical analysis. In accordance with the previous study [125], the appearance of skin tumors occurred earlier in irradiated animals than in unirradiated animals. However, there was no significant difference between unirradiated and irradiated animals of the control ($p = 0.5417$, **Fig. 4.5A**), L2 vaccination ($p = 0.8049$, **Fig. 4.5B**) and VLP vaccination groups ($p = 0.3611$, **Fig. 4.5C**), respectively. Furthermore, the difference between each subgroup was also not statistically significant (**Table 4.5**). Overall, these comparisons could not demonstrate an efficient tumor prevention by vaccination in the context of UV irradiation.

Table 4.5 Comparison of tumor incidence in different vaccination groups. Statistical analysis was performed using log-rank test.

Comparison Group	P-value
ctrl, w/o UV vs. L2 vacc, w/o UV	0.8084
ctrl, w/o UV vs. VLP vacc, w/o UV	0.6171
L2 vacc, w/o UV vs. VLP vacc, w/o UV	0.6171
ctrl, UV vs. L2 vacc, UV	> 0.9999
ctrl, UV vs. VLP vacc, UV	0.845
L2 vacc, UV vs. VLP vacc, UV	0.8888

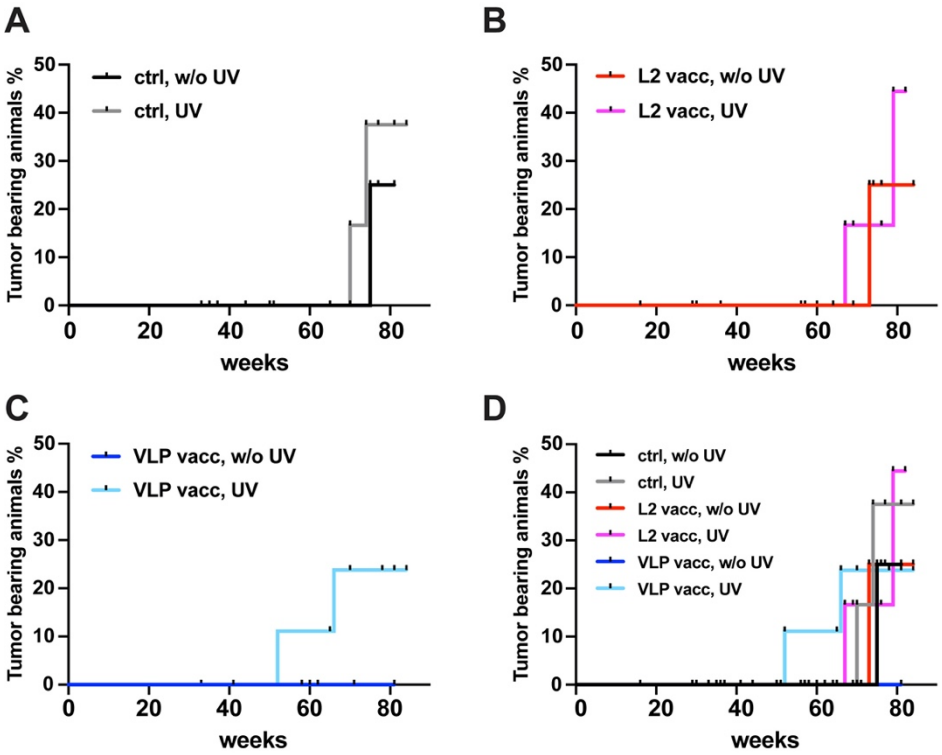

Fig. 4.5 Incidence of tumor development in the different groups. Kaplan-Meier curves show tumor occurrence in animals of control (**A**), L2 vaccination (**B**), VLP vaccination (**C**), and all groups side-by-side (**D**), respectively. The grey, pink and light blue lines represent incidence curves of unirradiated animals and the black, red and dark blue lines indicate incidence curves of irradiated animals in each group. The data of animals that died without developing tumors were censored and shown as small vertical lines.

4.6 Histological Analysis of Spontaneous and UV-induced Tumors

Keratoacanthomas, tongue papillomas, eye papillomas, condylomas as well as squamous cell carcinomas were previously reported in virus-bearing *Mastomys* [121, 148]. A recent study described two distinct types of squamous cell carcinomas in UV-irradiated *Mastomys*: well-differentiated keratinizing SCCs (KSCC) and poorly differentiated non-keratinizing SCCs (nKSCC) [125]. In order to address whether MnPV vaccines can protect against a variety of tumor types under UV conditions, it was essential to characterize the histological features and examine the MnPV DNA status in skin tumors.

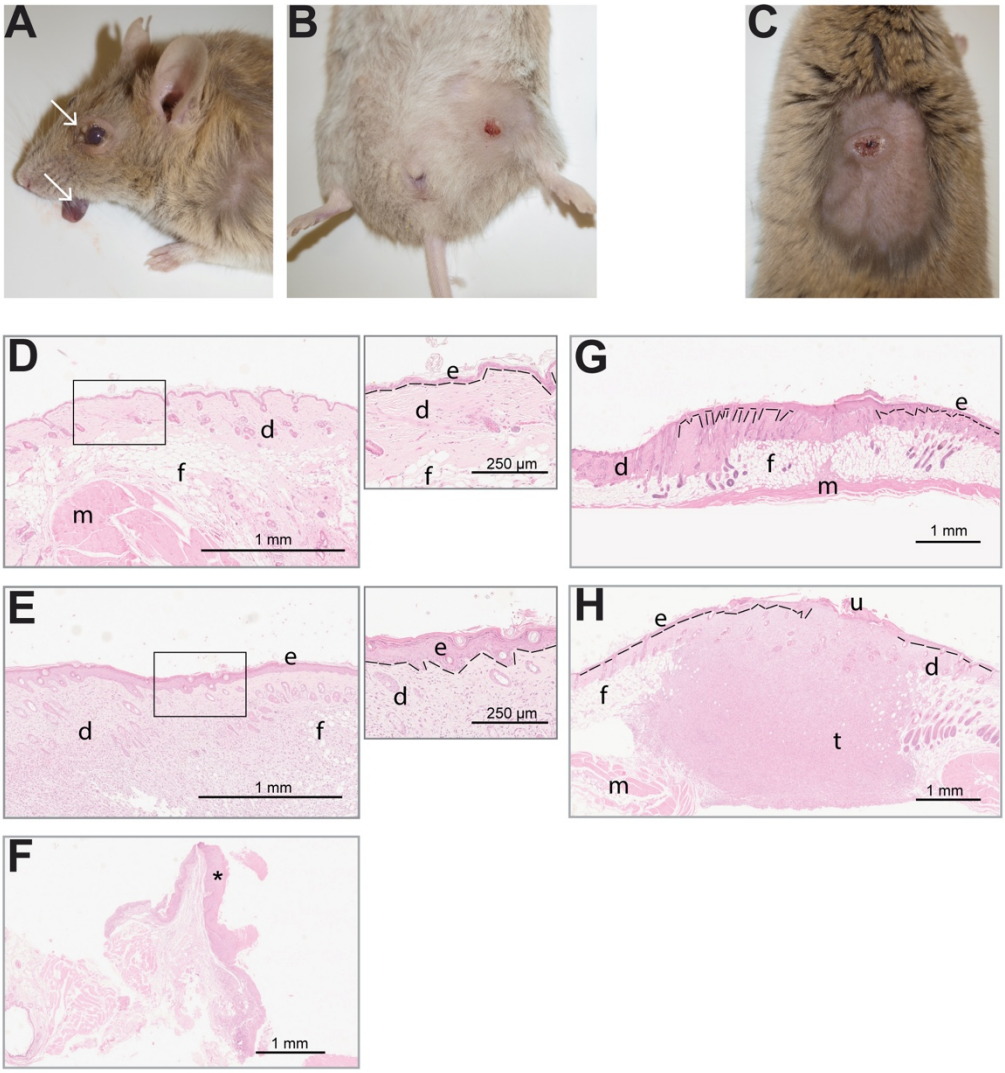

Fig. 4.6 Spontaneous and UV-induced tumors occurring on *Mastomys*. (**A**-**B**) Spontaneous tumors developed on the tongue, eye (indicated by white arrows) and lower abdomen. (**C**) A representative UV-induced tumor on the shaved area of the back. Representative HE-stained sections of normal skin (**D**), UV irradiated skin (**E**), eye tumor (**F**), UV-induced nKSCC with moderate differentiation (**G**) and poorly differentiated nKSCC (**H**). The insets show a higher magnification of respective sections. Dashed lines indicate the border of epidermis and dermis. d: dermis, e: epidermis, f: fat, m: muscle, t: tumor, u: ulcerations, *: dysplastic epithelium. Scale bar = 1 mm.

In this study, irrespective of the different groups, skin tumors spontaneously appeared on the tongue, eye (**Fig. 4.6A**), lower abdomen (**Fig. 4.6B**) and outside of the anus of animals. Also, typically UV-induced tumors were found at the irradiated area of the back (**Fig. 4.6C**). Compared to normal control skin from the same animal (**Fig. 4.6D**), chronic UV exposure led to a thicker epidermis (**Fig. 4.6E**). As depicted in **Fig. 4.6F**, eye papillomas exhibited thickened and hyperproliferative epithelium, which is a common histological feature in papillomavirus-induced lesions [149]. Keratinocyte proliferation and epidermal hyperplasia stimulated by UV may favor viral replication, leading to the formation of well-differentiated KSCC (median = 736.2 MnPV genome copies/cell), which commonly contain a central keratin plug [125]. The occurrence of typical KSCCs was not observed in this study. nKSCCs with

different differentiation grades were found here. The nKSCC with moderate differentiation (28.54 MnPV genome copies/cell) showed that altered keratinocytes invading into the dermis and the epidermis-dermis junction was not obvious (**Fig. 4.6G**). The poorly differentiated nKSCCs with ulcerations were frequently occurred on irradiated animals (**Fig. 4.6C**), which is faster-growing and more aggressive and contains a relatively low viral load (median = 0.020 MnPV genome copies/cell) [125]. The poorly differentiated nKSCC found in this study also displayed an indistinguishable border between epidermis and dermis and tended to infiltrate into the adipose tissue, or even the muscle (**Fig. 4.6H**).

4.7 Effect of MnPV Vaccination on Viral Load

As another read-out for MnPV vaccine efficacy, the viral load was analyzed by qPCR in normal skin and tumor samples obtained from animals after 50 weeks of age. Few animals died early (e.g. the earliest one died at week 16), therefore, vaccine efficacy and the influence of chronic UV exposure were hard to assess. Also, the time of the first tumor appearance was at week 52 in this study (**Fig. 4.5D**), and the increase of MnPV viral load in skin is dependent on the occurrence of tumors in virus-infected animals [121]. Tumors that occurred at the irradiated area (referred to as UV-induced tumor), the other body parts (referred to as non-UV tumor) of the same animal and unirradiated animals (referred to as spontaneous tumor) were examined separately.

Generally, no significant differences were observed between normal skin from unirradiated animals (skin), skin taken from unirradiated area (ctrl skin) and irradiated area (UV skin) of UV-irradiated animals in the control (**Fig. 4.7A**), L2 vaccination (**Fig. 4.7B**) and VLP vaccination (**Fig. 4.7C**) groups. Spontaneous tumors from the L2 vaccination group had a significantly higher viral load when compared to skin ($p = 0.0295$, Kruskal-Wallis test) or ctrl skin ($p = 0.0092$, Kruskal-Wallis test). Of note, all these MnPV-positive tumors were obtained from one single L2-vaccinated animal. The prevalence of MnPV DNA in UV-induced or non-UV tumors in irradiated animals was not remarkably different from other skin samples within the same group. Unfortunately, only one or two samples for each tumor type could be obtained for viral load quantification, due to the low tumor incidence. In order to evaluate the direct impact of the vaccine on virus-bearing animals, the comparison of viral load between skin, ctrl skin and UV skin from the control, L2 vaccination and VLP vaccination groups is shown in **Fig. 4.7D**. There were only statistically significant differences ($p = 0.0235$, Kruskal-Wallis test) between UV skin of control group and UV skin of the L2 vaccination group. Since sample sizes were not big enough, the effect of MnPV L2/PADRE and VLP vaccination on viral load could not be determined here.

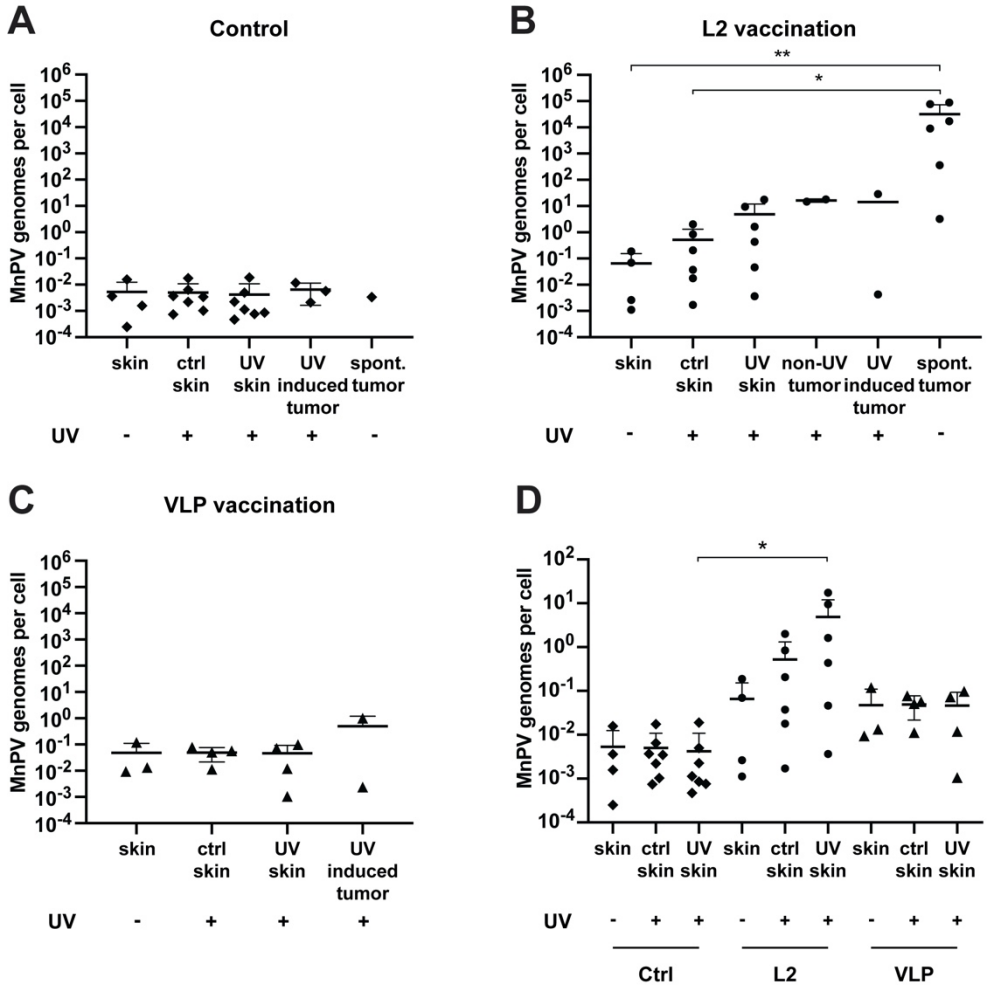

Fig. 4.7 Viral load in tissue specimens. The viral load of different skin samples was analyzed by qPCR (**A**-**D**). All samples were tested in duplicates and normalized to a reference. Scatter dot plots show viral loads with mean ± SD indicated. UV+/- represents whether animals were exposed to UV or not. skin: normal skin from unirradiated animals; ctrl skin: skin taken from unirradiated areas of UV-irradiated animals; UV skin: skin obtained from irradiated area of UV-irradiated animals; spont. tumor: tumors developed in unirradiated animals; non-UV tumor: tumors developed in unirradiated area of UV-irradiated animals; UV induced tumor: tumors occurred on UV-irradiated area. Statistical analysis was performed using non-parametric Kruskal-Wallis test followed by Dunn's multiple comparison test. * $p < 0.05$, ** $p < 0.01$.

As shown in **Table 4.7**, in the control group, one out of 16 (6.3%) unirradiated animals developed a spontaneous tumor and it was found at the abdomen but only harbored a very low viral load of MnPV (0.00339 MnPV genomes/cell). Two out of 19 irradiated animals (10.5%) developed three UV-induced nKSCCs tumors with a low MnPV load (mean of viral load = 0.00654 ± 0.00399). In the MnPV L2/PADRE vaccination group, one out of 16 (6.3%) unirradiated animal developed eye and tongue papillomas with a significantly high viral load (mean of viral load = 32087.93 ± 36610.78). nKSCCs with different differentiation grades occurred in two out of 18 (11.1%) irradiated animals (mean of viral load = 14.27 ± 14.27). Additionally, one irradiated animal of this group developed condylomas (mean of viral load = 16.26 ± 1.59). As for the VLP vaccination group, unsurprisingly, no tumors were observed in

unirradiated animals, which is consistent with the previous study [126]. However, two out of 14 (14.3%) irradiated animals developed nKSCCs after vaccination (mean of viral load = 0.49951 ± 0.49715). Furthermore, nKSCCs were the predominant type of UV-induced tumors in both unvaccinated and vaccinated animals.

Table 4.7 Summary of tumor incidences and MnPV viral loads in different tissue specimens.

Group	Tumor Incidence rate % (n)	Sample	Range (genomes/cell)	Mean (genomes/cell)
Control	UV-: 6.3% (1/16)	skin	0.00025 - 0.01577	0.00530
		spontaneous tumor	0.00339	
	UV+: 10.5% (2/19)	control skin	0.00074 - 0.01758	0.00503
		UV skin	0.00047 - 0.01891	0.00420
		UV-induced tumor	0.00212 - 0.01179	0.00654
MnPV L2/PADRE	UV-: 6.3% (1/16)	skin	0.00112 - 0.18764	0.06535
		spontaneous tumor	3.20070 - 88961.69281	32087.92785
	UV+: 11.1% (2/18)	control skin	0.00170 - 2.00682	0.51784
		UV skin	0.00364 - 17.48565	4.83607
		non-UV tumor	14.67164 - 17.84932	16.26048
		UV-induced tumor	0.00426 - 28.54415	14.274205
VLP	UV-: 0% (0/11)	skin	0.00938 - 0.11965	0.04744
	UV+: 14.3% (2/14)	control skin	0.01126 - 0.07730	0.04922
		UV skin	0.00105 - 0.09819	0.04598
		UV-induced tumor	0.00236 - 0.99665	0.49951

In summary, MnPV L2/PADRE vaccination apparently did not prevent the formation of eye papillomas, tongue papillomas or condylomas. In addition, vaccination with MnPV L2/PADRE or VLPs did not prevent the development of UV-induced nKSCCs, where the MnPV viral load was low or undetectable.

4.8 Establishment of an *in vitro* Model for MnPV Infection

4.8.1 Maintenance of Viral Genomes and Transcripts in Murine 308 Keratinocytes

Despite rising evidences for the role of cutaneous HPVs in skin carcinogenesis, their exact mode of action is still not fully understood. Furthermore, since cutaneous PVs do not persist in cell culture systems, investigations of them are hampered and therefore E6/E7-transduced cell lines are usually used as substitute [150]. However, in these systems PV gene expression is not regulated by the natural viral promotor.

Therefore, to establish an *in vitro* system, the murine 308 keratinocyte cell line derived from Balb/c mouse back skin (contains mutated but activated *Hras* and wildtype *Tp53*) was used [138]. The establishment and initial characterization were done by Dr. D. Hasche. For infection of 308 cells, frozen tissue from naturally occurring *Mastomys* skin lesions was homogenized (**Fig. 4.8.1A**) and cleared supernatant that contained intact MnPV virions was further used (**Fig. 4.8.1B**). Infection with tumor extracts was performed for 24 h, and afterwards cells were passaged every two or three days after infection (eight passages in total). In order to analyze the maintenance of viral genomes, a portion of infected 308 cells was harvested at each passage. The latent infection of 308 keratinocytes was detected for up to 16 days and quantified by qPCR on the late gene *L1* similar to the method used *in vivo* (**Fig. 4.8.1C** and **D**). Infected 308 cells initially harbored up to 84 MnPV copies per cell, however, the viral load decreased after passage 5 (P5, less than 10 copies/cell), indicating that the MnPV infection was not persistent in the murine 308 cell line. Next, to test whether the viral genomes were transcriptionally active in the cells, the detection of viral transcripts from both the early (*E6, E1^E4*) and the late (*E1^E4, L1*) promoter was performed by semi-quantitative RT-PCR. As expected, *E1^E4*, which is the most abundant viral transcript found in naturally developed tumors [127] and *E6* transcripts were detected in 308 cells post infection, showing that isolated MnPV virions efficiently infected the murine 308 keratinocytes (**Fig. 4.8.1E**). Notably, activation of the viral late promotor was confirmed by a significant increase of *L1* transcripts in early passages (P1-P3), a gene that is tightly controlled and activated in a differentiation-dependent manner [151]. However, the viral transcripts decreased with higher passages, which correlated with the maintenance of viral genomes as shown in **Fig. 4.8.1C** and **D**. With this short-term *in vitro* infection system, it is possible to explore the underlying mechanisms of the naturally regulated MnPV gene expression, their effects on the host cell during initial virus infection and cell responses to extracellular stress (e.g. differentiation and UV irradiation).

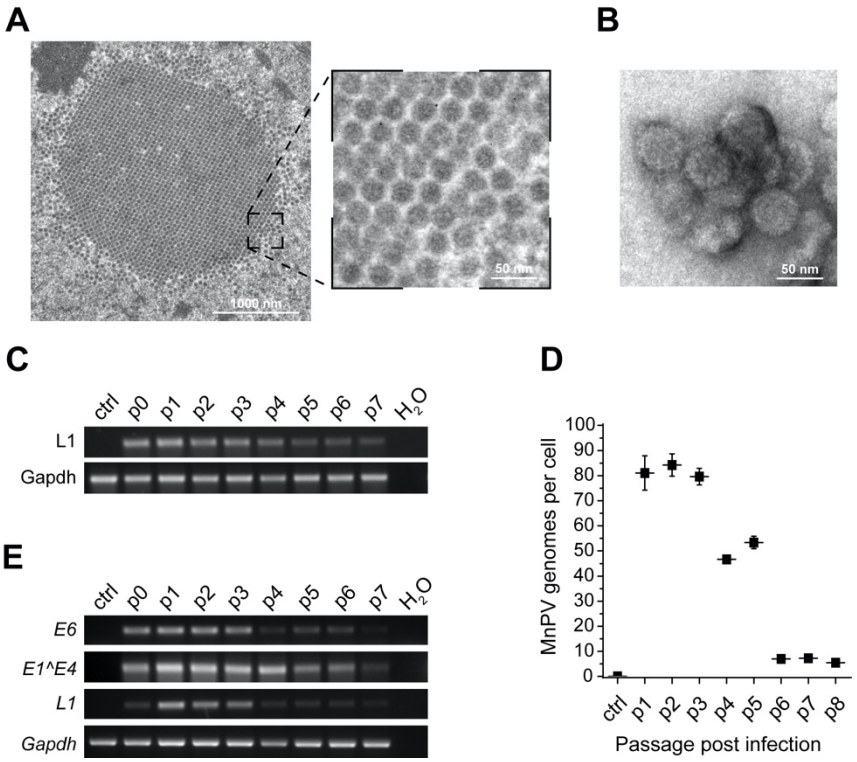

Fig. 4.8.1 Establishment of an *in vitro* model for MnPV infection. (**A**) Representative electron microscopy negative staining image shows numerous virus particles with uniform size (55 nm) within a MnPV-induced papilloma. 308 cells were infected with *Mastomys*-derived tumor extracts containing intact MnPV virions (**B**) for 24 h. (**C**) MnPV genomes are detectable by semi-quantitative PCR in infected 308 cells for eight passages (ca. 16 days). (**D**) Quantification of MnPV loads via qPCR correlates with the pattern shown in (**C**). The number of MnPV genomes was normalized to the single copy gene *Hbb*. Genomic DNA from uninfected 308 cells was used as control (ctrl). (**E**) RT-PCR of viral transcripts. RNA was isolated from each passage and *E6*, *E1^E4* and *L1* were detected by semi-quantitative RT-PCR after reverse transcription (P0 represents samples harvested 24 h post infection). *Gapdh* was used as a reference gene. These figures were provided by Dr. D. Hasche.

4.8.2 The Half-live of MnPV Transcripts

As already reported, the genome of MnPV remained episomal in naturally occurring tumors, corresponding to cutaneous HPVs [127]. In addition, the stability of viral mRNAs is tightly associated with the viral life cycle and influences virus-host interactions. Since the *in vitro* system is supposed to also be used to investigate the impact of UV irradiation, which globally affects cellular and viral mRNAs, the basal half-life of MnPV transcripts had to be analyzed. Therefore, 308 cells were treated with Actinomycin D (ActD), an inhibitor of transcription, for 1, 2, 4 and 8 h, respectively. The decay rates of viral mRNA (*E1^E4*, *E6*, *E7* and *L1*) were quantified by qRT-PCR (**Fig. 4.8.2A**). The half-life (defined as the time point where the initial amount of mRNA is reduced by 50%) of the different viral transcripts was calculated based on the equation: $t_{1/2} = \ln 2 / k_{decay}$ (**Fig. 4.8.2B**). The mRNA half-lives of *E1^E4*, *E6*, *E7* and *L1* were 1.74 h, 2.71 h, 2.58 h and 5.14 h, respectively. These results showed that the stability varied among different MnPV transcripts: *E1^E4* transcripts were the least stable while *L1* transcripts

were the most stable. Since encoded by a polycistronic transcript [127], *E6* and *E7* showed the same decay pattern after ActD treatment.

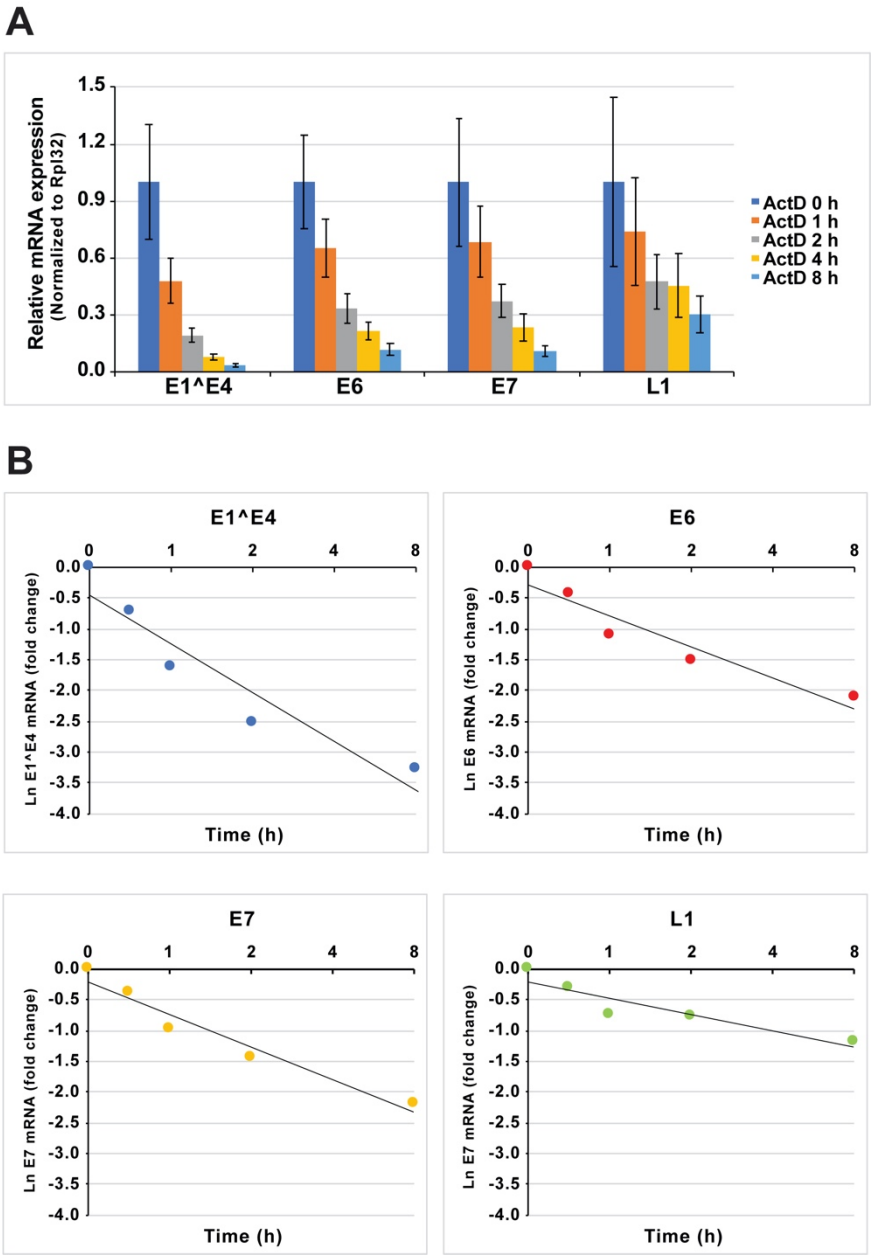

Fig. 4.8.2 Determination of the half-lives of different MnPV mRNAs. (**A**) Infected 308 cells were treated with 5 µg/ml Actinomycin D (ActD) for 0, 1, 2, 4 and 8 h prior to RNA extraction. Viral transcripts were measured by qRT-PCR at indicated times after addition of ActD. The results are shown as a ratio to the base line value measured before ActD addition (in natural logarithmic scale). Data are normalized to *Rpl32*, and represented as mean ± SD of six independent experiments. (**B**) The half-lives of MnPV mRNAs were calculated from data shown in (**A**) based on first order kinetics ($t_{1/2} = \ln 2 / k_{decay}$).

4.8.3 Analysis of Viral Early Protein E4 in Infected 308 Keratinocytes

As next, it was of interest to investigate whether the viral transcripts were also translated in this *in vitro* model system. For this purpose, a monoclonal antibody against MnPV E4, which recognizes 40 amino acids within the E4 region, was produced in our lab, allowing to study of naturally regulated MnPV protein production. The full-length MnPV E1^E4 contains 266 amino acids, with a calculated molecular weight of 31 kDa. In Western blot analysis of MnPV-infected cells, it could be detected with a major band close to 40 kDa using the anti-E4 monoclonal antibody (**Fig. 4.8.3A**). The early protein E4 of several HPV types has been reported to be localized in the cytoplasm, the nucleus or the perinuclear space, altering its function during infection [37]. Here, by immunofluorescence staining, it was possible to detect MnPV E4 in the cytoplasm (**Fig. 4.8.3B**), which was essential for further functional analyses. Moreover, the detection of the E4 protein in infected 308 cells suggested that the viral early protein E4 could serve as a potential marker of MnPV infection both *in vitro* and *in vivo*.

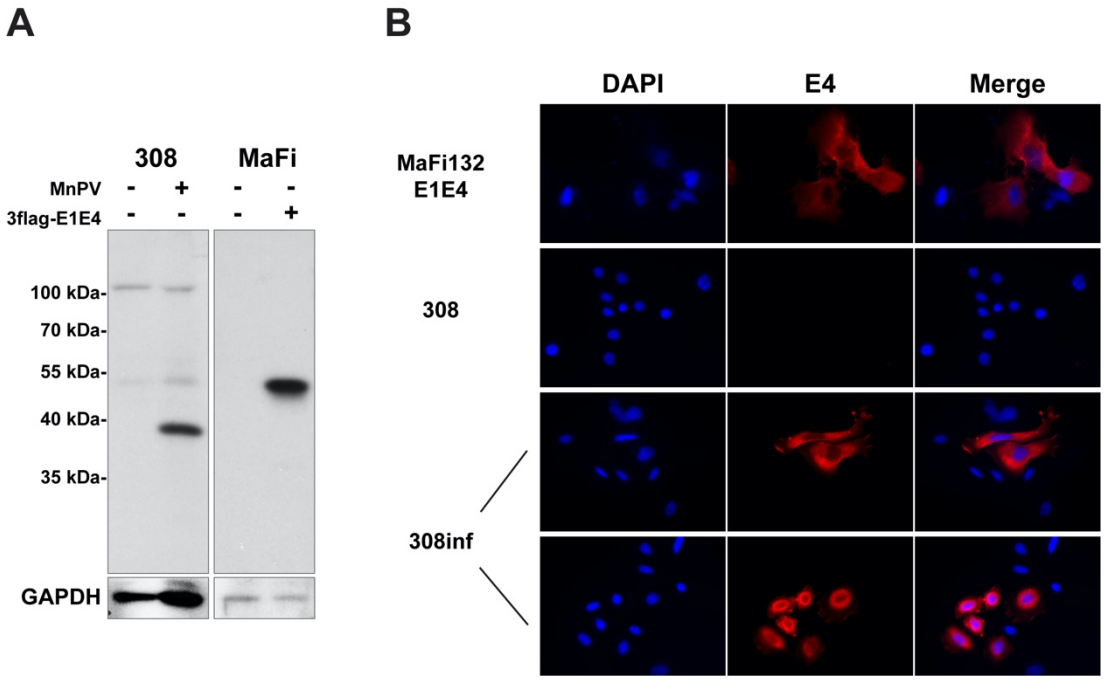

Fig. 4.8.3 Detection of MnPV E4 protein in infected murine 308 keratinocytes. (**A**) The product of the *E1^E4* transcript was detected in MnPV-infected 308 cells by using a self-made monoclonal anti-E4 antibody. Lysate of MaFi132 (*Mastomys coucha*-derived fibroblasts) transfected with a plasmid that encodes full-length *E1^E4* mRNA served as a control and was incubated with an anti-flag antibody (Note that the size differences in the control are due to the additional flag tags). GAPDH was used as a loading control. (**B**) Intracellular localization of MnPV E4 in infected 308 cells (308inf) was visualized by immunofluorescence. Cells were stained with anti-E4 monoclonal antibody and anti-mouse IgG conjugated with Alexa 594 (red). Nuclei were counterstained with DAPI (blue). Images were acquired with a Zeiss Cell observer equipped with a 40 ×/0.75 EC PlnN Ph2 air objective lens.

4.8.4 Analysis of Viral Early Protein E7 in Infected 308 Keratinocytes

Provided that the function of E7 varies among cutaneous papillomaviruses, the availability of a monoclonal antibody against viral early protein E7 would enable to investigate the role of MnPV E7 involved in skin carcinogenesis. Western blot analyses of infected 308 cells using a homemade anti-E7 monoclonal antibody however still need to be optimized. As shown in **Fig. 4.8.4**, the mainly nuclear and partially cytoplasmic distribution of E7 was observed in MaFi191 cells transfected with a plasmid that encodes full-length *E7* mRNA as a control. Of note, as describe previously, MaFi132 fibroblasts harbor *Tp53* mutations, resulting the loss of p53 in the late-passage MaFi132 [132]. Another *Mastomys coucha*-derived fibroblast cell line, namely MaFi191 which was freshly established and contains wildtype *Tp53*, served as a control for antibody specificity. Interestingly, the subcellular localization of MnPV E7 in infected 308 keratinocytes was also found in both nucleus and cytoplasm in some MnPV E7-positive cells, while others showed a predominantly cytoplasmic distribution. However, all the observations are in conformity with the expression pattern of reported high-risk HPV E7 [27].

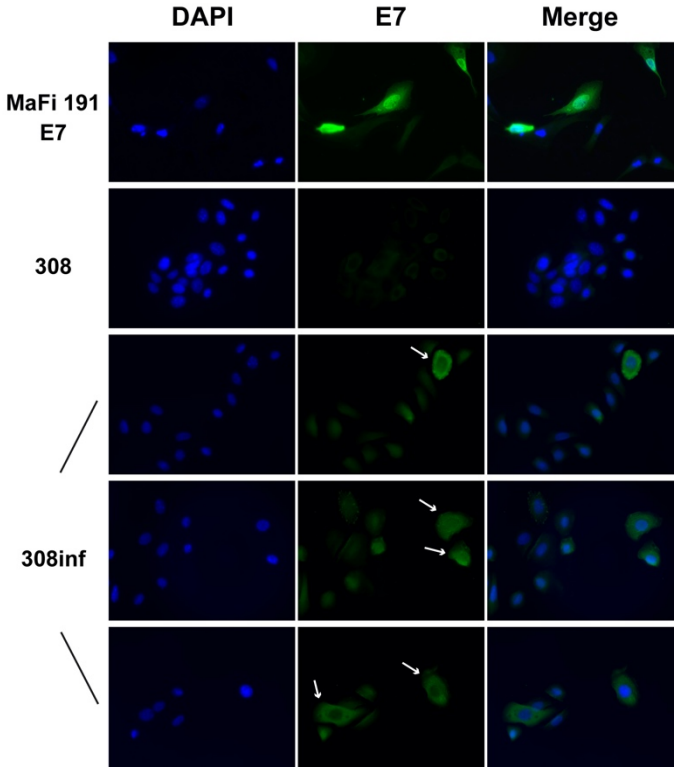

Fig. 4.8.4 Localization of MnPV E7 protein in infected murine 308 keratinocytes. Intracellular localization of MnPV E7 in infected 308 cells (308inf) was visualized by immunofluorescence. Cells were stained with anti-E7 monoclonal antibody and anti-mouse IgG conjugated with Alexa 488 (green). Nuclei were counterstained with DAPI (blue). MaFi191 transfected with full-length *E7* mRNA served as a control to ensure antibody reactivity. The white arrows indicate 308inf expressing *E7*. Images were acquired with a Zeiss Cell observer equipped with a 40 ×/0.75 EC PlnN Ph2 air objective lens.

4.9 The Effect of Differentiation and UV Exposure on Infected 308 Keratinocytes

4.9.1 Optimization of Differentiation Conditions for 308 Keratinocytes

Unlike undifferentiated primary keratinocytes, the murine 308 cell line was selected against a high concentration of calcium (1.4 mM) to prevent terminal differentiation [138]. However, several studies reported that 308 cells can be differentiated with even higher concentrations of calcium alone or supplemented with staurosporine or ionomycin, which was confirmed by increased expression of differentiation makers [152-154]. From this finding, several questions arose: 1) Can murine 308 cells be committed to terminal differentiation via differentiation inducers (e.g. calcium or methylcellulose)? 2) If so, are islands of cells in close contact capable of differentiation? 3) Is the detection of MnPV *L1* late transcripts in this *in vitro* system due to those islands of cells? Since it is known that expression of *L1* is tightly controlled by epithelial differentiation. Therefore, it was hypothesized that the detection of L1 transcripts (see **Fig. 4.8.1E**) might be largely due to the differentiation of infected cells with close contact.

However, as mentioned above, the murine 308 cell line was selected against high concentration of Ca^{2+}. Therefore, in order to answer the abovementioned questions, it was necessary to optimize differentiation conditions in this system. Here, 308 cells were incubated with different concentrations of Ca^{2+} or 2% methylcellulose (MC), which is commonly used for the induction of differentiation *in vitro*, for 48 h. In addition, cells were seeded with distinct densities (3×10^5 or 9×10^5 cells per 6 cm dish, referred to as low or high confluence, respectively). Cell density was demonstrated to influence the differentiation status of keratinocytes, as a high confluence would increase cell-to-cell interactions to induce keratinocyte differentiation, which is mediated by cadherin [155, 156]. After treatment, the upregulated expression of the terminal differentiation makers Involucrin and Loricrin was observed in highly confluent cells compared to low confluence ones (**Fig. 4.9.1A** and **B**). Moreover, the low and high confluence cells were induced to differentiate with additional calcium in culture medium. This phenomenon was more pronounced at higher confluency when cells were treated with calcium, especially at a concentration of 2.8 mM, demonstrated by stronger induction of Involucrin and Loricrin (**Fig. 4.9.1B**). The levels of Involucrin and Loricrin were also increased when 308 cells were suspended in 2% MC, where the cell-to-cell contact was lost (**Fig. 4.9.1C**). Here, Vinculin was used as a loading control in Western blot analysis. Although, the levels of Vinculin varied remarkably among different settings, confirming that the 2% MC treatment can significantly change the protein profile of 308 keratinocytes, it was still the best loading control of the ones tested (e.g. Actin, not shown).

In conclusion, increased cell-to-cell contact and differentiation inducers activated differentiation of 308 cells. Culture medium with the addition of 2.8 mM Ca^{2+} and 2% MC was therefore applied for further experiments.

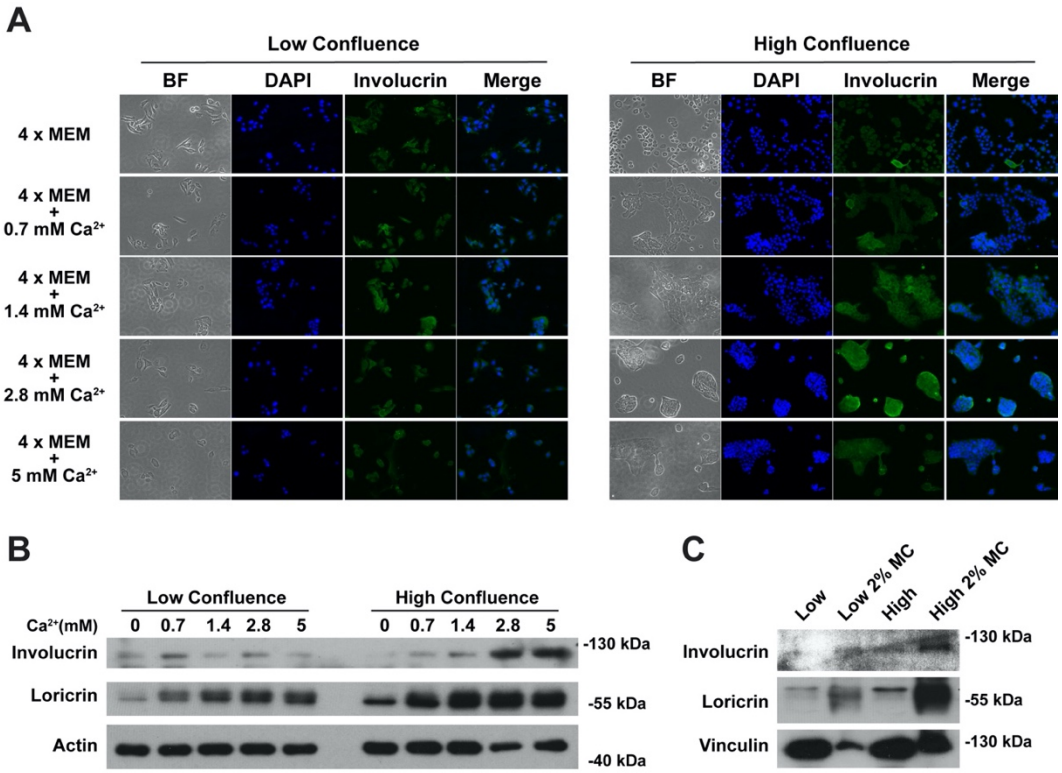

Fig. 4.9.1 Induction of differentiation in 308 cells. 308 cells were seeded with distinct densities (low or high confluence) and treated with different concentrations (0.7, 1.4, 2.8 and 5 mM) of calcium (Ca^{2+}) or 2% methylcellulose (MC) for 48 h. (**A**) Cells were incubated with anti-Involucrin antibody and anti-rabbit IgG conjugated with Alexa 488 (green). Nuclei were counterstained with DAPI (blue). Images were acquired by a Zeiss Cell observer equipped with a 20 ×/0.4 LD PlnN Ph2 air objective lens. (**B** and **C**) Involucrin and Loricrin protein levels were analyzed by Western blot. Actin (**B**) and Vinculin (**C**) were used as loading controls.

4.9.2 Induction of Differentiation in Infected 308 Keratinocytes

Next, MnPV-infected 308 cells were differentiated. Briefly, infected cells were seeded with low or high confluence, and cells with higher density were treated with 2.8 mM Ca^{2+} or suspended in 2% MC culture medium for 48 h. As depicted in **Fig. 4.9.2A**, the undergoing differentiation was indicated by increased levels of Involucrin and Loricrin in Western blot. The induction of terminal differentiation induced by 2% MC was more potent in comparison with calcium treatment. Moreover, the levels of the E4 protein were not obviously changed during differentiation, which was also confirmed by the unchanged levels of *E1^E4* transcripts determined by qRT-PCR (**Fig. 4.9.2B**). Meanwhile, other viral early (*E6* and *E7*) and late (*L1*) transcripts were also measured. Similar to *E1^E4*, post differentiation, the mRNAs of *E6* and *E7* were not expressed differently in infected 308 cells. These data show that the expression of *E6* and *E7* from the viral early promoter as well as *E1^E4* controlled by both the viral early and later promoter seemingly does not respond to the calcium- or MC- mediated differentiation. In contrast, there was a trend of up-regulation of *L1* mRNA in differentiated infected keratinocytes. This suggests

that a potential differentiation-regulated activation of *L1* arose from the late promoter in this *in vitro* infection model.

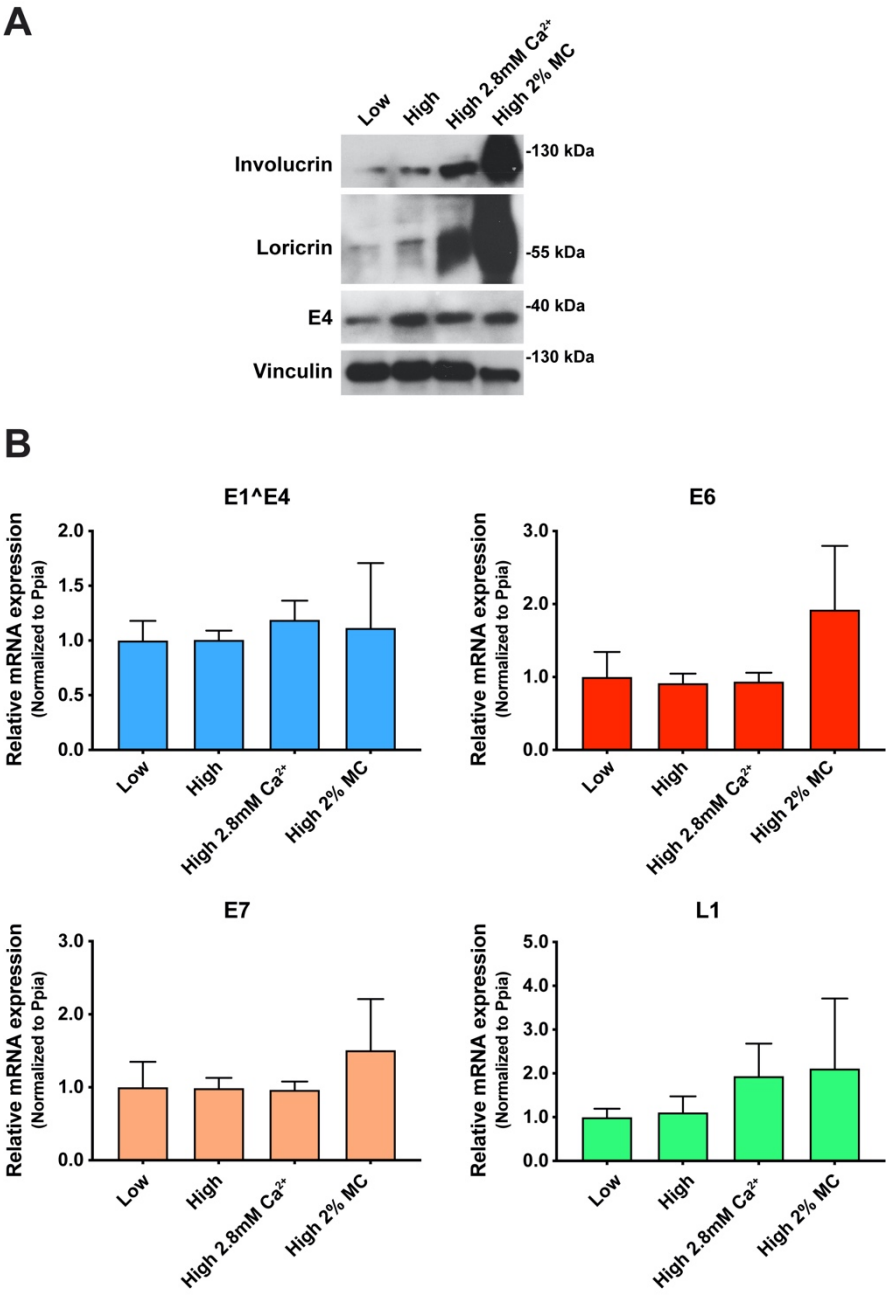

Fig. 4.9.2 Induction of differentiation in infected 308 cells. (**A**) Infected 308 cells were seeded with distinct densities (low or high confluence) and cells with high confluence were treated with 2.8 mM calcium (Ca^{2+}) or 2% methylcellulose (MC) for 48 h. Involucrin, Loricrin and E4 protein levels were assessed by Western blot. Vinculin was used as a loading control. (**B**) The relative abundance of MnPV transcripts (*E1^E4*, *E6*, *E7* and *L1*) was quantified by qRT-PCR. Data were normalized to *Ppia* and represented as mean ± SD of three independent experiments (High 2% MC includes data from two independent experiments).

4.9.3 Characterization of Antibodies against Different MnPV L1 Isoforms

As abovementioned, an increase of *L1* mRNA was observed after differentiation. Additionally, seroconversion against various MnPV L1 isoforms (defined as $L1_{short}$, $L1_{middle}$ and $L1_{long}$, expressed from different start codons within *L1* ORFs) during different life stages of *Mastomys* were detected by GST-ELISA, suggesting a possible immune escape mechanism of MnPV infection [140]. Therefore, it was interesting to explore whether these isoforms were also differentially produced in the infected 308 keratinocytes.

Previously, three monoclonal antibodies (mAb 2E2, mAb 2D11 and mAb 3H8) against conformational epitopes of $L1_{short}$ and two monoclonal (mAb 2D6 and mAb 5E5) against linear epitopes were produced and analyzed by native and denatured ELISA[140]. However, only mAb 2D11 and mAb 3H8 were able to detect the same single band in Western blot analysis (data not shown). In addition, serum mix, which is sera from five tumor-bearing MnPV-positive animals, showed positive signals in the detection of all three L1 isoforms by GST-ELISA. To further characterize the specificity and sensitivity of aforementioned antibodies, MaFi132 cells were transfected with HA-tagged plasmids encoding humanized MnPV $L1_{short}$, $L1_{middle}$, $L1_{long}$ as well as genuine viral full-length of *L1* ORFs ($L1_{wt}$) that can putatively express all three L1 isoforms for 48 h. The expression of MnPV L1 isoforms was visualized by immunofluorescence. Cells transfected with $L1_{short}$ or $L1_{wt}$ showed positive staining using mAb 2D11, serum mix or anti-HA antibody as primary antibody (**Fig. 4.9.3A**, **B** and **C**), while the expression of $L1_{middle}$ or $L1_{long}$ was only detectable when serum mix or anti-HA antibody were applied (**Fig. 4.9.3B** and **C**). Therefore, mAb 2D11 can be used to detect $L1_{short}$ and $L1_{wt}$, while serum mix can react with all L1 isoforms.

Consistent with immunofluorescence results, in Western blot (**Fig. 4.9.3D**, upper panel), detection with the mAb 2D11 displayed one prominent band below 250 kDa in the lysates in which $L1_{short}$ or $L1_{wt}$ were expressed. Serum mix reacted with the monomer of $L1_{short}$ (approximately 55 kDa), $L1_{middle}$ (58 kDa) and $L1_{long}$ (60 kDa). Interestingly, by comparing the band sizes and intensities, the presence of $L1_{short}$ and $L1_{long}$, but not $L1_{middle}$, was detected in cells transfected with $L1_{wt}$ using serum mix and the levels of $L1_{short}$ were higher than those of $L1_{long}$. Moreover, the reactivity of serum mix with the band below 250 kDa, as with mAb 2D11, was also detected in both $L1_{short}$ and $L1_{wt}$. Furthermore, serum mix detected an additional band above 100 kDa in lysates containing $L1_{short.}$ The observation of bands of large molecular weights and mAb 2D11-positive staining for $L1_{short}$ and $L1_{wt}$ suggested the formation of higher order structures in MaFi132 transfected with $L1_{short}$ or $L1_{wt}$. Therefore, to verify whether these two bands represent accumulation of the dimeric and trimeric MnPV L1, comparable to sizes of HPV16 and BPV1 [54, 157], additional DTT and β-mercaptoethanol were added to cell lysates prior to incubation for 1 h at room temperature and heating at 95 °C for 10 min. In principle, this harsh denaturation condition can disrupt disulfide bonds, which are essential for the maturation of papillomavirus capsids. After the

treatment, the two high molecular weight bands disappeared while the monomers were still detectable (**Fig. 4.9.3D**, lower panel), demonstrating that mAb 2D11 specifically detects L1 trimer and serum mix can be used for the detection of L1 monomers, dimers and trimers.

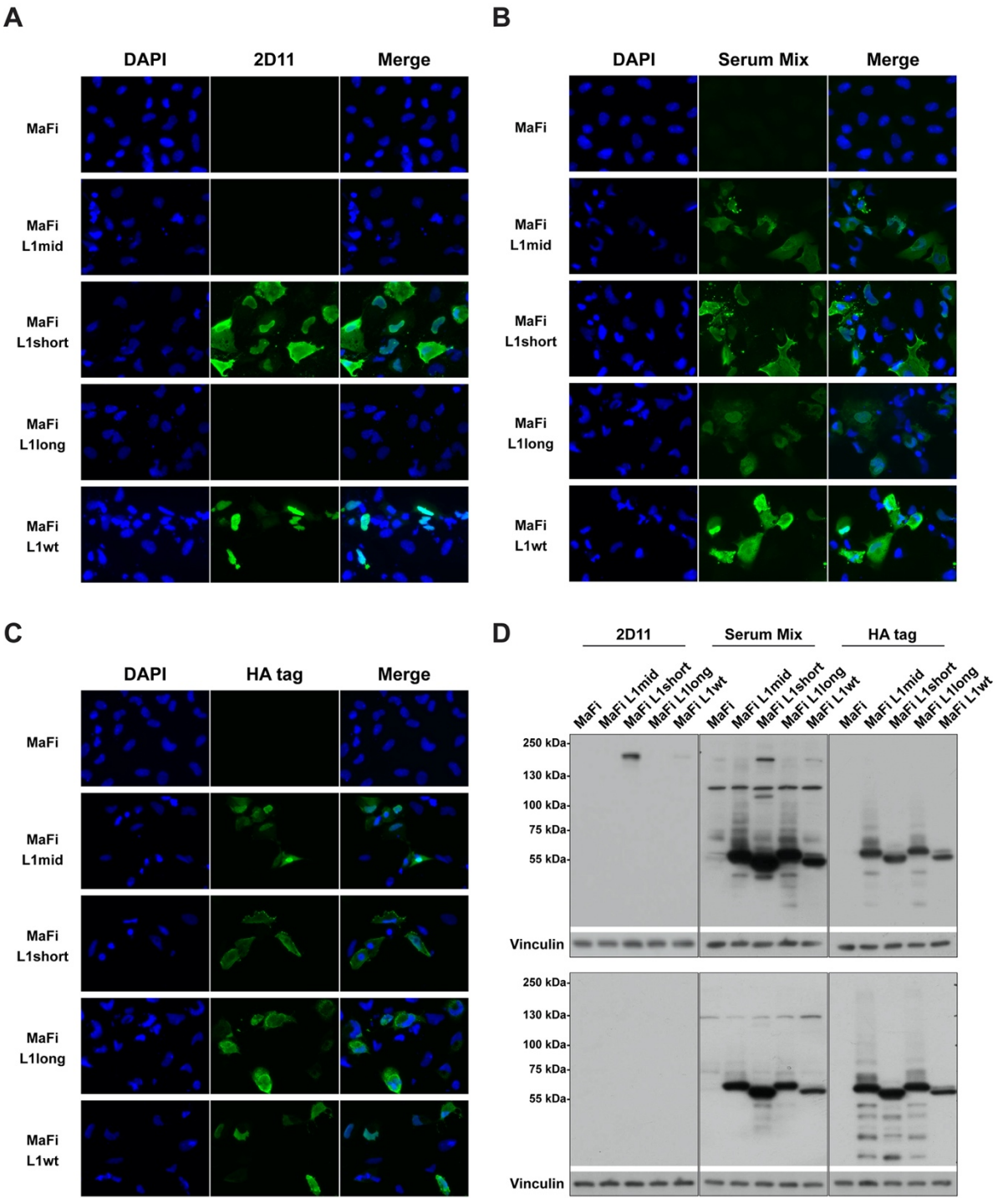

Fig. 4.9.3 Expression of different MnPV L1 isoforms in MaFi132 cells. MaFi132 cells were transfected with HA-tagged $L1_{short}$, $L1_{middle}$ or $L1_{long}$ (humanized codons), or $L1_{wt}$ (encodes the genuine viral full-length of *L1* ORFs possibly expressing three L1 isoforms). Presence of L1 isoforms was visualized by immunofluorescence with mAb 2D11 (**A**), serum mix (**B**) and anti-HA antibody (**C**). Nuclei were stained with DAPI (blue). Images were acquired by a Zeiss Cell observer equipped with a 40 ×/0.75 EC PlnN Ph2 air objective lens. (**D**) The abundance of different L1 isoforms and the same cell lysate after harsh denaturation are assessed by Western blot using antibody 2D11, serum mix or anti-HA antibody. Vinculin was used as a loading control. Partial results of the presented figure have been published in [140].

4.9.4 MnPV L1 Protein Production Varies during Keratinocyte Differentiation

As shown previously, the levels of MnPV $L1_{short}$ and $L1_{long}$ differ in transfected MaFi132 cells. MnPV $L1_{long}$ encodes additional 31 amino acids compared to $L1_{short}$ but cannot form capsids *in vitro* and *in vivo* [140]. Therefore, to explore whether different MnPV L1 isoforms can be induced in differentiated 308 cells with the abovementioned protocol, 308 cells were transiently transfected with humanized MnPV $L1_{short}$ and $L1_{long}$ under control of a CMV promoter for 24 h. Subsequently, transfected cells were subjected to differentiation by high cell density, 2.8 mM Ca^{2+} or 2% MC. Interestingly, MnPV $L1_{short}$ and $L1_{long}$ showed different protein amounts after treatments (**Fig. 4.9.4**). As expected, keratinocyte differentiation increased $L1_{short}$ protein levels, particularly a strong induction of $L1_{short}$ was found in cells suspended in MC. However, increased cell-to-cell contact, high dose Ca^{2+} concentration or suspension in MC could not enhance the levels of $L1_{long}$ compared to $L1_{short}$.

Here, the protein level of Histone H3 (di methyl K4) served a s a loading control in Western blot analysis since it was relatively stable in MC-treated cells. However, it has been reported that HPV31 can affect the protein levels of several post-translationally modified histones, including Histone H3 (di methyl K4) [158]. Therefore, the loading control was changed to Vinculin in infected cells in further experiments.

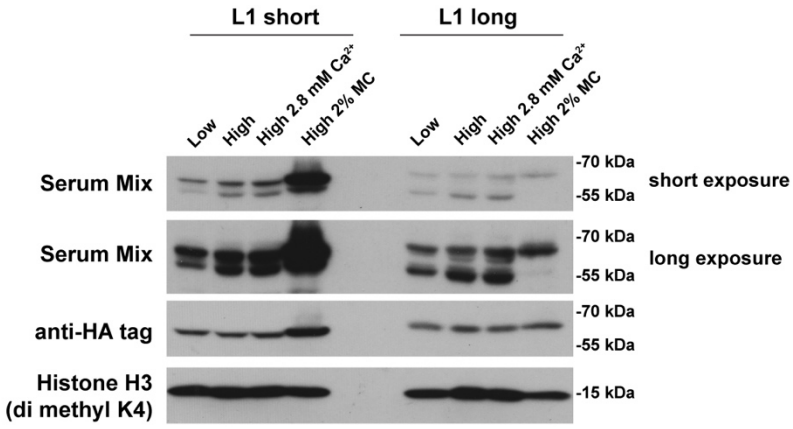

Fig. 4.9.4 Protein levels of transfected L1 in differentiated 308 cells. 308 cells were transfected with MnPV $L1_{short}$ or $L1_{long}$ for 24 h, afterwards, seeded with distinct densities (low or high confluence) and treated with 2.8 mM calcium (Ca^{2+}) or 2% methylcellulose (MC) for 48 h. The abundance of transfected $L1_{short}$ or $L1_{long}$ was assessed by Western blot using serum mix and anti-HA tag as primary antibodies. Histone H3 (di methyl K4) was used as a loading control.

In addition, keratinocytes transfected with $L1_{wt}$ were also subjected to differentiation by calcium and MC treatment, however, probably due to the extremely low protein levels, it was hard to distinguish the difference between $L1_{short}$ and $L1_{long}$ (data not shown).

Furthermore, calcium and methylcellulose were applied to differentiate infected cells for the detection of L1 protein. Unfortunately, strong unspecific bands were detected using serum mix as primary antibody. Also, mAb 2D11 was used to examine the presence of L1 protein in infected 308 cells by immunofluorescence, but again, no positive staining was found (data not shown).

To sum up, $L1_{short}$, but not $L1_{long}$, protein levels were induced in differentiated keratinocytes. However, all isoforms of MnPV L1 protein remained at relatively low levels in the *in vitro* infection system. Hence, more specific and sensitive antibodies against various MnPV L1 isoforms are required for further analyses.

4.9.5 The Impact of UV Irradiation on Viral Transcripts and E4 Protein Levels

UV irradiation affects the seroconversion in naturally infected *Mastomys*, and causes the formation of well-differentiated KSCC and poorly differentiated nKSCCs [125]. Nevertheless, the underlying mechanism is still unknown, hence, the *in vitro* infection system using 308 cells may provide new insights into the interplay of UV irradiation and MnPV infection as co-factors in skin carcinogenesis.

For this purpose, infected 308 cells were exposed to UVB with 50 mJ/cm^2 and harvested at different time points post UV. As expected, UV rapidly increased p53 protein levels and UV-induced p53-mediated p21 induction in infected 308 cells (**Fig. 4.9.5A**). p53 and p21 accumulations reached maximum levels at 8 h after UV irradiation. Subsequently, MnPV transcription activities in infected 308 cells after UV irradiation were quantified by qPCR. Intriguingly, *E1^E4*, *E6* and *E7* transcript levels were reduced following irradiation. The dramatic decrease occurred at 4 h after UV exposure, where *E1^E4*, *E6* and *E7* gene expression were reduced by 78.3%, 55.9% and 67.2%, respectively, when compared to unirradiated infected cells harvested at 0.5 h (**Fig. 4.9.5B**). As for *L1*, an up-regulation post UV was observed and the *L1* mRNA levels went back to base line 24 h after UV. However, the increase in *L1* did not show a statistically significant difference (w/o UV 0.5 h vs. UV 8 h, $p = 0.4385$). To further verify that the dysregulation of MnPV transcripts following UV irradiation was due to a transient transcription blockage, infected keratinocytes were irradiated with 50 mJ/cm^2, and afterwards the transcription was inhibited by the addition of ActD. UV did not affect the stability of viral transcripts after ActD treatment, since the viral transcripts (*E1^E4*, *E6*, *E7* and *L1*) of unirradiated and irradiated cells showed highly similar decay patterns after ActD treatment (**Suppl. Fig. 4**), indicating the changes of MnPV mRNAs, except for *L1*, after UV irradiation were regulated at the transcriptional level.

It is known that the expression of *L1* is restricted to terminally differentiated cells. Consequently, it was interesting to explore whether UV can activate the differentiation of infected cells to induce the

expression of *L1*. The induction of Involucrin and Loricrin was therefore visualized by Western blot (**Fig. 4.9.5C**) after UV irradiation. Involucrin and Loricrin were remarkably increased at 24 h but decreased 48 h after UV treatment. A slightly up-regulated amount of Involucrin and Loricrin was observed in cells harvested after 24 h without UV, which was likely on account of the increased confluence of cells (**Fig. 4.9.5D**). In spite of the down-regulated *E1^E4* mRNA post UV exposure, the E4 protein remained at steady-state levels, suggesting a post-translational stabilization mechanism might be involved.

Overall, UV irradiation transiently inhibited the transcription of MnPV *E1^E4*, *E6*, *E7* and slightly induced *L1* expression *in vitro*, while the E4 protein did not show significant changes in response to UV irradiation. In addition, UV activated differentiation in infected keratinocytes, explaining the increase of *L1* transcript levels to certain extent.

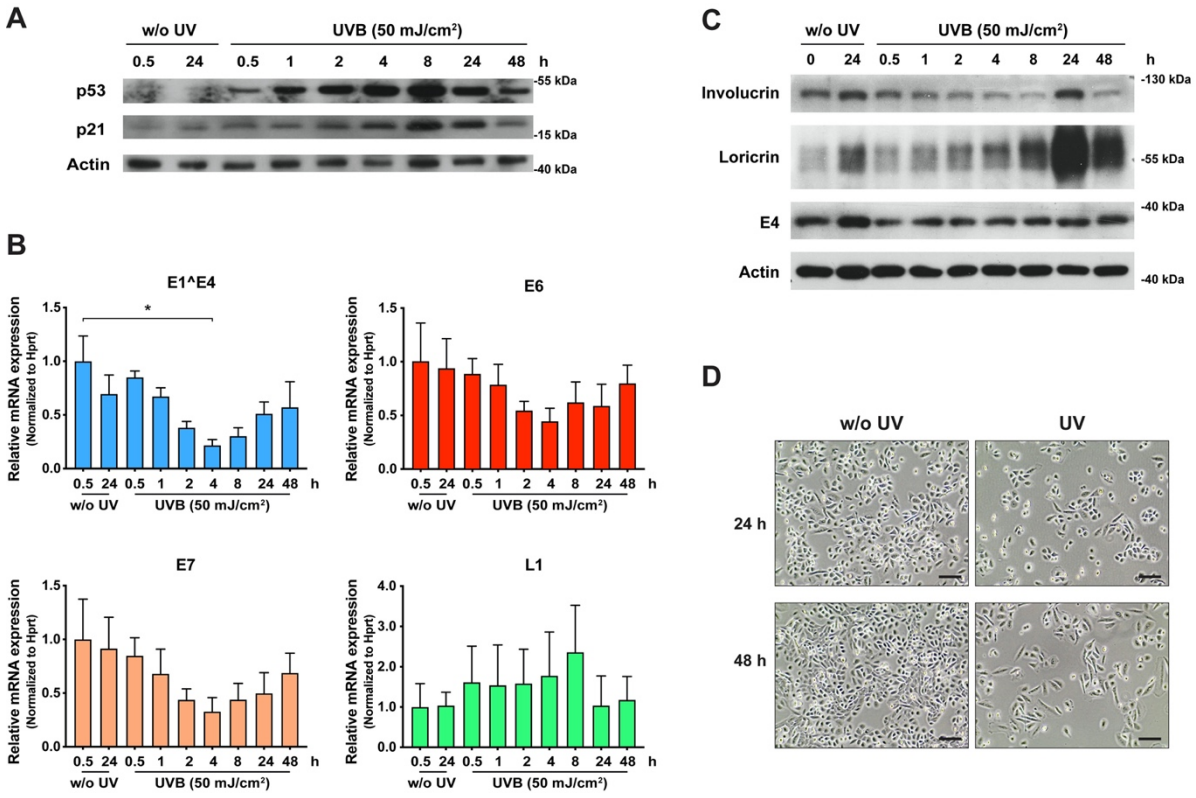

Fig. 4.9.5 MnPV transcription activities after UV irradiation. (**A**) Infected 308 cells were irradiated by UVB (50 mJ/cm²) and collected at time points 0.5 (with or without UV), 1, 2, 4, 8, 24 (with or without UV) and 48 h after irradiation. Both p53 and p21 protein levels were analyzed by Western blot. Actin served as a loading control. (**B**) MnPV transcription activities (*E1^E4*, *E6*, *E7*, *L1*) were measured by qRT-PCR. Data were normalized to *Hprt* and represented as mean ± SD of three independent experiments. Statistical analysis was performed using non-parametric Kruskal-Wallis test followed by Dunn's multiple comparison test. * $p < 0.05$. (**C**) Involucrin, Loricrin and E4 protein levels were analyzed by Western blot. Actin served as a loading control. (**D**) Bright field microscopy images of infected 308 cells 24 h and 48 h after irradiation when compared to unirradiated cells. Scale bar = 100 µm.

5. Discussion

In order to evaluate the efficacy of MnPV L2- and VLP-based vaccine in naturally infected *Mastomys*, the present study analyzed serological responses, tumor occurrence and viral loads in animals after vaccination. In addition, to explore the MnPV/host cell interplay in response to extracellular stress, a novel *in vitro* infection system was established. The viral transcripts and proteins as well as effects of differentiation inducers and UVB exposure on the infected cells were investigated. In the following, the findings based on abovementioned investigations are discussed in detail.

5.1 Immunogenicity of the MnPV Vaccine

The highly conserved epitope in the HPV L2 N-terminus is a promising antigen for next-generation vaccine development. Antibodies induced by L2 vaccination can elicit broadly cross-neutralizing reactions against various HPV types. The rodent *Mastomys coucha* is naturally and persistently infected with the cutaneous MnPV and the mucosal McPV2 types, making this animal model ideal for monitoring L2-based vaccine efficacy.

In a pilot study designed to assess which antigen and adjuvant combination was most immunogenic, both MnPV L2 and MnPV L2/PADRE elicited high anti-L2 titers while only the latter, but not MnPV L2, showed neutralizing MnPV antibody responses in L1-based PBNA (**Fig. 4.1.2**). This might be due to the lack of the helper T cell peptide PADRE in MnPV L2 which appears to have poor immunogenicity (see section 4.1). The high binding affinity of PADRE to DR on the surface of APCs facilitates the antigen presentation, and consequently the production of L2-specific neutralizing antibodies [145]. However, anti-MnPV L2 antibodies induced by MnPV L2/PADRE only weakly cross reacted with McPV2 (**Suppl. Fig. 3**), possibly due to the relatively poor conservation between the N-terminal epitope of MnPV L2 (QT**C**KQA**G**T**CPPDVVNKVEG**) and McPV2 L2 (RQ**C**QVT**G**N**CPPDVVNKVEG**). In agreement with a previous study, the cross-reactivity of antibodies against HPV16 L2 was weak with HPV31 L2, where 6 non-conserved amino acids between HPV16 and 31 were found after sequence alignment [111]. Moreover, cross-neutralization capacity with HPV31 was improved when the immunogen contained the conserved epitope of L2 from HPV16, 31 and 51, providing a possible optimization for broad coverage in MnPV L2 vaccine design by the insertion of both MnPV and McPV2 L2 peptides [159].

In the subsequent performed MnPV L2 main study, vaccination with MnPV L2/PADRE was able to elicit a relatively strong immune response against L2 in animals of the virus-bearing colony (**Fig. 4.4.2B**). As mentioned in section 4.4.2, the mean anti-L2 titer of 0.437 in virus-bearing animals (n = 33) was much lower than that of 2.413 in vaccinated virus-free animals of the pilot study (n = 5; **Fig. 4.1.2A**). In addition, the geometric mean titer of anti-L2 specific neutralizing antibodies was relatively low in the pilot study (2.4×10^2). However, the high anti-VLP response, which correlates with the production of

neutralizing antibodies, with a geometric mean titer of 1.7×10^5, was elicited by MnPV VLPs in naturally infected animals (**Fig. 4.4.3B**). These results demonstrate that immunogenicity elicited by MnPV L2/PADRE or VLP against MnPV is different, which can be affected by various characteristics of the antigens. As is commonly known, the HPV VLP-based vaccine is highly immunogenic, mainly due to the highly ordered and repetitive capsid structure. VLPs can rapidly and sufficiently activate dendritic cells (DCs) and B cells via the Toll-like receptor 4 (TLR4) and MyD-88 dependent pathway, which is essential for antibody generation and the induction of an Ig class switch [160, 161]. Therefore, even a single dose of bivalent or quadrivalent HPV VLP vaccine can efficiently induce the production of protective antibodies [162, 163], while the antibody response elicited by capsomers is less robust [164]. However, α-helices and β-sheets are major secondary structural features of thioredoxin, which served as an L2 display platform, possibly resulting in low levels of anti-L2 specific antibodies in response to vaccination with MnPV L2/PADRE [112].

Furthermore, the immunogenic differences could also be influenced by the number of L2 molecules incorporated into the capsid and the efficiency of furin cleavage. Up to 80 copies (approximately 24 to 36 copies on average) of L2 assemble with 360 monomers of L1 into the capsid and the L2 is buried under the surface of the capsomers (**Fig. 1.2.2**) [43, 44, 57]. The limited copies of L2 are separated from each other in the capsid and only the N-termini of some L2 proteins are exposed after a conformational change upon viral entry [58]. Consequently, the chance of L2-specific antibodies to bind to the papillomavirus capsid is lower, resulting in the poor immunogenicity of the L2-based vaccines [104]. In addition, during viral entry, HPV L2 is cleaved by the furin convertase at its consensus site (R-X-K/R-R) and the cleavage primarily occurs on the basement membrane [165]. However, furin cannot completely cleave L2 molecules *in vitro*, where the cleavage efficiency is up to 35% [166]. Therefore, a probably incomplete exposure of L2 *in vivo* would also affect the efficacy of the L2 vaccine.

Furthermore, the low anti-L2 peptide and neutralizing antibody titers may also be due to limitations of the employed detection methods. The GST-ELISA and L1-based PBNA are not as sensitive as the L2-based PBNA, where the L2 molecules within PsVs have a higher chance to be cleaved by furin and subsequently be bound by L2-specific antibodies [167]. The L2-based PBNA can increase the sensitivity of L2-specific antibody detection by at least 100-fold. Therefore, the detection limit of GST-ELISA might be the reason that 32% (11 of 34 animals) of MnPV L2/PADRE-vaccinated, virus-bearing animals showed anti-L2 antibody titers below the cut-off after the final immunization. However, there is also the possibility that those animals actually did not react to the L2 antigen even following a booster dose. In fact, in case of hepatitis B vaccination, “non or low responders", which correspond to up to 10% of healthy individuals, do not develop detectable antibody titers even after boosting [168]. In spite of antigen-associated factors, the host-associated properties such as age-related immunosenescence, obesity, smoking, genetic predisposition and immune status, can also have great impact on the immune

response to hepatitis B antigens [169, 170]. Thus, the low levels of antibodies against MnPV L2 in some animals could also be attributed to host genetics and individual health conditions. However, none of them developed skin tumors during the observation period. Similarly, acute hepatitis B or chronic antigen carriage has also not been reported even in vaccinated individuals who failed to respond serologically [171-173]. Hence, hepatitis B vaccine apparently still provided protection against HBV infection in "non-responders", which most likely resulted from detectable antigen-specific memory T cells in blood [169]. This could also be the case in "non-responding" animals in this study.

5.2 Protection against Papillomavirus Infection by MnPV Vaccines

Despite the different immunogenicity of L2 peptides and VLPs, vaccination of animals with MnPV L2/PADRE or VLPs led to decreased serological levels against E2, indicative for reduced MnPV replication and in turn viral spread (**Fig. 4.4.2A** and **Fig. 4.4.3A**). As reported previously in a heterologous system, antibody-mediated prevention of infection was slightly different between VLP- and L2-based vaccines. For instance, mice were passively immunized with sera from animals vaccinated with HPV16 VLP or L2 peptides, and afterwards vaginally challenged with pseudoviruses [174]. The inhibition of infection by VLP vaccination was microscopically observed in an antibody concentration dependent manner. High concentration of anti-L1 antibodies hampered HSPGs-binding of pseudoviruses on the basement membrane during the initiation of infection while low concentration of anti-L1 antibodies caused non-HSPG cell receptor blockage on the surface of basal cells (**Fig. 1.2.3**). As for L2 vaccination, following the exposure of the N-terminus of pseudovirus L2 after furin cleavage, anti-L2 antibodies would have a higher chance to bind the exposed epitope, subsequently inhibiting the non-HSPG cell receptor binding to prevent the infection [174]. Of note, the efficient inhibition of infection via the blockage of non-HSPG cell receptor binding also would not require higher concentration of protective antibodies induced by L2 antigen. For example, the mean geometric titer of neutralizing antibodies against HPV31, elicited by vaccination of PfTrx-8-mer-OVX313 (8-mer: eight heterologous HPV types), in mice was around 1×10^2 in L1-based PBNA (~1×10^3 in HPV16), but these antibodies with low titers were still protective against murine vaginal challenge with HPV31 pseudoviruses [175].

However, in comparison with the long-term persistence of anti-MnPV VLP antibodies (**Fig. 4.4.3B**), anti-L2 titers significantly decreased below the cut-off after 46 weeks and persisted for maximal 7 months post final immunization in this study (**Fig. 4.4.2B**). The long-lasting protection of vaccine is therefore directly linked to the persistence of protective antibodies [176]. As shown in follow-up studies, the long-term effectiveness of Cervarix, Gardasil and Gardasil-9 remained at least ten, nine, and six years, respectively [177-179]. In several L2 vaccine-related studies, the efficient protection lasts up to one year in mice, rabbit or cattle, when passively immunized animals were vaginally re-challenged [110, 180, 181]. Interestingly, the anti-L2 peptide antibody levels declined faster than neutralizing antibody levels in

rabbits vaccinated with HPV16/31 L2(17-36) displayed on AAV2-like particles, indicating that the L2-specific neutralizing antibodies are more stable [180]. This might suggest that MnPV L2-specific neutralizing antibodies would probably persist longer than anti-L2 peptide antibodies to provide long-term protection, but further analyses are needed to confirm this assumption.

The long-lasting persistence of vaccine-specific antibodies is determined by several factors. The vaccination schedule might influence the immune response to vaccination, consequently affecting longevity of the antibody response [182]. In the MnPV L2 vaccination group, 56% of animals (19/34) after three and 68% (23/34) after four and five doses of vaccine elicited anti-L2 antibody titers above the cut-off, suggesting that booster doses improved the immune response to L2 vaccines (**Fig. 4.4.2B**). In healthy individuals administered with hepatitis B vaccine, longer intervals (e.g. 7 or 14 weeks instead of 4 weeks) between vaccinations elicited high and persistent protective antibody titers [183]. A similar conclusion has been drawn with acellular pertussis (aP) and diphtheria-tetanus-pertussis (DTP) vaccine [184, 185]. Hence, an extended schedule could be chosen to increase immunogenicity of L2-based vaccines in further studies.

Moreover, the choice of adjuvant is also a determinants of vaccine efficacy [182]. Therefore, two various adjuvants, Montanide ISA 720 and AddaVax™, were tested in a pilot study. Montanide ISA 720 is derived from metabolizable nonmineral oil and enhances humoral and cellular immune responses by depot effect (slow release of antigens) and the recruitment of APCs at the injection site [186]. AddaVax™ is an MF59-like, squalene-based oil-in-water emulsion, and this class of emulsions has been demonstrated to recruit APCs and stimulate proinflammatory cytokines, consequently enhancing immune responses [187]. As shown in **Fig. 4.1.2**, no appreciable differences between Montanide ISA 720 and AddaVax™ were found in the induction of anti-L2 antibody or neutralizing antibody. But AddaVax™ was easier to formulate with MnPV L2/PADRE.

Overall, the persistence of antibodies is primarily determined by a potent induction of long-lived plasma cells (LLPCs). Vaccine antigen activates the B cell response via binding to B cell receptors (BCR) on the surface of naïve B cells. This interaction is enhanced by cross-linking of adjacent BCRs, consequently inducing strong signals for activation and survival of antigen-specific B cells. Subsequently, antigen-specific B cells continuously proliferate and further differentiate into plasma cells in germinal centers (GCs) or memory B cells. A small portion of antigen-specific plasma cells migrates toward and accumulates in the bone marrow, where plasma cells reside and therefore antibody generation can prevail for years [188]. Hence, unlike VLPs, MnPV L2/PADRE may not induce sufficient LLPCs to produce durable antibody responses. Moreover, except for the vaccination schedule and adjuvants, the induction of LLPCs can also be influenced by antigen properties themselves, such as the multivalency and structure (e.g. VLP), which can be optimized in the vaccine design.

5.3 Papillomaviruses and UV-induced Skin Tumors

The ultimate criterion to assess the efficacy of a vaccine against oncogenic papillomaviruses is the prevention of tumors. However, in the current study there was no remarkable difference of tumor incidence between unirradiated animals from the vaccinated (L2: 6.3%; VLP: 0%) or control (6.3%) group (**Fig. 4.5** and **Table 4.7**). Although, one L2-vaccinated unirradiated animal developed papillomas on eye and tongue with high viral loads of MnPV, skin tumors that typically occur on the neck and dorsum were not found. Condylomas, positive for MnPV, were also observed in one vaccinated irradiated animal. Those animals elicited anti-VLP antibody responses during the late stage of observation. In a previous study, both MnPV and McPV2 DNA could be detected in 66.7% of eye papillomas, 62.5% of tongue papillomas and 66.7% of condylomas when animals exclusively developed one type of tumor, suggesting that infections with multiple papillomaviruses frequently occurred in *Mastomys* [147]. Actually, infections with two or more HPV types have been frequently observed in 20%-50% of infected women and 34%-51% of infected men [189-192]. Moreover, the presence and persistence of mucosal types, such as HPV6, 16, 31, 33 and 51, was identified in skin lesions of immunocompetent individuals, indicating mucosal HPVs might be an additional possible risk factor for NMSC development [193-196]. Therefore, it is possible that these vaccinated animals suffering from eye and tongue papillomas as well as condylomas might be co-infected with McPV2. If so, it would not be unexpected that MnPV L2 vaccination might not protect animals against McPV2-associated tumors, since antibodies elicited by MnPV L2/PADRE showed only weak cross-reactivity with McPV2 L2 (**Suppl. Fig. 3**). However, in order to verify this assumption, the antibody response against McPV2 has to be analyzed in future investigations. Overall, the development of broadly protective HPV vaccines is crucial for the prevention of infections with multiple HPV types.

It is well-known that UV irradiation is a major risk factor for the development of NMSC by inducing the accumulation of mutations and suppressing the immune system [197]. Here, UV-induced skin tumors appeared slightly earlier than spontaneous tumors (**Fig. 4.5**), in accordance with previously published data [125]. Intriguingly, in this study, the UV-induced skin tumors were predominantly poorly differentiated nKSCCs with low or undetectable viral loads (**Fig. 4.6H** and **Table 4.7**). For instance, in the L2 vaccination group, the mean viral load of spontaneously occurring tumors was 32087.93 ± 36610.78 MnPV genomes/cell, while the mean viral load of nKSCCs was 14.27 ± 14.27, which was even lower in the control (mean = 0.00654 ± 0.00399) and VLP vaccination (mean = 0.49951 ± 0.49715) group. As described above, pre-cancerous skin lesions often harbor a high viral load of cutaneous HPVs, while viral DNA is absent after lesions progressed into SCCs, indicating that the maintenance and progression of skin tumors does not require the persistence of cutaneous HPV DNA [83]. This proposed "hit-and-run" mechanism was also well demonstrated in *Mastomys coucha* in the context of chronic UV exposure, where nKSCCs could be observed in seropositive animals [125]. The

similar case was found here in control and L2-vaccinated groups, where two irradiated animals from each group developed nKSCCs and were also positive for anti-VLP antibodies, indicating that a productive viral infection occurred in unvaccinated and L2-vaccinated animals. Thus, protective anti-L2 antibodies might not persist long enough to prevent the development of UV-induced skin tumors, while the anti-VLP titers still remained relatively high (mean geometric titer of 8.1×10^3) in the two VLP-vaccinated animals suffering from nKSCCs. As previously reported, the formation of nKSCCs was also found in few seronegative or virus-free animals and the *Tp53* gene was more frequently found mutated in nKSCCs [125]. The accumulation of *Tp53* mutations induced by UV impairs the function of p53 and might play a pivotal role in the development and progression of human SCCs [198]. The percentage of tumor-bearing animals was also no appreciably different between the vaccinated (L2: 11.1%; VLP: 14.3%) and unvaccinated (10.5%) group (**Table 4.7**), indicating that vaccination with either L2 or VLPs may not protect against nKSCCs. Therefore, the development of nKSCCs in VLP-vaccinated animals may be caused merely by chronic UV exposure.

Unfortunately, the low percentage of tumor-bearing animals (6.3%) in the MnPV-infected colony of present study might hamper the assessment of vaccine efficacy. In previous studies, the 64% of naturally infected animals developed MnPV-associated tumors at the end of the observation period, whereas this rate was declined to 28% in later studies [126, 147]. Hence, even vaccinated unirradiated animals did not develop any skin tumors, so there was no statistically significant difference of tumor incidence (p = 0.6171) between unirradiated animals from the VLP vaccination and control groups. Outbred *Mastomys coucha* have been housed at the DKFZ for decades. Genetic diversity, captivity, diet and other possible reasons might contribute to alter the animals' immune responses to MnPV [199, 200]. Additionally, tumor-bearing animals had to be sacrificed according to the animal welfare regulations when they showed signs of disease. Consequently, this "artificial selection" possibly results in the preservation of animals, which are more resistant to virus (and other) infection and tumor development. Currently, new external animals have been progressively introduced into the present colony to overcome abovementioned shortcomings.

With regard to the prevalence of MnPV DNA in skin samples (**Fig. 4.7D**), there were no statistically significant variations between normal skin from unvaccinated and VLP-vaccinated animals, which was contradictory to the decreasing viral load in VLP-vaccinated animals in the previous study [126]. However, here the method for skin sample collection was different. Previously, skin, containing dermis and epidermis, was dissected from animals for DNA extraction and may have resulted in the dilution of virus, which is only present in the epidermis. Here, skin samples were scratched from the target area of frozen skin, yet the depth of scratching was hard to standardize, possibly affecting the sample reproducibility. Most importantly, the sample size was exceedingly small for statistical analysis, and more animals will have to be included in the future. Prior to the submission of this thesis, some animals

in the experiments did not yet reach the end of the observation time and could therefore not be included here.

5.4 Characterization of an *in vitro* Infection System for Studying Cutaneous Papillomaviruses

Several questions need to be addressed that were raised in the *in vivo* part of this study. How, for instance, does UV promote the development of KSCCs and nKSCCs in the context of MnPV infection? What causes the loss of MnPV DNA during the progression to nKSCC? Detailed investigations of involved pathways were hampered by the lack of an appropriate *in vitro* system. Previously, a *Mastomys coucha*-derived keratinocyte cell line (Kera5), which is spontaneously immortalized by a *Tp53* point mutation, was generated [132]. However, for unknown reasons, these natural host cells could not be infected with MnPV.

Here, murine 308 keratinocytes could be infected with tumor extracts containing intact MnPV virions (**Fig. 4.8.1A** and **B**), mimicking the initial stage after cutaneous papillomavirus infection. The presence of viral DNA as well as early and late viral transcripts were detected, but declined over time (**Fig. 4.8.1C**, **D** and **E**), which is probably due to the instability of the episomal MnPV genome during cell division. A previous transcriptome analysis revealed no MnPV-cell fusion transcripts indicating that no MnPV integration took place in naturally occurring tumors [127]. The instability of HPV episomes, which consequently affects viral transcriptional activities, may be influenced by DNA damage response (DDR) signaling, like inhibition of ATR/CHK1 and MRE11, restoration of STAT-1 as well as interferon engagement, which might be triggered by cellular defense response [201-205]. Another possibility causing the decreasing MnPV DNA could be the viral early protein E4. Several studies have shown that the predominantly cytoplasmic high-risk HPV E4 proteins induced G2 arrest in monolayer cell culture or organotypic raft tissue culture [206-208]. Similarly, MnPV E4 protein was present mostly in the cytoplasm of infected cells (**Fig. 4.8.3B**), indicating that the function of MnPV E4 might be similar to that of high-risk HPV E4. Hence, the potentially arrested infected cells may lose their proliferation advantage and consequently, MnPV DNA would be lost during daily culture and passaging.

The stability of mRNA can greatly influence transcript levels, which in turn strongly impact protein levels in response to various external changes [209]. Therefore, the half-lives of MnPV transcripts were measured. The mRNA stability varied greatly among MnPV early and late transcripts (**Fig. 4.8.2**), but was comparable to reported half-lives of other HPV mRNAs. For instance, the half-life of the HPV16 *E6/E7* mRNAs from an extrachromosomal genome status was 3 h [210]. In addition, the half-life of transfected HPV6b L1 and BPV1 L1 was slightly longer in undifferentiated keratinocytes (around 5 h) than that in differentiated cells (around 4 h) [211]. The AU-rich elements (AREs) within the HPV early three prime untranslated region (3'-UTR) are one possible factor influencing the stability of viral early mRNAs, where the loss of AREs after HPV integration increased *E6/E7* mRNA stability [210]. Moreover,

the negative regulatory element (NRE) within the HPV late 3'-UTR was also involved in the modulation of polyadenylation and the steady-state levels of mRNAs [212, 213]. Apart from regulatory elements within the UTR, the mRNA stability could also be influenced by alternative splicing and codon usage [214, 215].

Apart from E4, also the MnPV E7 protein could be visualized in infected 308 keratinocytes (**Fig. 4.8.4**). MnPV E7 was detected in both nucleus and cytoplasm, and in some cases predominantly in the cytoplasm. One study reported that the subcellular localization of the HPV16 E7 protein is dependent on cell confluence [216]. HPV16 E7 protein localized to the nucleus and cytoplasm in subconfluent cells, while it was mostly present in the cytoplasm of confluent cells in a cell cycle-independent manner. As for cutaneous HPVs, HPV8 E7 protein was predominantly found in the nucleus of transfected RTS3b cells, however, no different cell densities were analyzed there [217]. Additionally, the presence of E7 protein was also linked to its structural state. Monomeric and dimeric HPV16 E7 was primarily found in the nucleus, consequently promoting the inactivation of pRb. In contrast, E7 existed as stable and soluble oligomers when it accumulated in the cytoplasm and different pH in distinct intracellular compartments may induce conformational changes [218, 219]. Moreover, the accumulation of E7 protein in the nucleus and/or cytoplasm was a dynamic and reversible process [218]. The nuclear-cytoplasmic shuttling ability originates in a nuclear localization signal (NLS) and nuclear export signal (NES) identified within the E7 protein [220-222]. Intriguingly, HPV16 E7 targets Steroid receptor coactivator 1 (SRC-1) and p130 were more obviously reduced when E7 largely accumulated in the cytoplasm, while its localization did not affect E7-mediated degradation of pRb [216]. These findings suggest that the localization of MnPV E7 might similarly influence its interactions with host cell proteins.

5.5 Differentiation of Infected 308 Keratinocytes

Expression of the papillomavirus major capsid protein L1 is tightly controlled by epithelial differentiation at transcriptional, post-transcriptional and translational levels [223]. Therefore, it was surprising that MnPV *L1* transcripts were readily detected after initial infection (**Fig. 4.8.1E**), since in contrast, the HPV *L1* mRNA was undetectable in human primary keratinocytes without the simultaneous induction of differentiation [74]. It was hypothesized that the differentiation in infected cells with close contact might activate keratinocyte differentiation [156]. Indeed, increased cell-to-cell contact was able to induce differentiation of uninfected and infected murine 308 keratinocytes, a process that was further augmented by the addition of calcium and culture in methylcellulose (MC) (**Fig. 4.9.1** and **Fig. 4.9.2A**). However, the individual underlying mechanisms of the induction of keratinocyte differentiation via cell-to-cell contact, calcium or MC are slightly different. Increased cell-to-cell contact promotes keratinocyte differentiation via E-cadherin [156]. Comparably, extracellular calcium induces keratinocyte differentiation via E-cadherin/Catenin/Phosphoinositide 3-kinase (PI3K), which in turn results in intracellular calcium release and activation of Protein kinase C (PKC) [224]. Murine 308 cells

have a higher level of intracellular free calcium than do primary mouse keratinocytes and the intracellular free calcium first increases rapidly and then declines to the basal level in a short time in response to the addition of extracellular calcium (1.2 mM) [225]. This unsustain increase of intracellular free calcium in 308 cells might explain why a higher concentration of calcium (e.g. 2.8 mM) was required for the induction of differentiation in the present study. The MC suspension culture can lead to the inhibition of the extracellular signal regulated kinase (ERK) pathway and activation of the c-Jun N-terminal kinase (JNK) pathway, subsequently activating AP-1 factors to achieve terminal differentiation of keratinocytes [75]. Therefore, after the addition of these differentiation inducers, an increase of *L1* mRNA was observed in infected 308 cells (**Fig. 4.9.2B**). In addition, MC suspension culture upregulated the transcription of viral early genes (*E6* and *E7*). Similarly, several studies have reported that both early and late promoters are activated in differentiated human keratinocytes via suspension culture or organotypic raft cultures [74, 129, 226]. Differentiation-mediated regulation of transcription factors (AP-1, NF-1, Sp-1, YY-1, etc.) probably contributes to the increase of viral early mRNAs in MC-treated cells [227].

The MnPV L1 protein was undetectable in the infected 308 cells in the current study, possibly due to the lack of specific antibodies and low abundance of MnPV L1, yet some interesting phenomena were noticed in the detection of different MnPV L1 isoforms ($L1_{short}$, $L1_{middle}$ and $L1_{long}$) in transfected MaFi132 cells (**Fig. 4.9.3**). Actually, MnPV $L1_{middle}$ could not be detected in MaFi132 transfected with plasmid encoding the full-length *L1* ORF ($L1_{wt}$) potentially expressing three L1 isoforms when comparing the band sizes, indicating that two isoforms of MnPV L1 exist in cells derived the natural host of MnPV. Thereby, it gives a hint that both $L1_{short}$ and $L1_{long}$ could be expressed in infected 308 cells. Additionally, only MnPV $L1_{short}$, but not $L1_{middle}$ or $L1_{long}$, formed dimers and trimers (detected as high molecular weight bands in Western blot) which resolved when the same cell lysates were harshly denatured (additional DTT, β-mercaptoethanol and heating; **Fig. 4.9.3D**). In fact, the higher order structure of L1 was reported to be stabilized via disulfide bonds between conserved cysteine residues in L1, since mutated cysteine residues or reducing agents, such as DTT and β-mercaptoethanol, can disrupt the VLP or capsid formation [228-231]. Interestingly, one cysteine (C18) was found within the additional 31aa of the $L1_{long}$ N-terminus and was predicted via DiANNA (a disulfide connectivity prediction website; http://clavius.bc.edu/~clotelab/DiANNA/) to have a strong interaction with the other cysteine residues within MnPV $L1_{short}$ (**Suppl. Fig. 5**) [232]. This indicates that the additional cysteine within $L1_{long}$ may affect the assembly of L1, therefore explaining why $L1_{long}$ failed to form dimers, trimers or capsids. However, further experiments (e.g. mutation of C18 in $L1_{long}$) are required to verify this hypothesis.

Interestingly, MnPV $L1_{short}$ and $L1_{long}$ were apparently regulated differently in 308 cells committed to differentiation, with MnPV $L1_{short}$ being induced and $L1_{long}$ levels remaining unchanged (**Fig. 4.9.4**). This correlates with previous *in vivo* findings that $L1_{long}$ was found in basal epithelial cells and the entire

epithelium, while capsid protein was specifically observed in keratinocytes that had committed to terminal differentiation and cornified layers [140]. Here, both $L1_{short}$ and $L1_{long}$ were detected in MaFi132 cells transfected with $L1_{wt}$, therefore post-transcriptional or post-translational modifications might lead to the differential regulation of $L1_{short}$ and $L1_{long}$ protein levels in differentiated keratinocytes. Multiple early and late splicing signals have been characterized within the HPV transcriptome with respect to different stages of infection [40, 223]. For instance, the late splice site SA5639 of HPV16 is located upstream of the L1 transcription start site, which is essential for the production of *L1* mRNA [233]. The activation of alternative splicing at this late splice site of HPV16 was dependent on epithelial differentiation [234]. A similar late splice site (SA5797) was found upstream of MnPV $L1_{short}$ [127], possibly resulting in preferential production of $L1_{short}$ and subsequently contributing to the efficient translation of $L1_{short}$ in differentiated cells. In addition, impaired interpentameric disulfide bonds can destabilize capsids in a differentiation-dependent manner [235]. Therefore, the capacity to form capsids might stabilize $L1_{short}$ upon epithelial differentiation.

Another important aspect addressed with this *in vitro* system was the potential effects of UV exposure on the regulation of MnPV at transcriptional and translational levels. As reported previously, the impact of UV exposure on URR activity is diverse and even controversial among different HPV types and cell lines [236-239]. Hence, with the benefits of the present *in vitro* infection system, the direct influence of UV on viral transcriptional activities could be revealed, where UV irradiation transiently caused a decrease of MnPV *E1^E4*, *E6* and *E7* mRNA and showed an increase of *L1* (**Fig. 4.9.5B**). The reduced levels of *E1^E4*, *E6* and *E7* were probably due to a general transcription blockage induced by UV exposure (**Suppl. Fig. 4**) [240]. E4 protein levels remained relatively stable post UV exposure, indicating a possible post-translational stabilization. Intriguingly, UV-mediated differentiation, evident by the increasing protein levels of Involucrin and Loricrin (**Fig. 4.9.5C**), may influence the relative abundance of *L1* mRNA, and the commitment to differentiation was not due to the change of cell confluence (**Fig. 4.9.5D**). In fact, UV irradiation was able to upregulate the terminal differentiation markers, Involucrin and Loricrin, *in vivo*, causing increases in the epidermal thickness (**Fig. 4.6D** and **E**) [241]. Therefore, apart from DDR and systemic immunosuppression, UV-induced differentiation may alter late promoter activity and post-transcriptional modification to favor the productive infection with cutaneous papillomavirus, consequently leading to the development of NMSC.

5.6 Conclusion and Future Perspectives

In the present study, the efficacies of MnPV L2 and VLP-based vaccine were assessed among naturally infected *Mastomys coucha* in the context of chronic UV exposure. Based on the analyses of serological responses, tumor occurrence and viral loads in the control, L2 vaccination and VLP vaccination groups, MnPV L2/PADRE has low immunogenicity compared to VLPs but prevents MnPV infection even under UV conditions. The anti-L2 antibody responses do not persist as long as anti-VLP antibody responses, which in turn influence their protective potential against eye papillomas, tongue papillomas or condylomas. However, the possible co-infection with McPV2 in tumorigenesis and the small sample size of tissue specimens hampered the direct assessment of tumor incidence and viral loads in this study. Hence, the antibody response against McPV2 and this type's overall prevalence need to be analyzed in future studies. Additionally, skin samples from animals at the end of this study will be included for viral load analysis to comprehensively evaluate the vaccine efficacy. Overall, in order to further enhance immunogenicity of L2, a platform with highly immunogenic structures, like OVX313 (heptameric nanoparticle) [175], can be used to display multiple copies of heterologous L2 peptides to achieve long-lasting antibody response and broader protection.

Moreover, murine 308 keratinocytes were successfully infected with isolated MnPV virions allowing the detection of MnPV genomes, viral transcripts as well as viral early proteins. Therefore, this *in vitro* infection system can extend the studies of cutaneous papillomaviruses that have previously been restricted to one or two viral gene products regulated by exogenous promoters to a complete viral life cycle. Meanwhile, MnPV is transcriptionally regulated by UV irradiation, which is interesting for further transcriptome-based investigations for a better understanding of MnPV and UV exposure in skin carcinogenesis.

Hence, the *in vitro* infection system will serve as a powerful tool for the study of pathogenesis of cutaneous papillomaviruses and biological effects of UV irradiation in the development of skin tumors. *Mastomys coucha* as a preclinical model will be of benefit for the development of prophylactic or therapeutic vaccines broadly acting against various cutaneous PVs for immunocompetent and immunosuppressed individuals.

6. Supplementary Figures

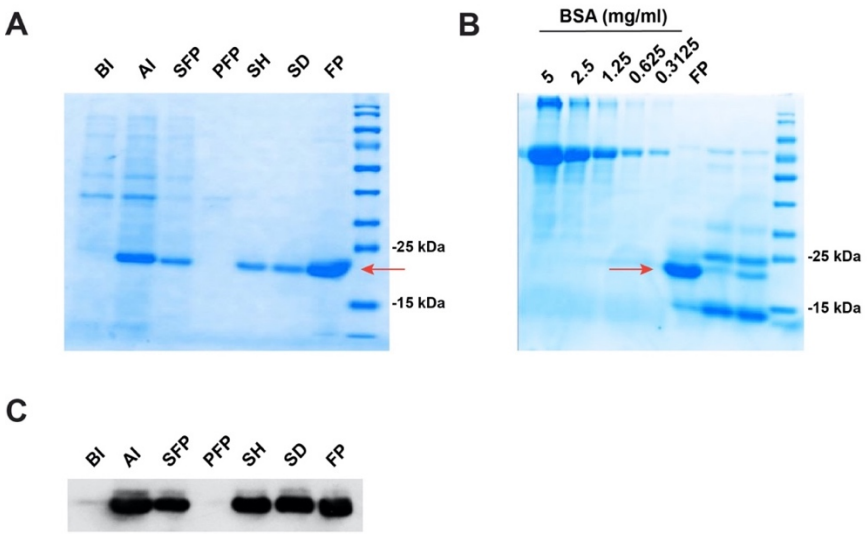

Suppl. Fig. 1 pET26 PfTrx-MnPV-L2(20-38)$_3$ production. (**A**) Samples collected during expression, extraction, and purification of pET26 PfTrx-MnPV-L2(20-38)$_3$ were stained by Coomassie Blue. Red arrow indicates pET26 PfTrx-MnPV-L2(20-38)$_3$. BI: before IPTG, AI: after IPTG, SFP: supernatant after French Press, PFP: pellet after French Press, SH: supernatant after heating, SD: supernatant after dialysis, FP: final protein. (**B**) The concentration of the antigen was determined by band densities using ImageJ when compared to different concentrations of BSA. Red arrow indicates pET26 PfTrx-MnPV-L2(20-38)$_3$. (**C**) pET26 PfTrx-MnPV-L2(20-38)$_3$ was analyzed by Western blot and samples are derived from (**A**).

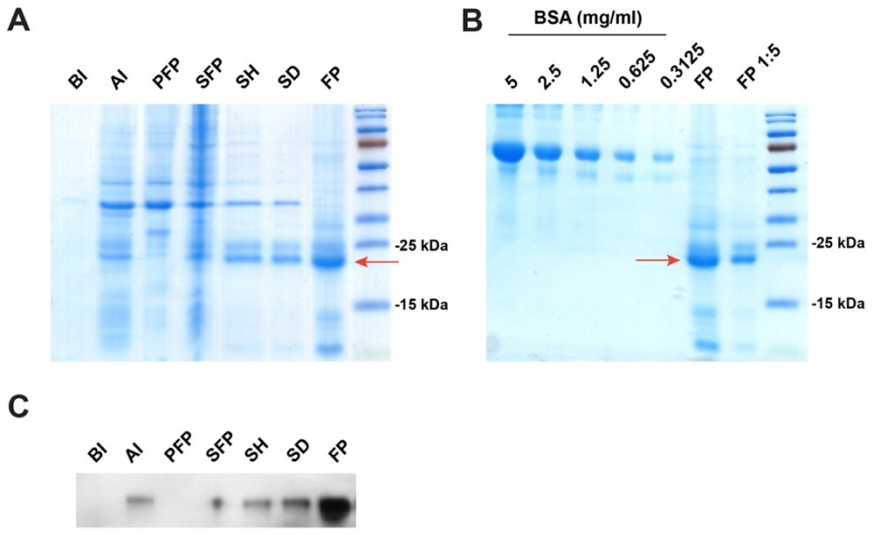

Suppl. Fig. 2 pET26-PADRE$_{2\times}$ PfTrx-MnPV-L2(20-38)$_3$ production. (**A**) Samples collected during expression, extraction, and purification of pET26-PADRE$_{2\times}$ PfTrx-MnPV-L2(20-38)$_3$ were stained by Coomassie Blue. BI: before IPTG, AI: after IPTG, PFP: pellet after French Press, SFP: supernatant after French Press, SH: supernatant after heating, SD: supernatant after dialysis, FP: final protein. Red arrow indicates pET26-PADRE$_{2\times}$ PfTrx-MnPV-L2(20-38)$_3$. (**B**) The concentration was determined by band densities using ImageJ when compared to different concentrations of BSA. Red arrow indicates pET26-PADRE$_{2\times}$ PfTrx-MnPV-L2(20-38)$_3$. (**C**) pET26-PADRE$_{2\times}$ PfTrx-MnPV-L2(20-38)$_3$ was analyzed by Western blot and samples are derived from (**A**).

Suppl. Table 1 Overview of MnPV L2 vaccination pilot study. Two antigens (pET26 PfTrx-MnPV-L2(20-38)$_3$ and pET26-PADRE$_{2\times}$ PfTrx-MnPV-L2(20-38)$_3$) with one dosage (80 µg) and two adjuvants (Montanide ISA 720 and AddaVax^{TM}) were applied in the pilot study. Animals were injected with PBS as negative control.

Antigen	Adjuvants	Antigen amount	n
PBS	-	-	5
PfTrx-MnPV-L2(20-38)$_3$	Montanide ISA 720	80 µg	5
	AddaVax^{TM}	80 µg	5
PfTrx-MnPV-L2(20-38)$_3$/PADRE$_{2\times}$	Montanide ISA 720	80 µg	5
	AddaVax^{TM}	80 µg	5

n = number of animals

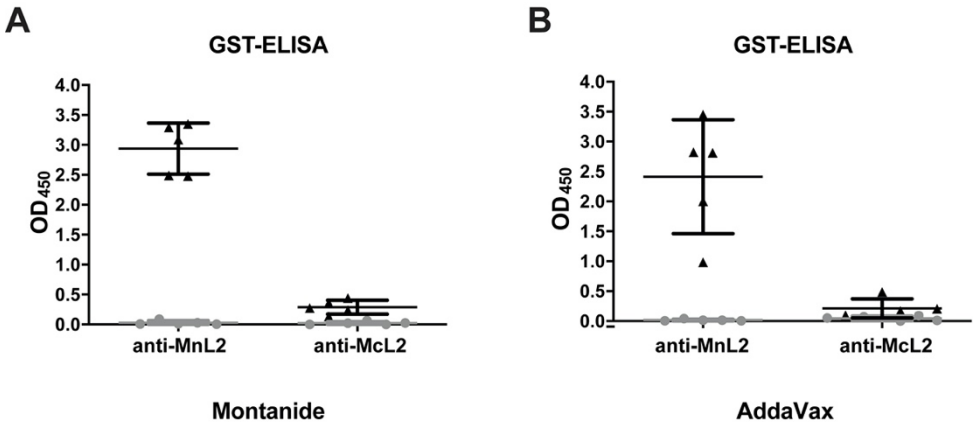

Suppl. Fig. 3 Anti-McPV L2 antibody response in the pilot study. Five virus-free animals were vaccinated with pET26-PADRE$_{2\times}$ PfTrx-MnPV-L2(20-38)$_3$ formulated in Montanide ISA 720 (**A**) or AddaVax^{TM} (**B**). Sera were collected before immunization (gray dots) and two weeks after 5th immunization (black triangles). Anti-MnPV L2 titers were obtained from Fig. 4.1.2A. Anti-McPV L2 titers were measured by GST-McPV2 ELISA.

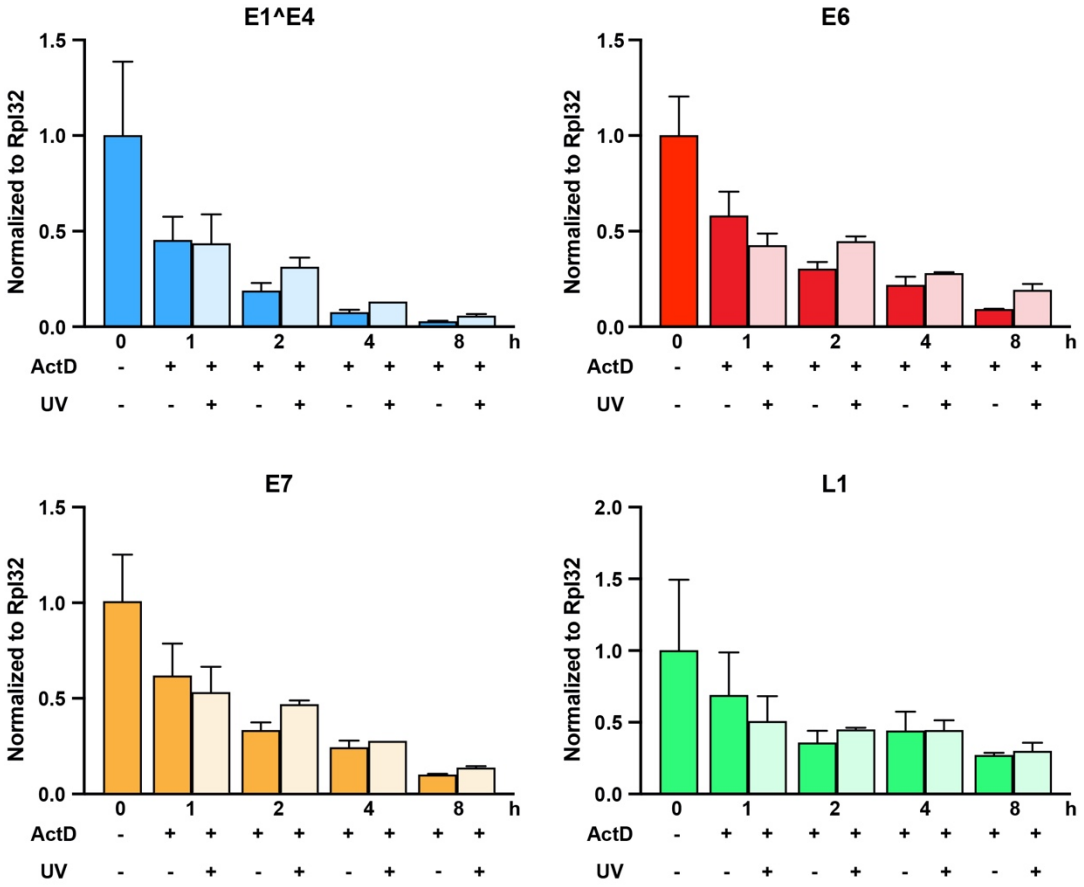

Suppl. Fig. 4 The effect of UV irradiation on the stability of MnPV viral transcripts. Infected 308 cells were exposed to UVB (50 mJ/cm^2) and afterwards treated with 5 µg/ml Actinomycin D (ActD) for 1, 2, 4 and 8 h, respectively. ActD +/- indicates whether cells were treated with ActD or not. UV+/- indicates whether cells were irradiated before the addition of ActD or not. MnPV transcription activities (*E1^E4*, *E6*, *E7*, *L1*) were measured by qRT-PCR. Data were normalized to *Rpl32* and are represented as mean ± SD of two independent experiments.

Predicted bonds	
18 - 104	IYTRHCPDAGV - YRVFRCKLPDP
130 - 214	QRLAWCIRGVE - VKKGDCPPIQR
190 - 458	MFIVGCVPAQG - SLATKCPDNVE
204 - 275	SRALTCSNQVV - THGNSCFFYAR

Suppl. Fig. 5 Predicted disulfide bonds within MnPV L1$_{long}$. The potential disulfide bonds in MnPV L1$_{long}$ was predicted using DiANNA (http://clavius.bc.edu/~clotelab/DiANNA/). The left panel indicates the cysteine position of the L1$_{long}$ sequence and the predicted bonds formed between two cysteine residues. The right panel shows the respective amino acid sequence of predicted bonds. C18 is located in the N-terminus of L1$_{long}$.

7. References

1. Vogelstein, B. and K.W. Kinzler, *The multistep nature of cancer.* Trends Genet, 1993. **9**(4): p. 138-41.
2. Parsa, N., *Environmental factors inducing human cancers.* Iran J Public Health, 2012. **41**(11): p. 1-9.
3. de Martel, C., et al., *Global burden of cancer attributable to infections in 2018: a worldwide incidence analysis.* Lancet Glob Health, 2020. **8**(2): p. e180-e190.
4. Feng, H., et al., *Clonal integration of a polyomavirus in human Merkel cell carcinoma.* Science, 2008. **319**(5866): p. 1096-100.
5. Dubrow, R., et al., *HIV infection, aging, and immune function: implications for cancer risk and prevention.* Curr Opin Oncol, 2012. **24**(5): p. 506-16.
6. Chang, Y., P.S. Moore, and R.A. Weiss, *Human oncogenic viruses: nature and discovery.* Philos Trans R Soc Lond B Biol Sci, 2017. **372**(1732).
7. Krump, N.A. and J. You, *Molecular mechanisms of viral oncogenesis in humans.* Nat Rev Microbiol, 2018. **16**(11): p. 684-698.
8. Van Doorslaer, K., et al., *The Papillomavirus Episteme: a major update to the papillomavirus sequence database.* Nucleic Acids Res, 2017. **45**(D1): p. D499-D506.
9. Shope, R.E. and E.W. Hurst, *Infectious Papillomatosis of Rabbits : With a Note on the Histopathology.* J Exp Med, 1933. **58**(5): p. 607-24.
10. Bernard, H.U., *Taxonomy and phylogeny of papillomaviruses: an overview and recent developments.* Infect Genet Evol, 2013. **18**: p. 357-61.
11. de Villiers, E.M., et al., *Classification of papillomaviruses.* Virology, 2004. **324**(1): p. 17-27.
12. Van Doorslaer, K., et al., *ICTV Virus Taxonomy Profile: Papillomaviridae.* J Gen Virol, 2018. **99**(8): p. 989-990.
13. Humans, I.W.G.o.t.E.o.C.R.t., *Vol. 100 B. Human papillomaviruses. IARC MonogrEvalCarcinog Risks Hum. 2012; 100B: 255–296.* 2016.
14. Arbyn, M., et al., *EUROGIN 2011 roadmap on prevention and treatment of HPV-related disease.* Int J Cancer, 2012. **131**(9): p. 1969-82.
15. Hellner, K. and L. Dorrell, *Recent advances in understanding and preventing human papillomavirus-related disease.* F1000Res, 2017. **6**.
16. Munoz, N., et al., *Epidemiologic classification of human papillomavirus types associated with cervical cancer.* N Engl J Med, 2003. **348**(6): p. 518-27.
17. Derkay, C.S. and B. Wiatrak, *Recurrent respiratory papillomatosis: a review.* Laryngoscope, 2008. **118**(7): p. 1236-47.
18. Miao, T., *Common types of infection with multitypes of HPV on uterine cervix.* 2018. **7**(1): p. 12.
19. Forslund, O., et al., *Identification of human papillomavirus in keratoacanthomas.* J Cutan Pathol, 2003. **30**(7): p. 423-9.
20. Pfister, H. and J. Ter Schegget, *Role of HPV in cutaneous premalignant and malignant tumors.* Clin Dermatol, 1997. **15**(3): p. 335-47.
21. Antonsson, A., et al., *General acquisition of human papillomavirus infections of skin occurs in early infancy.* J Clin Microbiol, 2003. **41**(6): p. 2509-14.
22. Chahoud, J., et al., *Association Between β-Genus Human Papillomavirus and Cutaneous Squamous Cell Carcinoma in Immunocompetent Individuals—A Meta-analysis.* JAMA Dermatology, 2016. **152**(12): p. 1354-1364.
23. Hampras, S.S., et al., *Natural history of cutaneous human papillomavirus (HPV) infection in men: the HIM study.* PLoS One, 2014. **9**(9): p. e104843.
24. Bacaj, P. and D. Burch, *Human Papillomavirus Infection of the Skin.* Arch Pathol Lab Med, 2018. **142**(6): p. 700-705.
25. Gheit, T., *Mucosal and Cutaneous Human Papillomavirus Infections and Cancer Biology.* Front Oncol, 2019. **9**: p. 355.

26. Narisawa-Saito, M. and T. Kiyono, *Basic mechanisms of high-risk human papillomavirus-induced carcinogenesis: roles of E6 and E7 proteins.* Cancer Sci, 2007. **98**(10): p. 1505-11.
27. Roman, A. and K. Munger, *The papillomavirus E7 proteins.* Virology, 2013. **445**(1-2): p. 138-68.
28. Cancer Genome Atlas Research, N., et al., *Integrated genomic and molecular characterization of cervical cancer.* Nature, 2017. **543**(7645): p. 378-384.
29. McBride, A.A. and A. Warburton, *The role of integration in oncogenic progression of HPV-associated cancers.* PLoS Pathog, 2017. **13**(4): p. e1006211.
30. Wendel, S.O. and N.A. Wallace, *Loss of Genome Fidelity: Beta HPVs and the DNA Damage Response.* Front Microbiol, 2017. **8**: p. 2250.
31. Bergvall, M., T. Melendy, and J. Archambault, *The E1 proteins.* Virology, 2013. **445**(1-2): p. 35-56.
32. Swindle, C.S. and J.A. Engler, *Association of the human papillomavirus type 11 E1 protein with histone H1.* J Virol, 1998. **72**(3): p. 1994-2001.
33. McBride, A.A., *The papillomavirus E2 proteins.* Virology, 2013. **445**(1-2): p. 57-79.
34. Clower, R.V., Y. Hu, and T. Melendy, *Papillomavirus E2 protein interacts with and stimulates human topoisomerase I.* Virology, 2006. **348**(1): p. 13-8.
35. Griffin, H., et al., *Stratification of HPV-induced cervical pathology using the virally encoded molecular marker E4 in combination with p16 or MCM.* Modern Pathology, 2015. **28**(7): p. 977-993.
36. Borgogna, C., et al., *β-HPV Infection Correlates with Early Stages of Carcinogenesis in Skin Tumors and Patient-Derived Xenografts from a Kidney Transplant Recipient Cohort.* Frontiers in Microbiology, 2018. **9**(117).
37. Doorbar, J., *The E4 protein; structure, function and patterns of expression.* Virology, 2013. **445**(1-2): p. 80-98.
38. Prescott, E.L., et al., *Human Papillomavirus Type 1 E1^E4 Protein Is a Potent Inhibitor of the Serine-Arginine (SR) Protein Kinase SRPK1 and Inhibits Phosphorylation of Host SR Proteins and of the Viral Transcription and Replication Regulator E2.* Journal of Virology, 2014. **88**(21): p. 12599-12611.
39. Maufort, J.P., et al., *A role for HPV16 E5 in cervical carcinogenesis.* Cancer Res, 2010. **70**(7): p. 2924-31.
40. Graham, S.V., *Keratinocyte Differentiation-Dependent Human Papillomavirus Gene Regulation.* Viruses, 2017. **9**(9).
41. Kirnbauer, R., et al., *Efficient self-assembly of human papillomavirus type 16 L1 and L1-L2 into virus-like particles.* Journal of virology, 1993. **67**(12): p. 6929-6936.
42. Chen, X.S., et al., *Structure of small virus-like particles assembled from the L1 protein of human papillomavirus 16.* Mol Cell, 2000. **5**(3): p. 557-67.
43. Guan, J., et al., *Cryoelectron Microscopy Maps of Human Papillomavirus 16 Reveal L2 Densities and Heparin Binding Site.* Structure, 2017. **25**(2): p. 253-263.
44. Wang, M., et al., *Expression of human papillomavirus type 6 L1 and L2 isolated in China and self assembly of virus-like particles by the products.* Sheng Wu Hua Xue Yu Sheng Wu Wu Li Xue Bao (Shanghai), 2003. **35**(1): p. 27-34.
45. Bronnimann, M.P., et al., *A Transmembrane Domain and GxxxG Motifs within L2 Are Essential for Papillomavirus Infection.* Journal of Virology, 2013. **87**(1): p. 464-473.
46. Campos, S.K., *Subcellular Trafficking of the Papillomavirus Genome during Initial Infection: The Remarkable Abilities of Minor Capsid Protein L2.* Viruses, 2017. **9**(12).
47. Wang, J.W. and R.B. Roden, *L2, the minor capsid protein of papillomavirus.* Virology, 2013. **445**(1-2): p. 175-86.
48. Schafer, F., L. Florin, and M. Sapp, *DNA binding of L1 is required for human papillomavirus morphogenesis in vivo.* Virology, 2002. **295**(1): p. 172-81.
49. Okun, M.M., et al., *L1 interaction domains of papillomavirus l2 necessary for viral genome encapsidation.* J Virol, 2001. **75**(9): p. 4332-42.
50. Finnen, R.L., et al., *Interactions between papillomavirus L1 and L2 capsid proteins.* Journal of virology, 2003. **77**(8): p. 4818-4826.

51. Kim, H.J., H.L. Kwag, and H.J. Kim, *Characterization of human papillomavirus type 16 pseudovirus containing histones.* BMC Biotechnol, 2016. **16**(1): p. 63.
52. Zhou, J., et al., *Interaction of human papillomavirus (HPV) type 16 capsid proteins with HPV DNA requires an intact L2 N-terminal sequence.* J Virol, 1994. **68**(2): p. 619-25.
53. Cerqueira, C., et al., *A Cell-Free Assembly System for Generating Infectious Human Papillomavirus 16 Capsids Implicates a Size Discrimination Mechanism for Preferential Viral Genome Packaging.* J Virol, 2016. **90**(2): p. 1096-107.
54. Buck, C.B., et al., *Maturation of papillomavirus capsids.* J Virol, 2005. **79**(5): p. 2839-46.
55. Zhao, K.N., et al., *DNA packaging by L1 and L2 capsid proteins of bovine papillomavirus type 1.* Virology, 1998. **243**(2): p. 482-91.
56. Kines, R.C., et al., *The initial steps leading to papillomavirus infection occur on the basement membrane prior to cell surface binding.* Proc Natl Acad Sci U S A, 2009. **106**(48): p. 20458-63.
57. Buck, C.B., et al., *Arrangement of L2 within the Papillomavirus Capsid.* Journal of Virology, 2008. **82**(11): p. 5190-5197.
58. Richards, R.M., et al., *Cleavage of the papillomavirus minor capsid protein, L2, at a furin consensus site is necessary for infection.* Proceedings of the National Academy of Sciences, 2006. **103**(5): p. 1522-1527.
59. Day, P.M., et al., *Mechanisms of human papillomavirus type 16 neutralization by l2 cross-neutralizing and l1 type-specific antibodies.* J Virol, 2008. **82**(9): p. 4638-46.
60. Horvath, C.A., et al., *Mechanisms of cell entry by human papillomaviruses: an overview.* Virol J, 2010. **7**: p. 11.
61. McBride, A.A., et al., *Hitchhiking on host chromatin: how papillomaviruses persist.* Biochim Biophys Acta, 2012. **1819**(7): p. 820-5.
62. Poddar, A., et al., *The human papillomavirus type 8 E2 tethering protein targets the ribosomal DNA loci of host mitotic chromosomes.* J Virol, 2009. **83**(2): p. 640-50.
63. Moody, C., *Mechanisms by which HPV induces a replication competent environment in differentiating keratinocytes.* Viruses, 2017. **9**(9): p. 261.
64. Doorbar, J., et al., *Specific interaction between HPV-16 E1–E4 and cytokeratins results in collapse of the epithelial cell intermediate filament network.* Nature, 1991. **352**(6338): p. 824-827.
65. Burley, M., S. Roberts, and J.L. Parish, *Epigenetic regulation of human papillomavirus transcription in the productive virus life cycle.* Seminars in Immunopathology, 2020.
66. Siadat-Pajouh, M., et al., *Detection of human papillomavirus type 16/18 DNA in cervicovaginal cells by fluorescence based in situ hybridization and automated image cytometry.* Cytometry, 1994. **15**(3): p. 245-57.
67. Stanley, M.A., et al., *Properties of a non-tumorigenic human cervical keratinocyte cell line.* Int J Cancer, 1989. **43**(4): p. 672-6.
68. Deau, M.-C., M. Favre, and G. Orth, *Genetic heterogeneity among human papillomaviruses (HPV) associated with epidermodysplasia verruciformis: evidence for multiple allelic forms of HPV5 and HPV8 E6 genes.* Virology, 1991. **184**(2): p. 492-503.
69. Boelsma, E., M.C. Verhoeven, and M. Ponec, *Reconstruction of a human skin equivalent using a spontaneously transformed keratinocyte cell line (HaCaT).* J Invest Dermatol, 1999. **112**(4): p. 489-98.
70. Dickson, M.A., et al., *Human keratinocytes that express hTERT and also bypass a p16(INK4a)-enforced mechanism that limits life span become immortal yet retain normal growth and differentiation characteristics.* Mol Cell Biol, 2000. **20**(4): p. 1436-47.
71. Yang, R., et al., *Combined Transcriptome and Proteome Analysis of Immortalized Human Keratinocytes Expressing Human Papillomavirus 16 (HPV16) Oncogenes Reveals Novel Key Factors and Networks in HPV-Induced Carcinogenesis.* mSphere, 2019. **4**(2).
72. Thomas, J.T., et al., *Cellular Changes Induced by Low-Risk Human Papillomavirus Type 11 in Keratinocytes That Stably Maintain Viral Episomes.* Journal of Virology, 2001. **75**(16): p. 7564-7571.
73. Purdie, K.J., et al., *Malignant transformation of cutaneous lesions in renal allograft patients: a role for human papillomavirus.* Cancer Res, 1993. **53**(21): p. 5328-33.

74. Bienkowska-Haba, M., et al., *A new cell culture model to genetically dissect the complete human papillomavirus life cycle.* PLoS Pathog, 2018. **14**(3): p. e1006846.
75. Levan, J., et al., *HPV type 16 E6 and NFX1-123 augment JNK signaling to mediate keratinocyte differentiation and L1 expression.* Virology, 2019. **531**: p. 171-182.
76. Andrei, G., et al., *Epithelial raft cultures for investigations of virus growth, pathogenesis and efficacy of antiviral agents.* Antiviral Res, 2010. **85**(3): p. 431-49.
77. Doorbar, J., *Model systems of human papillomavirus-associated disease.* J Pathol, 2016. **238**(2): p. 166-79.
78. Akgül, B., et al., *The E7 protein of cutaneous human papillomavirus type 8 causes invasion of human keratinocytes into the dermis in organotypic cultures of skin.* Cancer research, 2005. **65**(6): p. 2216-2223.
79. Westphal, K., et al., *Cutaneous human papillomavirus E7 type-specific effects on differentiation and proliferation of organotypic skin cultures.* Cell Oncol, 2009. **31**(3): p. 213-26.
80. Bray, F., et al., *Global cancer statistics 2018: GLOBOCAN estimates of incidence and mortality worldwide for 36 cancers in 185 countries.* CA Cancer J Clin, 2018. **68**(6): p. 394-424.
81. Coghill, A.E., et al., *Immunosuppressive Medications and Squamous Cell Skin Carcinoma: Nested Case-Control Study Within the Skin Cancer after Organ Transplant (SCOT) Cohort.* Am J Transplant, 2016. **16**(2): p. 565-73.
82. Chahoud, J., et al., *Association Between beta-Genus Human Papillomavirus and Cutaneous Squamous Cell Carcinoma in Immunocompetent Individuals-A Meta-analysis.* JAMA Dermatol, 2016. **152**(12): p. 1354-1364.
83. Weissenborn, S.J., et al., *Human papillomavirus-DNA loads in actinic keratoses exceed those in non-melanoma skin cancers.* Journal of Investigative Dermatology, 2005. **125**(1): p. 93-97.
84. White, E.A., et al., *Genus beta human papillomavirus E6 proteins vary in their effects on the transactivation of p53 target genes.* J Virol, 2014. **88**(15): p. 8201-12.
85. Mesplede, T., et al., *p53 degradation activity, expression, and subcellular localization of E6 proteins from 29 human papillomavirus genotypes.* J Virol, 2012. **86**(1): p. 94-107.
86. Cornet, I., et al., *Comparative analysis of transforming properties of E6 and E7 from different beta human papillomavirus types.* J Virol, 2012. **86**(4): p. 2366-70.
87. Howie, H.L., et al., *Beta-HPV 5 and 8 E6 promote p300 degradation by blocking AKT/p300 association.* PLoS Pathog, 2011. **7**(8): p. e1002211.
88. Bedard, K.M., et al., *The E6 oncoproteins from human betapapillomaviruses differentially activate telomerase through an E6AP-dependent mechanism and prolong the lifespan of primary keratinocytes.* J Virol, 2008. **82**(8): p. 3894-902.
89. Wang, N.J., et al., *Loss-of-function mutations in Notch receptors in cutaneous and lung squamous cell carcinoma.* Proc Natl Acad Sci U S A, 2011. **108**(43): p. 17761-6.
90. South, A.P., et al., *NOTCH1 mutations occur early during cutaneous squamous cell carcinogenesis.* J Invest Dermatol, 2014. **134**(10): p. 2630-2638.
91. Meyers, J.M., et al., *Cutaneous HPV8 and MmuPV1 E6 Proteins Target the NOTCH and TGF-beta Tumor Suppressors to Inhibit Differentiation and Sustain Keratinocyte Proliferation.* PLoS Pathog, 2017. **13**(1): p. e1006171.
92. Saidj, D., et al., *Oncoprotein E7 from beta human papillomavirus 38 induces formation of an inhibitory complex for a subset of p53-regulated promoters.* J Virol, 2013. **87**(22): p. 12139-50.
93. Hufbauer, M., et al., *Expression of betapapillomavirus oncogenes increases the number of keratinocytes with stem cell-like properties.* J Virol, 2013. **87**(22): p. 12158-65.
94. Errol, C.F., et al., *DNA Repair and Mutagenesis, Second Edition*. 2006: American Society of Microbiology.
95. Snow, J.A., et al., *beta-HPV 8E6 Attenuates ATM and ATR Signaling in Response to UV Damage.* Pathogens, 2019. **8**(4).
96. Wallace, N.A., et al., *HPV 5 and 8 E6 abrogate ATR activity resulting in increased persistence of UVB induced DNA damage.* PLoS Pathog, 2012. **8**(7): p. e1002807.
97. Wallace, N.A., et al., *HPV 5 and 8 E6 expression reduces ATM protein levels and attenuates LINE-1 retrotransposition.* Virology, 2013. **443**(1): p. 69-79.

98. Muschik, D., et al., *Cutaneous HPV23 E6 prevents p53 phosphorylation through interaction with HIPK2.* PLoS One, 2011. **6**(11): p. e27655.
99. Underbrink, M.P., et al., *E6 proteins from multiple human betapapillomavirus types degrade Bak and protect keratinocytes from apoptosis after UVB irradiation.* J Virol, 2008. **82**(21): p. 10408-17.
100. Harper, D.M., *Currently approved prophylactic HPV vaccines.* Expert Rev Vaccines, 2009. **8**(12): p. 1663-79.
101. Kirby, T., *FDA approves new upgraded Gardasil 9.* Lancet Oncol, 2015. **16**(2): p. e56.
102. Drolet, M., et al., *Population-level impact and herd effects following the introduction of human papillomavirus vaccination programmes: updated systematic review and meta-analysis.* Lancet, 2019. **394**(10197): p. 497-509.
103. Harper, D.M. and L.R. DeMars, *HPV vaccines - A review of the first decade.* Gynecol Oncol, 2017. **146**(1): p. 196-204.
104. Roden, R.B.S. and P.L. Stern, *Opportunities and challenges for human papillomavirus vaccination in cancer.* Nat Rev Cancer, 2018. **18**(4): p. 240-254.
105. Christensen, N.D., et al., *The open reading frame L2 of cottontail rabbit papillomavirus contains antibody-inducing neutralizing epitopes.* Virology, 1991. **181**(2): p. 572-9.
106. Chandrachud, L.M., et al., *Vaccination of cattle with the N-terminus of L2 is necessary and sufficient for preventing infection by bovine papillomavirus-4.* Virology, 1995. **211**(1): p. 204-8.
107. Gambhira, R., et al., *Protection of rabbits against challenge with rabbit papillomaviruses by immunization with the N terminus of human papillomavirus type 16 minor capsid antigen L2.* J Virol, 2007. **81**(21): p. 11585-92.
108. Gambhira, R., et al., *A protective and broadly cross-neutralizing epitope of human papillomavirus L2.* J Virol, 2007. **81**(24): p. 13927-31.
109. Karanam, B., et al., *Developing vaccines against minor capsid antigen L2 to prevent papillomavirus infection.* Immunol Cell Biol, 2009. **87**(4): p. 287-99.
110. Schellenbacher, C., et al., *Efficacy of RG1-VLP vaccination against infections with genital and cutaneous human papillomaviruses.* J Invest Dermatol, 2013. **133**(12): p. 2706-2713.
111. Rubio, I., et al., *Potent anti-HPV immune responses induced by tandem repeats of the HPV16 L2 (20 -- 38) peptide displayed on bacterial thioredoxin.* Vaccine, 2009. **27**(13): p. 1949-56.
112. Canali, E., et al., *A high-performance thioredoxin-based scaffold for peptide immunogen construction: proof-of-concept testing with a human papillomavirus epitope.* Sci Rep, 2014. **4**: p. 4729.
113. Seitz, H., et al., *Robust In Vitro and In Vivo Neutralization against Multiple High-Risk HPV Types Induced by a Thermostable Thioredoxin-L2 Vaccine.* Cancer Prev Res (Phila), 2015. **8**(10): p. 932-41.
114. Cladel, N.M., et al., *Mouse papillomavirus infection persists in mucosal tissues of an immunocompetent mouse strain and progresses to cancer.* Sci Rep, 2017. **7**(1): p. 16932.
115. Handisurya, A., et al., *Characterization of Mus musculus papillomavirus 1 infection in situ reveals an unusual pattern of late gene expression and capsid protein localization.* J Virol, 2013. **87**(24): p. 13214-25.
116. Uberoi, A., S. Yoshida, and P.F. Lambert, *Development of an in vivo infection model to study Mouse papillomavirus-1 (MmuPV1).* J Virol Methods, 2018. **253**: p. 11-17.
117. Cladel, N.M., et al., *Mouse papillomavirus infections spread to cutaneous sites with progression to malignancy.* J Gen Virol, 2017. **98**(10): p. 2520-2529.
118. Brake, T. and P.F. Lambert, *Estrogen contributes to the onset, persistence, and malignant progression of cervical cancer in a human papillomavirus-transgenic mouse model.* Proc Natl Acad Sci U S A, 2005. **102**(7): p. 2490-5.
119. Viarisio, D., et al., *Beta HPV38 oncoproteins act with a hit-and-run mechanism in ultraviolet radiation-induced skin carcinogenesis in mice.* PLoS Pathog, 2018. **14**(1): p. e1006783.
120. Schaper, I.D., et al., *Development of skin tumors in mice transgenic for early genes of human papillomavirus type 8.* Cancer Res, 2005. **65**(4): p. 1394-400.
121. Nafz, J., et al., *Persistence of Mastomys natalensis papillomavirus in multiple organs identifies novel targets for infection.* J Gen Virol, 2007. **88**(Pt 10): p. 2670-8.

122. Nafz, J., et al., *A novel rodent papillomavirus isolated from anogenital lesions in its natural host.* Virology, 2008. **374**(1): p. 186-97.
123. Hasche, D. and F. Rosl, *Mastomys Species as Model Systems for Infectious Diseases.* Viruses, 2019. **11**(2).
124. Salvermoser, M., et al., *Transcriptome analysis of Mastomys natalensis papillomavirus in productive lesions after natural infection.* J Gen Virol, 2016. **97**(7): p. 1658-1669.
125. Hasche, D., et al., *The interplay of UV and cutaneous papillomavirus infection in skin cancer development.* PLoS Pathog, 2017. **13**(11): p. e1006723.
126. Vinzon, S.E., et al., *Protective vaccination against papillomavirus-induced skin tumors under immunocompetent and immunosuppressive conditions: a preclinical study using a natural outbred animal model.* PLoS Pathog, 2014. **10**(2): p. e1003924.
127. Salvermoser, M., et al., *Transcriptome analysis of Mastomys natalensis papillomavirus in productive lesions after natural infection.* J Gen Virol, 2016. **97**(7): p. 1658-69.
128. Sankovski, E., et al., *Mapping of betapapillomavirus human papillomavirus 5 transcription and characterization of viral-genome replication function.* J Virol, 2014. **88**(2): p. 961-73.
129. Grassmann, K., et al., *Identification of a differentiation-inducible promoter in the E7 open reading frame of human papillomavirus type 16 (HPV-16) in raft cultures of a new cell line containing high copy numbers of episomal HPV-16 DNA.* J Virol, 1996. **70**(4): p. 2339-49.
130. Wang, X., et al., *Construction of a full transcription map of human papillomavirus type 18 during productive viral infection.* J Virol, 2011. **85**(16): p. 8080-92.
131. Graham, S.V. and A.A.A. Faizo, *Control of human papillomavirus gene expression by alternative splicing.* Virus Res, 2017. **231**: p. 83-95.
132. Hasche, D., et al., *Establishment of an Immortalized Skin Keratinocyte Cell Line Derived from the Animal Model Mastomys coucha.* PLoS One, 2016. **11**(8): p. e0161283.
133. Hanahan, D., *Studies on transformation of Escherichia coli with plasmids.* J Mol Biol, 1983. **166**(4): p. 557-80.
134. Towbin, H., T. Staehelin, and J. Gordon, *Electrophoretic transfer of proteins from polyacrylamide gels to nitrocellulose sheets: procedure and some applications.* Proceedings of the National Academy of Sciences, 1979. **76**(9): p. 4350-4354.
135. *SDS-PAGE Laemmli Buffer, 5×.* Cold Spring Harbor Protocols, 2015. **2015**(7): p. pdb.rec087924.
136. Buck, C.B., et al., *Efficient intracellular assembly of papillomaviral vectors.* J Virol, 2004. **78**(2): p. 751-7.
137. Sehr, P., et al., *High-throughput pseudovirion-based neutralization assay for analysis of natural and vaccine-induced antibodies against human papillomaviruses.* PLoS One, 2013. **8**(10): p. e75677.
138. Strickland, J.E., et al., *Development of murine epidermal cell lines which contain an activated rasHa oncogene and form papillomas in skin grafts on athymic nude mouse hosts.* Cancer Res, 1988. **48**(1): p. 165-9.
139. Hao, S. and D. Baltimore, *The stability of mRNA influences the temporal order of the induction of genes encoding inflammatory molecules.* Nat Immunol, 2009. **10**(3): p. 281-8.
140. Fu, Y., et al., *Expression of different L1 isoforms of Mastomys natalensis papillomavirus as mechanism to circumvent adaptive immunity.* eLife, 2020. **9**: p. e57626.
141. Sehr, P., K. Zumbach, and M. Pawlita, *A generic capture ELISA for recombinant proteins fused to glutathione S-transferase: validation for HPV serology.* J Immunol Methods, 2001. **253**(1-2): p. 153-62.
142. Schafer, K., T. Waterboer, and F. Rosl, *A capture ELISA for monitoring papillomavirus-induced antibodies in Mastomys coucha.* J Virol Methods, 2010. **163**(2): p. 216-21.
143. MacArthur, H. and G. Walter, *Monoclonal antibodies specific for the carboxy terminus of simian virus 40 large T antigen.* J Virol, 1984. **52**(2): p. 483-91.
144. Pinto, L.A., et al., *Immunogenicity of HPV prophylactic vaccines: Serology assays and their use in HPV vaccine evaluation and development.* Vaccine, 2018. **36**(32 Pt A): p. 4792-4799.
145. Alexander, J., et al., *Linear PADRE T helper epitope and carbohydrate B cell epitope conjugates induce specific high titer IgG antibody responses.* J Immunol, 2000. **164**(3): p. 1625-33.

146. Sari, D., et al., *The MultiBac Baculovirus/Insect Cell Expression Vector System for Producing Complex Protein Biologics.* Adv Exp Med Biol, 2016. **896**: p. 199-215.
147. Schafer, K., et al., *Serological markers for papillomavirus infection and skin tumour development in the rodent model Mastomys coucha.* J Gen Virol, 2011. **92**(Pt 2): p. 383-94.
148. Amtmann, E. and K. Wayss, *The Mastomys natalensis papillomavirus.* The Papovaviridae, 1987. **2**: p. 187-198.
149. Akgul, B., J.C. Cooke, and A. Storey, *HPV-associated skin disease.* J Pathol, 2006. **208**(2): p. 165-75.
150. Hasche, D., S.E. Vinzon, and F. Rosl, *Cutaneous Papillomaviruses and Non-melanoma Skin Cancer: Causal Agents or Innocent Bystanders?* Front Microbiol, 2018. **9**: p. 874.
151. Barksdale, S.K. and C.C. Baker, *Differentiation-specific expression from the bovine papillomavirus type 1 P2443 and late promoters.* J Virol, 1993. **67**(9): p. 5605-16.
152. Jaken, S. and S.H. Yuspa, *Early signals for keratinocyte differentiation: role of Ca2+-mediated inositol lipid metabolism in normal and neoplastic epidermal cells.* Carcinogenesis, 1988. **9**(6): p. 1033-8.
153. KRUSZEWSKI, F., et al. *REGULATION OF INTRACELLULAR FREE CALCIUM IN PRIMARY MOUSE KERATINOCYTES DIFFERS FROM THAT IN MOUSE TRANSFORMED KERATINOCYTE CELL-LINES*. in *PROCEEDINGS OF THE AMERICAN ASSOCIATION FOR CANCER RESEARCH*. 1988. AMER ASSOC CANCER RESEARCH 615 CHESTNUT ST, 17TH FLOOR, PHILADELPHIA, PA ….
154. Stanwell, C., A.A. Dlugosz, and S.H. Yuspa, *Staurosporine induces a complete program of terminal differentiation in neoplastic mouse keratinocytes via activation of protein kinase C.* Carcinogenesis, 1996. **17**(6): p. 1259-65.
155. Poumay, Y. and M.R. Pittelkow, *Cell density and culture factors regulate keratinocyte commitment to differentiation and expression of suprabasal K1/K10 keratins.* J Invest Dermatol, 1995. **104**(2): p. 271-6.
156. Charest, J.L., et al., *Cadherin-mediated cell-cell contact regulates keratinocyte differentiation.* J Invest Dermatol, 2009. **129**(3): p. 564-72.
157. Cardone, G., et al., *Maturation of the human papillomavirus 16 capsid.* mBio, 2014. **5**(4): p. e01104-14.
158. Wooldridge, T.R. and L.A. Laimins, *Regulation of human papillomavirus type 31 gene expression during the differentiation-dependent life cycle through histone modifications and transcription factor binding.* Virology, 2008. **374**(2): p. 371-80.
159. Seitz, H., et al., *A three component mix of thioredoxin-L2 antigens elicits broadly neutralizing responses against oncogenic human papillomaviruses.* Vaccine, 2014. **32**(22): p. 2610-7.
160. Yang, R., et al., *Papillomavirus-like particles stimulate murine bone marrow-derived dendritic cells to produce alpha interferon and Th1 immune responses via MyD88.* J Virol, 2004. **78**(20): p. 11152-60.
161. Yang, R., et al., *B lymphocyte activation by human papillomavirus-like particles directly induces Ig class switch recombination via TLR4-MyD88.* J Immunol, 2005. **174**(12): p. 7912-9.
162. Cuschieri, K., et al., *Impact of partial bivalent HPV vaccination on vaccine-type infection: a population-based analysis.* Br J Cancer, 2016. **114**(11): p. 1261-4.
163. Sankaranarayanan, R., et al., *Immunogenicity and HPV infection after one, two, and three doses of quadrivalent HPV vaccine in girls in India: a multicentre prospective cohort study.* Lancet Oncol, 2016. **17**(1): p. 67-77.
164. Thönes, N., et al., *A Direct Comparison of Human Papillomavirus Type 16 L1 Particles Reveals a Lower Immunogenicity of Capsomeres than Viruslike Particles with Respect to the Induced Antibody Response.* Journal of Virology, 2008. **82**(11): p. 5472-5485.
165. Day, P.M. and J.T. Schiller, *The role of furin in papillomavirus infection.* Future Microbiol, 2009. **4**(10): p. 1255-62.
166. Bronnimann, M.P., et al., *Furin Cleavage of L2 during Papillomavirus Infection: Minimal Dependence on Cyclophilins.* J Virol, 2016. **90**(14): p. 6224-6234.

167. Day, P.M., et al., *A human papillomavirus (HPV) in vitro neutralization assay that recapitulates the in vitro process of infection provides a sensitive measure of HPV L2 infection-inhibiting antibodies.* Clin Vaccine Immunol, 2012. **19**(7): p. 1075-82.
168. Kubba, A.K., et al., *Non-responders to hepatitis B vaccination: a review.* Commun Dis Public Health, 2003. **6**(2): p. 106-12.
169. Wiedermann, U., E. Garner-Spitzer, and A. Wagner, *Primary vaccine failure to routine vaccines: Why and what to do?* Hum Vaccin Immunother, 2016. **12**(1): p. 239-43.
170. Saco, T.V., A.T. Strauss, and D.K. Ledford, *Hepatitis B vaccine nonresponders: Possible mechanisms and solutions.* Ann Allergy Asthma Immunol, 2018. **121**(3): p. 320-327.
171. Fitzsimons, D., et al., *Long-term efficacy of hepatitis B vaccine, booster policy, and impact of hepatitis B virus mutants.* Vaccine, 2005. **23**(32): p. 4158-66.
172. Leuridan, E. and P. Van Damme, *Hepatitis B and the need for a booster dose.* Clin Infect Dis, 2011. **53**(1): p. 68-75.
173. Garner-Spitzer, E., et al., *Correlation between humoral and cellular immune responses and the expression of the hepatitis A receptor HAVcr-1 on T cells after hepatitis A re-vaccination in high and low-responder vaccinees.* Vaccine, 2009. **27**(2): p. 197-204.
174. Day, P.M., et al., *In vivo mechanisms of vaccine-induced protection against HPV infection.* Cell Host Microbe, 2010. **8**(3): p. 260-70.
175. Pouyanfard, S., et al., *Minor Capsid Protein L2 Polytope Induces Broad Protection against Oncogenic and Mucosal Human Papillomaviruses.* J Virol, 2018. **92**(4).
176. Sarkander, J., S. Hojyo, and K. Tokoyoda, *Vaccination to gain humoral immune memory.* Clin Transl Immunology, 2016. **5**(12): p. e120.
177. Naud, P.S., et al., *Sustained efficacy, immunogenicity, and safety of the HPV-16/18 AS04-adjuvanted vaccine: final analysis of a long-term follow-up study up to 9.4 years post-vaccination.* Hum Vaccin Immunother, 2014. **10**(8): p. 2147-62.
178. Kjaer, S.K., et al., *A 12-Year Follow-up on the Long-Term Effectiveness of the Quadrivalent Human Papillomavirus Vaccine in 4 Nordic Countries.* Clin Infect Dis, 2018. **66**(3): p. 339-345.
179. Huh, W.K., et al., *Final efficacy, immunogenicity, and safety analyses of a nine-valent human papillomavirus vaccine in women aged 16-26 years: a randomised, double-blind trial.* Lancet, 2017. **390**(10108): p. 2143-2159.
180. Jagu, S., et al., *Durable immunity to oncogenic human papillomaviruses elicited by adjuvanted recombinant Adeno-associated virus-like particle immunogen displaying L2 17-36 epitopes.* Vaccine, 2015. **33**(42): p. 5553-5563.
181. McGarvie, G., et al., *Vaccination of cattle with L2 protein prevents BPV-4 infection*, in *Immunology of human papillomaviruses*. 1994, Springer. p. 283-290.
182. Zimmermann, P. and N. Curtis, *Factors That Influence the Immune Response to Vaccination.* Clinical Microbiology Reviews, 2019. **32**(2): p. e00084-18.
183. Bock, H.L., et al., *Accelerated Schedule for Hepatitis B Immunization.* J Travel Med, 1995. **2**(4): p. 213-217.
184. Simondon, F., et al., *Randomised study of the possible adjuvant effect of BCG vaccine on the immunogenicity of diphtheria-tetanus-acellular pertussis vaccine in Senegalese infants.* Eur J Clin Microbiol Infect Dis, 1999. **18**(1): p. 23-9.
185. Booy, R., et al., *Immunogenicity of combined diphtheria, tetanus, and pertussis vaccine given at 2, 3, and 4 months versus 3, 5, and 9 months of age.* Lancet, 1992. **339**(8792): p. 507-10.
186. Aucouturier, J., et al., *Montanide ISA 720 and 51: a new generation of water in oil emulsions as adjuvants for human vaccines.* Expert Rev Vaccines, 2002. **1**(1): p. 111-8.
187. Ott, G., et al., *The adjuvant MF59: a 10-year perspective*. 2000, Springer. p. 211-228.
188. Siegrist, C.-A., *Vaccine immunology.* Vaccines, 2008. **5**(1): p. 17-36.
189. Liaw, K.L., et al., *A prospective study of human papillomavirus (HPV) type 16 DNA detection by polymerase chain reaction and its association with acquisition and persistence of other HPV types.* J Infect Dis, 2001. **183**(1): p. 8-15.
190. Clifford, G.M., et al., *Worldwide distribution of human papillomavirus types in cytologically normal women in the International Agency for Research on Cancer HPV prevalence surveys: a pooled analysis.* Lancet, 2005. **366**(9490): p. 991-8.

191. Chan, P.K., et al., *Distribution of human papillomavirus types in anogenital warts of men.* J Clin Virol, 2009. **44**(2): p. 111-4.
192. Lajous, M., et al., *Determinants of prevalence, acquisition, and persistence of human papillomavirus in healthy Mexican military men.* Cancer Epidemiol Biomarkers Prev, 2005. **14**(7): p. 1710-6.
193. Shamanin, V., et al., *Human papillomavirus infections in nonmelanoma skin cancers from renal transplant recipients and nonimmunosuppressed patients.* J Natl Cancer Inst, 1996. **88**(12): p. 802-11.
194. Clavel, C.E., et al., *Mucosal oncogenic human papillomaviruses and extragenital Bowen disease.* Cancer, 1999. **86**(2): p. 282-7.
195. Deguchi, M., et al., *Detection of human papillomavirus type 33 DNA in extragenital Bowen's disease with the polymerase chain reaction.* Dermatology, 1998. **196**(3): p. 292-4.
196. Zakrzewska, K., et al., *Pattern of HPV infection in basal cell carcinoma and in perilesional skin biopsies from immunocompetent patients.* Virol J, 2012. **9**: p. 309.
197. Garssen, J., et al., *Transcription-coupled and global genome repair differentially influence UV-B-induced acute skin effects and systemic immunosuppression.* J Immunol, 2000. **164**(12): p. 6199-205.
198. Tomas, D., *[Apoptosis, UV-radiation, precancerosis and skin tumors].* Acta Med Croatica, 2009. **63 Suppl 2**: p. 53-8.
199. Spielman, D., et al., *Does Inbreeding and Loss of Genetic Diversity Decrease Disease Resistance?* Conservation Genetics, 2004. **5**(4): p. 439-448.
200. Taylor, C.H., et al., *Immune state is associated with natural dietary variation in wild mice Mus musculus domesticus.* Functional ecology, 2019. **33**(8): p. 1425.
201. Edwards, T.G., et al., *Human papillomavirus episome stability is reduced by aphidicolin and controlled by DNA damage response pathways.* J Virol, 2013. **87**(7): p. 3979-89.
202. Edwards, T.G., et al., *DNA damage repair genes controlling human papillomavirus (HPV) episome levels under conditions of stability and extreme instability.* PLoS One, 2013. **8**(10): p. e75406.
203. Hong, S., K.P. Mehta, and L.A. Laimins, *Suppression of STAT-1 expression by human papillomaviruses is necessary for differentiation-dependent genome amplification and plasmid maintenance.* J Virol, 2011. **85**(18): p. 9486-94.
204. Herdman, M.T., et al., *Interferon-beta treatment of cervical keratinocytes naturally infected with human papillomavirus 16 episomes promotes rapid reduction in episome numbers and emergence of latent integrants.* Carcinogenesis, 2006. **27**(11): p. 2341-53.
205. Chang, Y.E., et al., *Long-term effect of interferon on keratinocytes that maintain human papillomavirus type 31.* J Virol, 2002. **76**(17): p. 8864-74.
206. Davy, C.E., et al., *Human Papillomavirus Type 16 E1[∧]E4-Induced G₂ Arrest Is Associated with Cytoplasmic Retention of Active Cdk1/Cyclin B1 Complexes.* Journal of Virology, 2005. **79**(7): p. 3998-4011.
207. Nakahara, T., et al., *Modulation of the cell division cycle by human papillomavirus type 18 E4.* J Virol, 2002. **76**(21): p. 10914-20.
208. Egawa, N., et al., *HPV16 and 18 genome amplification show different E4-dependence, with 16E4 enhancing E1 nuclear accumulation and replicative efficiency via its cell cycle arrest and kinase activation functions.* PLoS pathogens, 2017. **13**(3): p. e1006282.
209. Ross, J., *mRNA stability in mammalian cells.* Microbiol Rev, 1995. **59**(3): p. 423-50.
210. Jeon, S. and P.F. Lambert, *Integration of human papillomavirus type 16 DNA into the human genome leads to increased stability of E6 and E7 mRNAs: implications for cervical carcinogenesis.* Proc Natl Acad Sci U S A, 1995. **92**(5): p. 1654-8.
211. Zhao, K.N., et al., *Gene codon composition determines differentiation-dependent expression of a viral capsid gene in keratinocytes in vitro and in vivo.* Mol Cell Biol, 2005. **25**(19): p. 8643-55.
212. Kennedy, I.M., J.K. Haddow, and J.B. Clements, *A negative regulatory element in the human papillomavirus type 16 genome acts at the level of late mRNA stability.* J Virol, 1991. **65**(4): p. 2093-7.

213. Koffa, M.D., et al., *The human papillomavirus type 16 negative regulatory RNA element interacts with three proteins that act at different posttranscriptional levels.* Proc Natl Acad Sci U S A, 2000. **97**(9): p. 4677-82.
214. Thiele, A., et al., *AU-rich elements and alternative splicing in the beta-catenin 3'UTR can influence the human beta-catenin mRNA stability.* Exp Cell Res, 2006. **312**(12): p. 2367-78.
215. Presnyak, V., et al., *Codon optimality is a major determinant of mRNA stability.* Cell, 2015. **160**(6): p. 1111-24.
216. Laurson, J. and K. Raj, *Localisation of human papillomavirus 16 E7 oncoprotein changes with cell confluence.* PLoS One, 2011. **6**(6): p. e21501.
217. Sperling, T., et al., *Human papillomavirus type 8 interferes with a novel C/EBPbeta-mediated mechanism of keratinocyte CCL20 chemokine expression and Langerhans cell migration.* PLoS Pathog, 2012. **8**(7): p. e1002833.
218. Dantur, K., et al., *Cytosolic accumulation of HPV16 E7 oligomers supports different transformation routes for the prototypic viral oncoprotein: the amyloid-cancer connection.* Int J Cancer, 2009. **125**(8): p. 1902-11.
219. Alonso, L.G., et al., *High-Risk (HPV16) Human Papillomavirus E7 Oncoprotein Is Highly Stable and Extended, with Conformational Transitions that Could Explain Its Multiple Cellular Binding Partners.* Biochemistry, 2002. **41**(33): p. 10510-10518.
220. Knapp, A.A., et al., *Identification of the nuclear localization and export signals of high risk HPV16 E7 oncoprotein.* Virology, 2009. **383**(1): p. 60-8.
221. Onder, Z. and J. Moroianu, *Nuclear import of cutaneous beta genus HPV8 E7 oncoprotein is mediated by hydrophobic interactions between its zinc-binding domain and FG nucleoporins.* Virology, 2014. **449**: p. 150-62.
222. Onder, Z., V. Chang, and J. Moroianu, *Nuclear export of cutaneous HPV8 E7 oncoprotein is mediated by a leucine-rich nuclear export signal via a CRM1 pathway.* Virology, 2015. **474**: p. 28-33.
223. Kajitani, N., et al., *Productive Lifecycle of Human Papillomaviruses that Depends Upon Squamous Epithelial Differentiation.* Frontiers in Microbiology, 2012. **3**(152).
224. Bikle, D.D., Z. Xie, and C.L. Tu, *Calcium regulation of keratinocyte differentiation.* Expert Rev Endocrinol Metab, 2012. **7**(4): p. 461-472.
225. Hennings, H., et al., *Intracellular calcium alterations in response to increased external calcium in normal and neoplastic keratinocytes.* Carcinogenesis, 1989. **10**(4): p. 777-80.
226. Apt, D., et al., *Nuclear factor I and epithelial cell-specific transcription of human papillomavirus type 16.* J Virol, 1993. **67**(8): p. 4455-63.
227. Carson, A. and S.A. Khan, *Characterization of transcription factor binding to human papillomavirus type 16 DNA during cellular differentiation.* J Virol, 2006. **80**(9): p. 4356-62.
228. Ishii, Y., K. Tanaka, and T. Kanda, *Mutational analysis of human papillomavirus type 16 major capsid protein L1: the cysteines affecting the intermolecular bonding and structure of L1-capsids.* Virology, 2003. **308**(1): p. 128-36.
229. Ryndock, E.J., et al., *Roles for human papillomavirus type 16 l1 cysteine residues 161, 229, and 379 in genome encapsidation and capsid stability.* PLoS One, 2014. **9**(6): p. e99488.
230. McCarthy, M.P., et al., *Quantitative disassembly and reassembly of human papillomavirus type 11 viruslike particles in vitro.* J Virol, 1998. **72**(1): p. 32-41.
231. Rajendar, B., et al., *A simple and rapid method to monitor the disassembly and reassembly of virus-like particles.* Anal Biochem, 2013. **440**(1): p. 15-7.
232. Ferre, F. and P. Clote, *DiANNA: a web server for disulfide connectivity prediction.* Nucleic Acids Res, 2005. **33**(Web Server issue): p. W230-2.
233. Wu, C., N. Kajitani, and S. Schwartz, *Splicing and Polyadenylation of Human Papillomavirus Type 16 mRNAs.* Int J Mol Sci, 2017. **18**(2).
234. Schwartz, S., *Papillomavirus transcripts and posttranscriptional regulation.* Virology, 2013. **445**(1-2): p. 187-96.
235. Conway, M.J., et al., *Differentiation-dependent interpentameric disulfide bond stabilizes native human papillomavirus type 16.* PLoS One, 2011. **6**(7): p. e22427.

236. Akgul, B., et al., *UV-B irradiation stimulates the promoter activity of the high-risk, cutaneous human papillomavirus 5 and 8 in primary keratinocytes.* Arch Virol, 2005. **150**(1): p. 145-51.
237. Vasiljevic, N., et al., *Differences in transcriptional activity of cutaneous human papillomaviruses.* Virus Res, 2008. **137**(2): p. 213-9.
238. Purdie, K.J., et al., *The promoter of a novel human papillomavirus (HPV77) associated with skin cancer displays UV responsiveness, which is mediated through a consensus p53 binding sequence.* EMBO J, 1999. **18**(19): p. 5359-69.
239. de Villiers, E.M., A. Ruhland, and P. Sekaric, *Human papillomaviruses in non-melanoma skin cancer.* Semin Cancer Biol, 1999. **9**(6): p. 413-22.
240. Rockx, D.A., et al., *UV-induced inhibition of transcription involves repression of transcription initiation and phosphorylation of RNA polymerase II.* Proc Natl Acad Sci U S A, 2000. **97**(19): p. 10503-8.
241. Yugawa, T., et al., *Regulation of Notch1 gene expression by p53 in epithelial cells.* Mol Cell Biol, 2007. **27**(10): p. 3732-42.

Appendix

Abbreviation

3'-UTR	Three prime untranslated region
6-4 PP	6-4 photoproducts
AAV	Adeno-associated virus
ActD	Actinomycin D
AHSS	Aluminium hydroxyphophate sulfate
AKs	Actinic keratosis
AKT	Serine/threonine kinase
aP	Acellular pertussis
APCs	Antigen-presenting cells
APS	Ammonium persulfate
AREs	AU-rich elements
ATM	Ataxia telangiectasia mutated
ATR	Ataxia telangiectasia and Rad3 related
BAK	BCL2 antagonist/killer 1
BCR	B cell receptor
BEVS	Balculovirus expression vector system
BM	Bone marrow
BPV1	Bovine papillomavirus 1
BRD4	Bromodomain-containing protein 4
BSA	Bovine serum albumin
CaCl2	Calcium chloride
CBB	Casein blocking buffer
CBR	Chromatin binding region
Cdk	Cyclin-dependent kinase
CDP	CCAAT displacement protein
cGMP	cyclic GMP
CIA	Chloroform-isoamylalcohol
CIN	Cervical intraepithelial neoplasia
CMV	Cytomegalovirus
CPDs	Cyclobutane pyrimidine dimers
CRPV	Cottontail rabbit PV
CYPB	Cyclophilin B
CYCS	Cytochrome c
DAPI	4′,6-diamidino-2-phenylindole
DCs	Dendritic cells

DDR	DNA damage response
DMEM	Dulbecco's Modified Eagle's Medium
DMSO	Dimethyl sulfoxide
DNMT1	DNA methyltransferase 1
DSBs	Double strand breaks
DTP	Diphtheria-tetanus-pertussis
DTT	Dithiothreitol
E2BSs	E2-binding sites
E2F	E2 factor
E6AP	E6-associated protein
EBV	Epstein-Barr virus
ECL	Enhanced chemiluminescent reaction
ECM	Extracellular matrix
EcTrx	*Escherichia coli* thioredoxin
EDTA	Ethylenediaminetetraacetic acid
EE	Early endosome
ELISA	Enzyme-linked immunosorbent assay
EM	Electron microscope
ERK	Extracellular signalregulated kinase
EV	Epidermodysplasia verruciformis
EZH2	Enhancer Of Zeste 2 polycomb repressive complex 2 subunit
FBS	Fetal bovine serum
GAPDH	Glycerinaldehyde 3-phosphate dehydrogenase
GC	Germinal center
GST	Glutathione S-transferase
GW	Genital warts
HA	Hemagglutinin
HBSS	Hank's balanced salt solution
HBV	Hepatitis B virus
HCV	Hepatitis C virus
HE	Hematoxylin and eosin
HFK	Human foreskin keratinocytes
HHV-8	Human herpes virus 8
HIPK2	Homeodomain-interacting protein kinase 2
HIV	Human immunodeficiency virus
HPV	Human papillomavirus
HR	High-risk
HRP	Horseradish peroxidase

HSPGs	Heparan sulfate proteoglycans
hTERT	Human telomerase reverse transcriptase
HTLV	Human T-lymphotropic virus
ICN	Intracellular cleaved Notch
ICTV	International Committee on Taxonomy of Viruses
IFN	Interferon
IKK-beta	Inhibitor of nuclear factor kappa-B kinase subunit beta
ILVs	Intraluminal vesicles
IPTG	Isopropyl β-D-1-thiogalactopyranoside
IRAC	International Agency for Research on Cancer
JNK	c-Jun N-terminal kinase
K14	Keratin 14
KAs	Keratoacanthomas
KLK8	Kallikrein-8
KSCC	Keratinizing SCCs
LCR	Long control region
LE	Late endosome
LR	Low-risk
MAML1	Mastermind-like protein 1
MC	Methylcellulose
MCC	Merkel cell carcinoma
MCM	Minichromosome maintenance complex
McPV2	*Mastomys coucha* papillomavirus 2
MCV	Merkel cell carcinoma
MEM	Minimum Essential Medium
MmuPV1	*Mus musculus* papillomavirus 1
MnPV	*Mastomys natalensis* papillomavirus
MPL	Monophosphoryl lipid A
MVBs	Multivesicular bodies
NEAA	Non-essential amino acid
NES	Nuclear export signal
nKSCC	Non-keratinizing SCC
NLS	Nuclear localization signal
NMSC	Non-melanoma skin cancer
NRE	Negative regulatory element
OD	Optical density
ORF	Open reading frame
OTRs	Organ transplant recipients

PADRE	pan HLA DR-binding epitope
pAL	Late polyadenylation
PBNA	Pseudovirion-based neutralization assay
PCR	Polymerase chain reaction
PFA	Paraformaldehyde
PfTrx	*Pyrococcus furiosus* thioredoxin
PI3K	Phosphoinositide 3-kinase
PKC	Protein kinase C
PML	Promyelocytic leukemia
POLη	DNA polymerase η
Ppia	Peptidylprolyl isomerase A
pRb	Prepro-retinoblastoma-associated protein
PsVs	Pseudoviruses
QVs	Quasivirions
RBPJ	Recombination signal binding protein for immunoglobulin kappa J region
rDNA	Ribosomal DNA
RPA	Replication A proteins
Rpl32	Ribosomal protein L32
SAS	Sigma Adjuvant System
SCC	Squamous cell carcinoma
SDS-PAGE	Sodium dodecyl sulfate-polyacrylamide gel electrophoresis
Sf9	*Spodoptera frugiperda* 9
SMAD 2/3/4	Mothers against decapentaplegic homolog 2/3/4
SPF	Specified pathogen-free
SR	Serine-arginine
SRC-1	Steroid receptor coactivator 1
SRPK1	Serine-arginine protein kinase 1
SV40	Simian Virus 40
TA	Tissue antigen
TGN	Trans-Golgi network
TLR4	Toll-like receptor 4
TMD	Transmembrane domain
TN-High-5	*Trichoplusia ni* High-5
Topo I	Topoisomerase I
TRAPPC8	Trafficking protein particle complex 8
URR	Upstream regulatory region
VCR	Vaccination coverage rate
vDNA	viral genomic DNA

VLPs	Virus like particles
WHO	World Health Organization
XPA	DNA repair protein complementing XP-A cells

Acknowledgement

I would like to express the deep appreciation to my supervisor Prof. Frank Rösl for giving me the chance to grow in this field and the persistent guidance and support to complete my dissertation. Moreover, Frank, thanks for all your fantastic recommendations that lead me to discover “beautiful things”.

I also would like to thank my TAC members Prof. Dr. Martin Müller and Prof. Dr. Baki Akgül for their invaluable advice and generous help in improving my project.

Thanks to Prof. Reinhard Kirnbauer for the contribution and efforts in the RG-1 collaborative project.

Also, thanks to Prof. Ralf Bartenschlager and PD. Karin Müller-Decker for their participation in my defense committee.

I would like to thank Dr. Damir Krunic for the guidance to using various light microscopes and kind help in image processing and Dr. Karsten Richter and Dr. Michelle Neßling for their support in electron microscopy.

I also thank Dr. Xueer Zhao, Dr. Fan Yang and Petra Galmbacher from Prof. Martin Müller’s lab for all their assistance in L2 antigen and VLP production.

I would like to express my gratitude to all the members in F030:
Dr. Daniel Hasche for sharing your work experience and continuous support throughout my project. Sonja and Ilona for your great work, caring and improving my German (Danke schön). Dr. Matthias Meister, Miriam and Melinda for your kind help with my experiments.

Dr. Martina Niebler for all your science-related or unrelated- “gifts”. Dr. Graciela Ruiz Ramirez, Linhan, Elke, Regina, Nadine and Diana for your enthusiastic support with my experiments and paperwork.

Dr. Ruwen Yang and Dr. Yingying Fu, yes, both of you had got the Dr.! Wo ye bi ye la! Thanks for all the great time we had been together and your always gracious support no matter where you are now. I will treasure all those hilarious and ridiculous moments together with you two and Martina, but I think we will create more.

感谢我的家人一直以来的理解，包容和付出，谢谢你们支持我尽可能自由自在地做自己。

Now, it's time for a new adventure.

“莫听穿林打叶声，何妨吟啸且徐行。竹杖芒鞋轻胜马，谁怕？一蓑烟雨任平生。”

— 苏轼《定风波》